DEVELOPMENT OF APTAMERS FOR TARGETED THERAPY AND BIOMARKER DISCOVERY

By

LING MENG

A DISSERTATION PRESENTED TO THE GRADUATE SCHOOL
OF THE UNIVERSITY OF FLORIDA IN PARTIAL FULFILLMENT
OF THE REQUIREMENTS FOR THE DEGREE OF
DOCTOR OF PHILOSOPHY

UNIVERSITY OF FLORIDA

2010

To my loving parents, husband and daughter

ACKNOWLEDGMENTS

It has been more than five years since I joined University of Florida as a graduate student in 2005. It is an interesting journey fulfilled with encourage, support, friendship and, of course, pains. There have been so many things and people I will always remember.

First of all, I would like to express my deep gratitude to my advisor, Dr. Weihong Tan, who has guided me through my five years of study. Dr. Tan not only provided many suggestions and support for my research, but also encouraged and enlightened me to seriously investigate the correct attitude to my future career and life. In addition, I would like to thank my committee members: Dr. Gail Fanucci, Dr. Richard Moyer, Dr. Jon Stewart, and Dr. Vaneica Young. Their advice, suggestions, and encouragement have helped me to refine this dissertation. Also, I appreciate the great help from Department of Chemistry faculties and staffs, especially Dr.Kathryn R. Willams, Dr. Benjamin W. Smith and Lori Clark.

I appreciate the tremendous efforts from Dr. Xiangxuan Zhao and Lucy Zhang from Dr. Chen Liu's group on the liver cancer drug project. This is a collaborative work between Dr Weihong Tan and Dr. Liu's Labs. The success was through the collective efforts of all members. I also thank Dr. Lei Zhou and Dr. Siqing Wang for discussion and suggestions on PTK7 function project.

Tan group is more like a big family than a research group and I am proud and thankful to have been a member of this family. All former and current members have contributed to my research and life. Here, and helped me in different aspects. I want to thank all of them, especially Dr. Shangguan Dihua, Dr. Zhiwen Tang, Dr. Kwame Sefah, Dr. Prabodhika Mallikaratchy, Dr. Liu Yang, Dr. Yanrong Wu, Dr. Yan Chen, Hui Wang

for their continuous support, suggestions and discussions of my research, as well as their kind friendship and encouragement.

There has been nothing more valuable and precious than my family to me. I am exceedingly thankful to my parents, Hongying Su and Xiangting Meng, and my husband, Yan Li, for their understanding, support, encouragement and love. I also thank my daughter, Connie M. Li for the endless happiness and joy that she has brought to me.

Without these help and support, I would never achieve any success. I would like to acknowledge all of them at this special moment.

TABLE OF CONTENTS

page

LIST OF TABLES

LIST OF FIGURES

LIST OF ABBREVIATIONS

7-AAD	7-Aminoactinomycin D
AEBSF	4-(2-aminoethyl)benzenesulfonyl fluoride
AFC	7-amino-4-trifluoromethyl coumarin
AFP	Alpha-fetoprotein
ALL	Acute lymphoblastic leukemia
AMA	Ammonium hydroxide/40% aqueous methylamine 1:1
AMD	Age-related macular degeneration
AML	Acute myeloid leukemia
ATCC	American Type Culture Collection
Bid	BCL-2 Interacting Domain
BrdU	Bromodeoxyuridine
BSA	Bis(trimethylsilyl)acetamide
Caspase	Cysteine-*asp*artic protease
CCK4	Colon carcinoma kinase-4
cDNA	Complementary DNA
CGH	Comparative genomic hybridization
CT	Computed tomography
Cy5.5	Cyanine derivative 5.5
DISC	Death-inducing signaling complex
DMEM	Dulbecco's Modified Eagle Medium
DNA	Deoxyribonucleic acid
DNase	Deoxyribonuclease
dNTP	Deoxyribonucleotide triphosphate
Dox	Doxorubicin

DPBS	Dulbecco's phosphate buffered saline
dsRNA	Double-straned RNA
ECL	Enhanced chemiluminescence
EDTA	Ethylenediaminetetraacetic acid
EGF	Epithelial growth factor
EGFR2	Epidermal growth factor receptor 2
EGTA	Ethylene glycol tetraacetic acid
FADD	Fas-Associated protein with Death Domain
FBS	Fetal bovine serum
FISH	Fluorescence *in situ* hybridization
FITC	Fluorescein isothiocyanate
FMK	Fluoromethyl ketone
FSC	Forward Scatter
GAPDH	Glyceraldehyde 3-phosphate dehydrogenase
H&E Stain	Hematoxylin and eosin stain
HBSS	Hank's buffered salt solution
HBV	Hepatitis B virus
HCC	Hepatocellular carcinoma
HCV	Hepatitis C virus
HER2	Human epidermal growth factor receptor 2
HEPES	4-(2-hydroxyethyl)-1-piperazineethanesulfonic acid
HPLC	High-performance liquid chromatography
HRP	Horseradish peroxidase
IDT	Integrated DNA Technologies
IGF	Insulin-like growth factors

IgG	Immunoglobulin G
JC-1	5,5',6,6'-tetrachloro-1,1',3,3'- tetraethylbenzimidazolylcarbocyanine iodide
K_d	Dissociation constant
kD	KiloDalton
MEAR	BNL 1ME A.7R.1 mouse hepatoma cell line
miRNA	microRNA
MRI	Magnetic resonance imaging
mRNA	Messenger ribonucleic acid
MTS	(3-(4,5-dimethylthiazol-2-yl)-5-(3-carboxymethoxyphenyl)-2-(4-sulfophenyl)-2H-tetrazolium)
NP-40	Nonidet P-40
PAGE	Polyacrylamide gel electrophoresis
PBS	Phosphate buffered saline
PBST	Phosphate buffered saline buffer containing 0.2% Tween 20
PCP	Planar cell polarity
PCR	Polymerase chain reaction
PDGF	Platelet-derived growth factor
PE	R-phycoerythrin
PET	Positron emission tomography
PI	Propidium iodide
PMS	Phenazine methosulfate
Poly(A)	Polyadenylate
PS	Phosphatidylserine
PSMA	Prostate Specific Membrane Antigen
rRNA	Ribosomal RNA

PTK7	Protein tyrosine kinase-7
PVDF	Polyvinylidene Fluoride
RISC	RNA-induced silencing complex
RNA	Ribonucleic acid
RNAi	RNA interference
RTKs	Receptor tyrosine kinases
RT-PCR	Reverse transcription polymerase chain reaction
SELEX	Systematic Evolution of Ligands by EXponential enrichment
siRNA	Small interfering RNA
SDS	Sodium dodecyl sulfate
SSC	Side Scatter
ssDNA	Single stranded deoxyribonucleic acid
tBid	Truncated BCL-2 Interacting Domain
T-cell ALL	T-cell acute lymphoblastic leukemia
Tm	Melting temperature
TMR	Tetramethylrhodamine
TNF	Tumor necrosis factor
tRNA	Transfer RNA
VEGF	Endothelial growth factors
WB	Western blot

Abstract of Dissertation Presented to the Graduate School
of the University of Florida in Partial Fulfillment of the
Requirements for the Degree of Doctor of Philosophy

DEVELOPMENT OF APTAMERS FOR TARGETED THERAPY AND BIOMARKER DISCOVERY

By

Ling Meng

December 2010

Chair: Weihong Tan
Major: Chemistry

Cancer, as the second leading cause of death worldwide, is one of the major public health concerns. Though great efforts have been made globally in cancer research, the incidence of cancer is still rising. The most difficult part for effective diagnosis and treatment of most cancers is the lack of effective and specific molecular markers. Defining molecular characteristics of cancer cells is useful in the prediction of tumor behavior and monitoring the response to treatment. The identification of molecular markers for cancers using antibody and mass spectrometry methodologies has been challenging. Therefore, the development of new strategies to identify new molecular markers specific for cancers is important.

Oligonucleotides were once considered mainly as molecules for the storage and translation of genetic information. However, the discovery of RNAzymes, and later, DNAzymes, revealed the potential use of oligonucleotides in many other biological applications. In the last two decades, these applications have been expanded through the introduction of Systematic Evolution of Ligands by EXponential enrichment (SELEX) which generates, by repeated rounds of *in vitro* selection, a type of molecular probe termed aptamers. Aptamers are oligonucleic acid (or peptide) molecules that can bind

to various molecular targets and are viewed as complements to antibodies. Aptamers have found applications in many areas, such as biotechnology, medicine, pharmacology, microbiology, and chemistry. The potential of aptamers in cancer research has been intensively studied in the past few decades, as a result of the unique ability of aptamers to identify molecular signatures of cancer cells. In this dissertation we have demonstrated the potential of aptamers in recognition of surface markers for human liver cancers and in targeted drug-delivery. We believe the successful development of these molecular probes will contribute immensely to the efforts in many research facilities to understand and manage human cancers.

CHAPTER 1
INTRODUCTION

Human Cancer

Overview

Cancer is the general name for a group of different diseases which are characterized by uncontrolled cell growth and spread of abnormal cells. Cancer starts when cells in a part of the body start to grow out of control. Normal cells grow, divide, and die in a very ordered fashion, but cancer cells continue growing and forming new cancer cells. Cancer cells can invade other tissues, but normal cells cannot. So uncontrolled cell growth and the capability to invade other tissue make cancer cells different from normal cells. Cancer is caused by lifestyle and environmental factors (tobacco, diet and obesity, infections, radiation, stress, lack of physical activity, and environmental pollutants) and genetics (oncogene activation and tumor suppressor gene inactivation).[1] Currently cancer is the second most common leading cause of death worldwide and in the United States, exceeded only by heart disease. In 2010, 1,529,560 new cancer cases are expected to be diagnosed and about 569,490 Americans are expected to die of cancer, accounting for nearly 1 of every 4 deaths.[2]

Cancer diagnosis methods include X-rays, computed tomography (CT), magnetic resonance imaging (MRI), and ultrasound, all of which help physicians determine the tumor's location and size. A biopsy is usually performed to confirm most cancer diagnoses; tissue samples are surgically removed from the suspected malignancy and studied under a microscope to check for cancer cells. Treatment varies based on the type and stage of the tumor, and is typically determined by the tumor size and whether it has metasized, or spread from its original location. If the cancer is confined to one

location and has not spread, the most common treatment is surgery. If surgery cannot remove all of the cancer tissue, treatment can include radiation, chemotherapy, or both. For some cancer cases, a combination of surgery, radiation, and chemotherapy is required.

Cancer Genomics

Cancer is characterized as a complex disease of genomic alteration, exploiting many different molecular mechanisms. All cancers occur due to abnormalities in DNA sequences. The identification of genes that are mutated and hence induce cancer has been a central aim of cancer research, although the actual number of mutations required for a particular cancer development is still unknown.[3] In order to understand the fundamental biology of cancers, it is important to identify these genetic alterations during cancer development. These gene mutations change the proteomic patterns of the cell and then induce abnormal cell proliferation. Many techniques have been introduced as genome-screening tools for chromosomal aberrations the identification of cancer cells, including fluorescence *in situ* hybridization (FISH), multicolor spectral karyotype (SKY)/multicolor FISH (m-FISH), comparative genomic hybridization (CGH), and array-based CGH. But there are limitations in using these methods. For instance, prior knowledge of genes is required for FISH, and CGH is unable to detect balanced translocations and inversions.

Gene Expression Profiling in Cancer

Gene expression profiling is a technique to measure the expression of thousands of genes simultaneously. In the context of cancer, gene expression profiling has been used to more accurately classify tumors and to predict a patient's clinical outcome. Microarrays of cDNA and oligonucleotides have been used as efficient tools for cancer

gene expression profiling. Microarray analysis can provide quantitative gene expression information allowing for the generation of a molecular signature and the classification of tumors into subtypes.[4-7] For example, acute lymphoblastic leukemia (ALL) was distinguished from acute myeloid leukemia (AML) by gene expression profiling. Comparison of the gene expression between cancer cells and normal cells can help identify the genes which are associated with cancer development.

DNA/RNA microarrays, which offer relatively high sensitivity and throughput, have been used as efficient tools for gene expression profiling. However, there are 25,000 genes in the human genome which produce 1,000,000 distinct proteins through posttranslational modification, such as cleavage, protein phosphorylation, and glycosylation. So a given gene serves as the basis for many different proteins. On the other hand, cells use many other mechanisms to regulate proteins without altering the amount of mRNA, so these genes may stay consistently expressed even when protein concentrations are rising and falling. For example proteolysis, recycling, and isolation in cell compartments can affect protein concentration, without gene influence. Therefore, gene expression profiling alone is not sufficient for disease (such as cancer) biomarker identification.

Protein Profiling in Cancer

All living cells rely on proteins for their survival and growth. The alteration of proteins, by changes in expression levels, posttranslational modifications (glycosylation, phenylation, formylation, acetylation), or mutations at the genetic level, can induce uncontrolled cell growth leading to cancer. Therefore, detection of alterations of protein expression levels and protein modifications is an important goal, which can lead to the invention of novel diagnostic approaches and targeted therapy strategies.

Many of the key cancer-related proteins discovered so far are membrane associated proteins, because they confer specific cellular functions and are easily accessible. The membrane proteins represent about 1/3 of all cell proteins and play important roles in the survival of the cell. Several growth factor proteins, such as epidermal growth factor receptor 2 (EGFR2),[8] vascular endothelial growth factors (VEGF),[9] platelet-derived growth factor (PDGF),[10] and insulin-like growth factors (IGF),[11] are classic tumor-related cell membrane proteins, and their misregulation plays a key role in tumor initiation. Membrane proteins are generally used as markers to classify cell types[12] and in drug therapy.[13] Seventy percent of all known drug targets are cell membrane proteins, such as HER2 (human epidermal growth factor receptor 2) and G-protein coupled receptors.[13]

However, not all cell membrane proteins are significant for cancer study and therapy, as most of these may also be equally expressed on normal cells. Therefore, it is important and clinically significant to exploit technologies that have the capacity to identify useful markers which associate with cancer. To achieve this goal, many monoclonal antibodies against cell surface proteins have been prepared. Cells can be classified or immunophenotyped according to their cell-surface-protein expression. However, most cell membrane proteins remain undetectable due to the lack of suitable antibodies or recognition probes.[14] Hence, the cell-SELEX strategy (described further below) provides an opportunity to generate probes, called aptamers, to recognize target cancer cells with high specificity and can be used for further discovery of new cancer biomarkers.

Aptamers

Overview

Aptamers are oligonucleic acid or peptide molecules that specifically bind to a target molecule. Nucleic acid aptamers are single-stranded oligonucleotides (DNA or RNA), and they typically contain fewer than 100 bases and have unique three-dimensional structures for target recognition through interactions such as van der Waals surface contacts, hydrogen bonding and base stacking. Nucleic acid aptamers are developed from random oligonucleotide pools through a process called Systematic Evolution of Ligands by EXponential enrichment (SELEX), and they bind to various molecular targets, such as small molecules (metal ions, organic dyes or amino acids), nucleic acids, and proteins, as well as to viruses and virus-infected cells, bacterial cells, tissues and organisms.[15-52] Both DNA and RNA aptamers can form complex secondary and tertiary structures, but the range of 3D structures achieved by RNA aptamers is more diverse compared to DNA aptamers.[53,54] However, DNA aptamers are more stable and less expensive than RNA aptamers. Peptide aptamers consist of a short variable peptide domain attached at both ends to a protein scaffold to interfere with other protein interactions inside cells. Aptamers were first developed in1990, and they are now widely used in biotechnology, medicine, pharmacology, cell biology, microbiology and bioanalysis.[55,56] This dissertation focuses on DNA aptamer selection and application.

SELEX

Aptamers are obtained through an *in vitro* selection process known as SELEX (Systematic Evolution of Ligands by EXponential enrichment), in which aptamers are selected from a library of random sequences of synthetic DNA or RNA by repetitive binding of the oligonucleotides to target molecules. Briefly, the SELEX process starts

with the incubation of the oligonucleotide library pool (DNA or RNA) with the target of interest. After incubation, the bound complexes (target and oligonucleotide sequences) are separated from the unbound sequences. After that, the sequences binding to the target are eluted and then incubated with the control, and the remaining sequences are amplified by PCR. The process is repeated and monitored until the pool is enriched for sequences that specifically recognize the target of interest. Then the enriched pool is cloned and sequenced to obtain the individual sequences. Potential aptamer candidates, usually grouped into families, are chemically synthesized, labeled with fluorescent dye and tested against the target.

Most aptamers reported so far have been selected by using simple targets, such as a purified protein. Recently, aptamer selection against complex targets, such as red blood cell membranes and endothelial cells, was also demonstrated.[36,38,57,58] To identify unique molecular features of target cancer cells, we have developed a cell-based SELEX (cell-SELEX) for the selection of a panel of target cell-specific aptamers.[40-44] The use of whole cells as targets to select aptamers offers several advantages: first, a panel of aptamers can be selected to target multiple proteins for the cancer study without prior knowledge of up/down regulation of proteins; second, the aptamers are selected against the native state of the proteins in the cellular environment; finally, aptamers selected against whole cells can lead to the discovery of novel biomarkers.

Our cell-SELEX process is illustrated in Figure 1-1. A counter-selection strategy is used to collect DNA sequences that interact only with the target cells but not the control cells. Consequently, aptamer candidates exclusively binding to the target cells are enriched. The membrane protein targets of the selected aptamers represent the

molecular-level differences between the two cell lines used in this study. Not only can molecular signatures of the cancer cells be easily discovered, but probes that can recognize such unique features with very high affinity and specificity are also generated at the same time. More importantly, the use of a panel of probes has a clear advantage over the single-biomarker-based assays in clinical practice, providing much more information for accurate disease diagnosis and prognosis. At the same time, the probes recognize the targets in their native states, creating a true molecular profile of the disease cells. This is important in clinical applications of the molecular probes. In addition, the aptamers selected from cell-SELEX offer valuable tools for isolating and identifying new biomarkers of the diseased cells, if desired. The development of specific probes for molecular signatures on the cancer cell surface will provide new opportunities in ‘‘personalized’’ medicine.

Aptamers versus Antibodies

As they serve similar functions, aptamers are often compared to antibodies. While both can offer selective binding and high affinity, aptamers have some advantages over antibodies:

- Through *in vitro* selection, aptamers can be made for any target molecule. Antibody production requires the induction of an animal’s immune response, which can kill the animal.
- The use of animals in antibody production results in batch-to-batch variation. However, aptamers are chemically synthesized and purified, which prevents batch-to-batch variation.

- Modification is much easier for aptamers than for antibodies. The modification of antibodies can cause the loss of binding affinity to the target molecules, but the modification position in aptamers can be easily changed to positions where binding is not affected.
- Nucleic acid aptamers are short DNA/RNA oligonucleotides, and they are more stable at high temperature and can be regenerated easily after denaturation. So aptamers have much longer shelf life compared to antibodies.
- Aptamers have low toxicity or immunogenicity (if any) compared to antibodies, and these are important features when used for *in vivo* applications, such as imaging.
- Aptamers have better tissue penetration ability than antibodies, which is important for *in vivo* studies, such as targeted drug delivery.

One of the most important disadvantages of nucleic acid aptamers is their susceptibility to enzymatic degration. However, this can be overcome by modification of nuclease resistance bases, such as locked nucleic acids and 2‘-O-methyl nucleotide analogues, to further enhance nuclease resistance when adopted for *in vivo* study.[59-61]

Applications of Aptamers

Aptamers, synthesized nucleic acid or short peptides, specifically recognize a wide range of targets with high binding affinity. Also they are easily modified. These properties allow wide application of aptamers for biosensors, targeted therapy, cancer imaging and detection.

Biosensor and Bio-analytical Applications

A biosensor is a device consisting of two main parts: a biological component, which reacts with a target substance, and a signal-generating component, which detects the resulting products. The specificity and high affinity of aptamers to a wide range of targets, coupled with the ease of design and molecular engineering, make aptamers highly suitable for development of molecular biosensors. Recently, the use of aptamers in different types of biosensor designs has been reviewed extensively. [62-66] There are three general paradigms that have appeared most frequently for the rational design of aptamer biosensors: structure-switching, enzyme-based, and aptazyme-based biosensors.[62] Structure-switching aptamer biosensors are the most common designs in the literature.[67-72] These usually utilize the aptamer's complementary DNA, which can either act as a separate molecule or can link to the aptamer. The easiest design for aptamer biosensors is to simply add the cDNA of an aptamer to act as a competitor to ligand binding. cDNA usually carries a signaling moiety that can be either enhanced or suppressed when in complex with the aptamer. So when the target molecule replaces the cDNA and binds to the aptamer, a signal change can be observed. If proteins or enzymes are involved in the design, it is called enzyme-based aptamer biosensor design.[73-75] These designs require good understanding of both aptamers and enzyme reactions. As many enzymes can be reused and have high catalytic rates, enzyme-based biosensors can give significant signal enhancement. In addition to protein enzymes, oligonucleotides themselves can act as catalytic molecules (DNAzymes and RNAzymes). In these aptazyme-based designs for biosensors, the fundamental strategy calls for the binding of an analyte to the aptazyme complex leading to activation of the enzyme activity.

Biomarker Identification

Disease biomarkers play critical roles in the management of various pathological conditions of diseases, including diagnosis prediction of disease progression, and monitoring the efficacy of treatment by charting the levels of the biomarker. Although there have been many attempts to identify specific disease biomarkers using a variety of technologies, the effective use of disease-specific biomarkers is still not routine. Recently, cell-SELEX-based biomarker identification has been explored.[76,77] As described above, a panel of aptamers for the molecular recognition of diseased cells can be generated without prior knowledge of the target molecule or cell biomarker population. And selected aptamers have high binding affinity to specific targets.[40,42-44,78]. Dr. Dihua Shangguan directed the first use of the cell-SELEX-based method for biomarker identification.[76] The strategy included two steps: aptamer selection and biomarker discovery. First, a group of aptamers was generated for a T-cell acute lymphoblastic leukemia (T-ALL) cell line, CCRF-CEM.[78] Aptamer sgc8, as one of the selected aptamers, showed high specificity and binding affinity to surface targets on most of T-ALL and acute myeloid leukemia (AML) cells, as well as some B-cell acute lymphoblastic leukemia (B-ALL) cells. However, sgc8 did not show a detectable level of binding to either lymphoma cells or normal human bone marrow cells.[40,78] This indicated that the target of sgc8 may act as an important biomarker for leukemia. Then, sgc8 was conjugated with magnetic beads and used to capture and purify the binding targets on the leukemia cell surface. Protein tyrosine kinase 7 (PTK7) was identified as the target protein of sgc8 on the cell surface, and was thereby established as a biomarker.[76] (The function of PTK7 is discussed in Chapter 4.) A cross-linking strategy was proposed by Dr. Probodhika Mallikaratchy, and the target protein of aptamer TD05 was identified

successfully.[77] Thus, cell-SELEX-based biomarker identification shows great promise for efficient discovery of new disease biomarkers.

Therapeutic Applications

In the past few years the therapeutic application of aptamers has been demonstrated in model systems.[37,57,79-83] The potential advantage of aptamers in therapeutic applications is that so far there is no indication that aptamers are immunogenic, whereas antibodies can elicit immune responses even within short periods of treatment.[84] One the other hand, the potential disadvantage of aptamers is their rapid clearance and correspondingly short circulation time *in vivo*. But this problem can be overcome by various modifications, such as conjugation with cholesterol,[85] polyethylene-glycol groups,[85] liposomes,[86] or modification with locked nucleic acids.[59] Aptamer function is not affected in a majority of these modifications.

Effective early diagnosis of cancer is very important in the management of the disease. Currently, a number of techniques have been used to image tumors, such as positron emission tomography (PET), magnetic resonance imaging (MRI), computed tomography (CT), ultrasound methods and optical technologies. However, these techniques lack sensitivity and cause many false positive readings, leading to unnecessary procedures. Use of tumor specific imaging probes would improve sensitivity and decrease misdiagnosis. In this regard, aptamers can serve as effective probes for sensitive cancer detection, while providing rapid blood clearance and tumor penetration. For example, aptamer TTA1A (selected against tenascin-C) was modified with ^{99m}Tc and used as an imaging probe to specifically recognize tenascin-abundant cell surfaces *in vivo*.[87] Another example is *in vivo* fluorescence imaging of tumors using the DNA aptamerTD05,[88] which was selected against Ramos (B-cell lymphoma). The

aptamer was modified with Cy5 dye and injected into mice bearing grafted tumors, followed by whole-body fluorescence imaging. The results demonstrated that the aptamers could effectively recognize tumors with high sensitivity and specificity *in vivo*. Furthermore, approaches have been investigated to conjugate aptamers with nano-materials or quantum dots for cancer cell or tissue detection and imaging.[89-92] In addition, aptamers generated by cell-SELEX have been used to reveal molecular differences of cancer cells in patient samples, demonstrating applicability of aptamers to real clinical settings.[40,44]

Currently, a number of aptamers targeting specific cell membrane receptors have been successfully investigated for the targeted delivery of active drugs both *in vitro* and *in vivo*, including anti-cancer drugs[89,93-97], toxins[98], viruses[99] and siRNAs[100-105]. For example, anti-PSMA (Prostate Specific Membrane Antigen, a cell-surface receptor overexpressed in prostate cancer cells and tumor vascular endothelium[106]) aptamers were conjugated to gelonin, a toxin which can cleave a specific glycosidic bond in rRNA, resulting in disruption of protein synthesis and cell death. The aptamer-toxin conjugates showed IC_{50} (Inhibition Concentration) of 27 nM for PSMA-positive prostate cancer cells, and displayed a 600-fold toxicity increase when compared to non-PSMA expressing cells.[98] In addition, three independent groups have specifically delivered siRNAs to target cells using anti-PSMA RNA aptamers (Figure 1-2).[107] Other aptamers that can be used for targeted delivery include anti-CD4 aptamer, anti-HIV gp120 aptamer, anti-PTK7 aptamer, anti-TfR aptamer.

In addition to conjugating aptamers to therapeutic drugs or siRNAs, some aptamers, like those for VEGF, thrombin, and nucleolin, have therapeutic effects

themselves. The binding of anti-VEGF aptamer to VEGF effectively inhibits VEGF from binding to its cellular receptors and therefore prevents further initiation and growth of unwanted blood vessels in patients with age-related macular degeneration (AMD).[108] Anti-thrombin aptamer, a 15-nucleotide G-quadruplex-forming DNA aptamer, binds thrombin's active site, making it a potent anticoagulant.[109,110] In addition, AS1411, another quadruplex-forming oligonucleotide aptamer that targets nucleolin, inhibits cancer cell proliferation by affecting the activities of certain nucleolin-containing complexes.[111,112] AS1411 is currently in clinical trials as a treatment for various cancers.

Overview of Dissertation Research

The research presented in this dissertation focuses on the development of aptamers for targeted therapy and biomarker discovery. Chapter 2 demonstrates successful utilization of cell-SELEX strategies to develop useful, specific and high-affinity DNA aptamers for liver cancer cells. Chapter 3 demonstrates the concept of targeted drug delivery to cancer cells using aptamers. Chapter 4 describes the discovery of the functional role of PTK7, a biomarker identified as the target protein of aptamer sgc8, in cancer cell apoptois and proliferation. Chapter 5 summarizes the overall significance and further direction of this research.

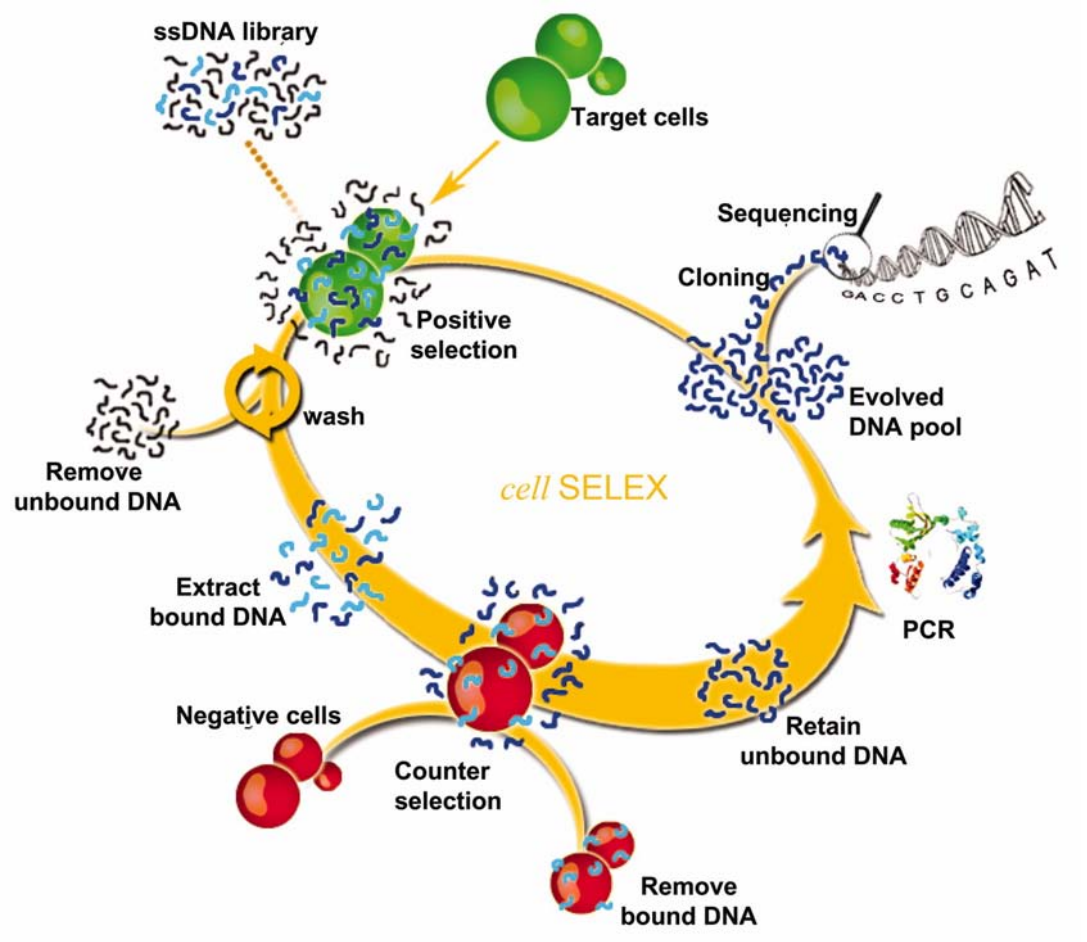

Figure 1-1. Schematic representation of the cell-based aptamer selection. Briefly, the ssDNA pool is incubated with target cells. After washing, the bound DNAs are eluted by heating to 95°C. The eluted DNAs are then incubated with negative cells for counterselection. After centrifugation, the supernatant is collected and the selected DNA is amplified by PCR. The PCR products are separated into ssDNA for the next-round of selection or are cloned and sequenced for aptamer identification in the final round of selection.[78] (copyright permission acquired)

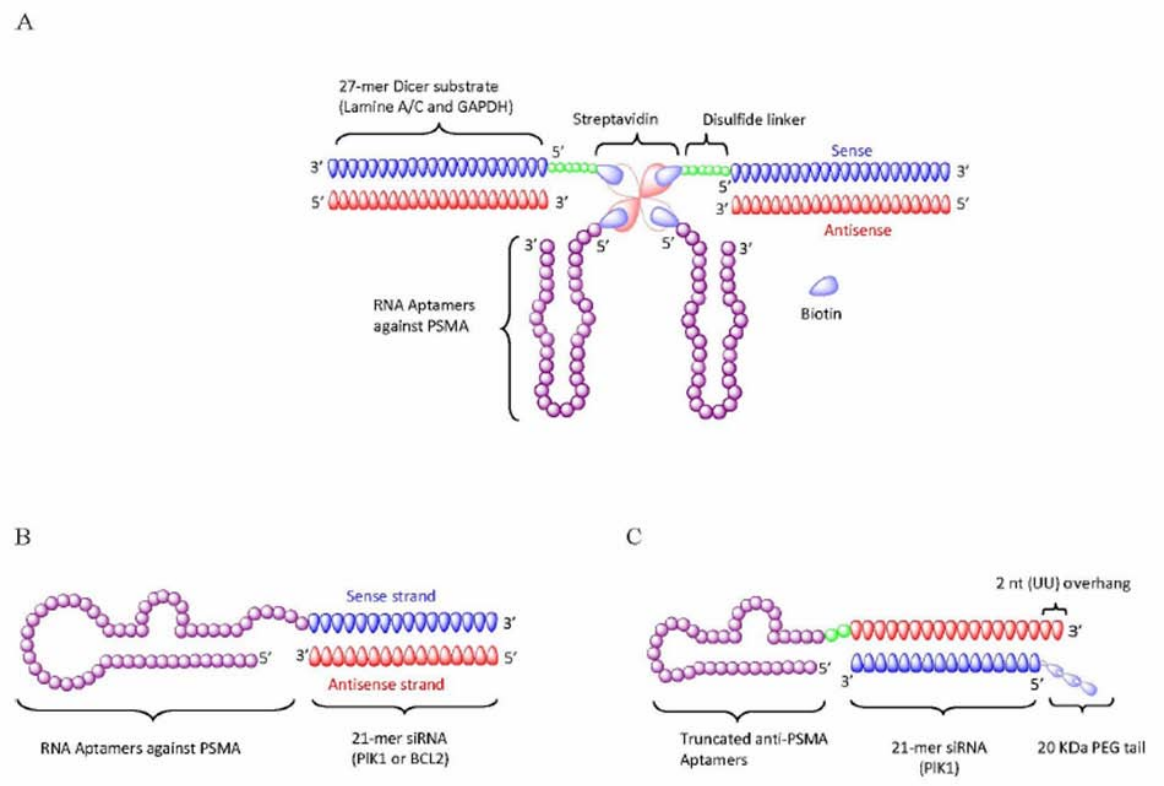

Figure 1-2. Anti-prostate-specific membrane antigen (PSMA) aptamer-mediated small interfering (si)RNA delivery. (a) Schematic of anti-PSMA aptamer-streptavidin-siRNA conjugates. The 27-mer Dicer substrate RNA duplex and RNA aptamers were chemically conjugated with a biotin group. Thus, two biotinylated siRNAs and two aptamers were non-covalently assembled via a streptavidin platform. (b) Schematic of the first generation anti-PSMA aptamer-siRNA chimeras. The 2'-fluoro-modified aptamer and siRNA sense strand were co-transcribed, followed by annealing of the complementary siRNA antisense strand to complete the chimeric molecule. (c) Schematic of the optimized second generation chimeras. Compared with the first generation chimeras, the aptamer portion of the chimera was truncated from 71 to 39 nucleotides, and the sense and antisense strands of the siRNA portion were swapped. A 2 nucleotide (UU)-overhang and a polyethylene glycol tail were added to the 3'-end of the guide strand and the 5'-end of passenger strand, respectively.[107] (copyright permission acquired)

CHAPTER 2
IDENTIFICATION OF LIVER CANCER-SPECIFIC APTMERS USING WHOLE LIVE CELLS

Introduction

Hepatocellular carcinoma (HCC) is one of the most common and highly malignant cancers in the world. Despite its severity and clinical significance, there is a limited understanding of the pathogenesis. Currently, surgical resection or liver transplantation is the only effective treatment for early cancers. However, the majority of these cancers are diagnosed at later stages when there are only a few therapeutic options with poor clinical outcomes.[113] It is known that most of liver cancers arise from patients who have long standing chronic infection with hepatitis B virus (HBV), hepatitis C virus (HCV), or other chronic liver diseases. The carcinogenesis usually takes decades, which provides a window of opportunity to detect the cancer in its earliest stages, a key factor for patient survival. Current screening methodologies for liver cancer in at-risk patients rely on measuring the serum level of alpha-fetoprotein (AFP), a biomarker, as well as ultrasound imaging. AFP's sensitivity and specificity are very limited since many other liver diseases can result in a very high blood level of AFP similar to that observed in HCC. In addition, AFP is not always elevated in the early stages of cancer development, when therapy is most effective. Imaging, on the other hand, only gives limited information with morphology.[114] To achieve the goal of early diagnosis, it is essential to have cancer-specific biomarkers or molecular probes.

Recent studies using genomic and proteomic approaches have generated a wealth of information on biomarkers.[113,114] The diagnostic values of these markers remain to be investigated clinically. One limitation of these approaches is the fact that the biomarker discovery is conducted by analyzing gene expression and protein

products out of contact of cancer cells. Alternative approaches that identification of biomarkers in context of intact cancer cells are clearly needed.

Recently, a new class of molecular probes termed aptamers has attracted much attention as molecular probes for disease diagnosis and therapy. Aptamers are single-stranded DNA (ssDNA), RNA, or modified nucleic acids. They have the ability to bind specifically to targets, which range from small organic molecules to proteins.[115] The basis for target recognition is the tertiary structures formed by the single-stranded oligonucleotides.[116] Aptamers have the following attractive features: low molecular weight, easy and reproducible synthesis, high binding affinity and molecular specificity, easy modification,[61,117-119] fast tissue penetration and low toxicity,[120] tunability in binding affinity and long-term stability.[115] These advantages have made aptamers excellent alternative molecular probes for biomedical studies and clinical applications.

Previously, our lab had developed an effective method to generate cancer cell-specific aptamers by employing the differences at the molecular level between any two cell lines.[78] Using this method known as cell-SELEX, we have systematically generated new probes recognizing molecular signatures of target cells without any prior knowledge of target molecules. Using a human T-cell acute lymphoblastic leukemia cell line, CCRF-CEM, as target and a human Burkitt's lymphoma cell line, Ramos, as control, we have generated a group of aptamers that specifically recognize leukemia cells.[78] The selected aptamers can bind to target cells with an equilibrium dissociation constant (K_d) in the nM to pM range. They can specifically recognize target leukemia cells mixed with normal human bone marrow aspirates, and can also identify cancer cells closely related to the target cell line in real clinical specimens.[40,78] We are also able to identify the

target of one of the binding aptamer by using the aptamer as ligand to capture it in leukemia cell lysate.[76] All of these demonstrated the great potential of the cell-SELEX in cancer research and clinical applications. In previous studies, we mainly used suspension cell lines derived from different sources. However, solid tumor cells are more common in clinics. Thus, developing methods using solid tumors are needed.

In this chapter, we establish a selection method for solid tumor cells (adherent cells). Using a paired non-cancer liver cell line and cancer liver cell line, we have selected and validated several liver cancer-specific aptamers. These aptamers have a great potential to be used for liver cancer studies and even diagnosis. Moreover, the method we developed would be a novel tool for biomarker discovery of other solid tumor cells.

Materials and Methods

Cell Lines and Buffers

The BNL 1ME A.7R.1 (MEAR) mouse liver hepatoma cell line and its normal counterpart BNL CL.2 (BNL) cell line, derived from Balb/cJ mice, were obtained from ATCC (Manassas, VA) and maintained in tissue culture at 37 °C and 5% CO2 in Dulbecco's minimal essential medium (DMEM)/F-12 media (1:1) medium (Cellgro) supplemented with 10% Fetal bovine serum (FBS) (heat inactivated, GIBCO), 5 μg/mL insulin, 5 μg/mL transferin, 5 ng/mL selenium, 100 U/mL penicillin-streptomycin (Cellgro), 40 ng/mL dexamethasone and 50 ng/mL EGF. Huh7 (a human Liver cancer) were cultured in Dulbecco's minimal essential medium (DMEM) (Cellgro) supplemented with 10% Fetal bovine serum (FBS) (heat inactivated, GIBCO), 5 μg/mL insulin, 5 μg/mL transferin, 5 ng/mL selenium, 100 U/mL penicillin-streptomycin (Cellgro). CCRF-CEM

(human acute lymphoblastic leukemia), Ramos, (human Burkitt's lymphoma), Jurkat (human acute T cell leukemia), K562 (chronic myelogenous leukemia) and H23 (non-small cell lung cancer) were purchased from ATCC (Manassas, VA), all the cells were cultured in RPMI 1640 medium (ATCC) supplemented with 10% fetal bovine serum (FBS) (heat inactivated, GIBCO) and 100 IU/mL penicillin-Streptomycin (Cellgro). Cells were washed before and after incubation with wash buffer (4.5 g/L glucose and 5 mM $MgCl_2$ in Dulbecco's phosphate buffered saline with calcium chloride and magnesium chloride (Sigma)). Binding buffer used for selection was prepared by adding yeast tRNA (0.1 mg/mL) (Sigma) and BSA (1 mg/mL) (Fisher) into wash buffer to reduce background binding.

SELEX Library and Primers

HPLC purified library contained a central randomized sequence of 45 nucleotides (nt) flanked by 20-nt primer hybridization sites (ACGCTCGGATGCCACTACAG-45nt-CTCATGGACGTGCTGGTGAC). A fluorescein isothiocyanate (FITC)-labeled 5'-primer (5'-FITC- ACGCTCGGATGCCACTACAG-3') or a tetramethylrhodamine anhydride (TMR)-labeled 5'-primer (5'-TMR-ACGCTCGGATGCCACTACAG-3'); and a biotinylated (Bio) 3'-primer (5'-Bio- GTCACCAGCACGTCCATGAG -3') were used in the PCR reactions for the synthesis of double-labeled, double-stranded DNA molecules. After denaturing in alkaline condition (0.2 M NaOH), the FITC or TMR -conjugated sense ssDNA aptamer is separated from the biotinylated anti-sense ssDNA strand by streptavidin-coated sepharose beads (Amersham Bioscience) and used for next round selection. The selection process was monitored using flow cytometry and confocal imaging.

SELEX Procedures

The procedure of selection was as follows: ssDNA pool (200 pmol) dissolved in 500 μL binding buffer was denatured by heating at 95 °C for 5 min and cooled on ice for 10 min before binding. Then the ssDNA pool was incubated with BNL 1ME A.7R.1 cell monolayer in T25 flask (target cells) on ice for 30 min. After washing, the adhesive cells were scraped off and washed again. The bound DNAs were eluted by heating at 95 °C for 5 min in 500 μL of binding buffer. The eluted DNAs were then incubated with BNL CL.2 cell monolayer in 60 cm^2 dish (control cells) for counter-selection on ice for 1 hour. The supernatant was desalted and then amplified by PCR with FITC- or TMR- and biotin-labeled primers (10-20 cycles of 0.5 min at 94 °C, 0.5 min at 58 °C, and 0.5 min at 72 °C, followed by 5 min at 72 °C; the Taq-polymerase and dNTP's were obtained from Takala). The selected sense ssDNA is separated from the biotinylated anti-sense ssDNA strand by streptavidin-coated sepharose beads (Amersham Bioscience). In the first round of selection, the amount of initial ssDNA pool was 10 nmol, dissolved in 1 mL binding buffer; and the counter selection step was eliminated. In order to acquire aptamers with high affinity and specificity, the wash strength was enhanced gradually by extending wash time (from 1 min to 10 min), increasing the volume of wash buffer (from 1 mL to 5 mL) and the number of washes (from 3 to 5). Additionally, 20% FBS and 50-300 fold molar excess 88 mer random DNA library were added to incubation solution. After 16 rounds of selection, selected ssDNA pool was PCR-amplified using unmodified primers and cloned into Escherichia coli using the TA cloning kit (Invitrogen). Cloned sequences were determined by Genome Sequencing Services Laboratory in University of Florida. The whole procedure of cell-SELEX was shown in Figure 1-1.

Flow Cytometric Analysis

Flow cytometry is a technique for counting and examining particles and cells in the size range of 0.2 µm to 150 µm diameter. It allows simultaneous multi-parametric analysis of the chemical and/or physical characteristics of up to thousands of particles or cells per second by suspending them in a stream of sheath fluid and passing them by an electronic detection apparatus-flow cytometer. Inside a flow cytometer, cells or particles in suspension are drawn into a stream created by a surrounding sheath of isotonic fluid, and then pass individually through a point. At that point, the cells or particles of interest intercept a beam of monochromatic light, usually a laser light, so they scatter light and fluorochromes are excited to a higher energy state. Scattered and emitted light from cells or particles is converted to electrical pulses by optical detectors. Forward SCatter (FSC) gives information on relative size and Side SCatter (SSC) give data on relative internal complexity. Figure 2-1 is a schematic diagram of the fluidic and optical components of a flow cytometer.[121]

Fluorescent dyes and antibodies or aptamers conjugated to fluorescent dyes may bind or intercalate with different cellular components such as DNA, RNA and specific proteins on cell membranes or inside cells. When labeled cells intercept a light source, the fluorescent molecules are excited to a higher energy state. Upon returning to their resting states, the fluorochromes emit light energy at higher wavelengths compared to excitation light source. By using multiple fluorochromes, each with similar excitation wavelengths but different emission wavelengths, different cell properties can be measured simultaneously.

To monitor the enrichment of aptamers in selected DNA pools or to test the binding capacity of selected aptamers, cells monolayers were detached by non-

enzymatic cell dissociation solution (Cellgro) and filtered with 40 μm Cell Strainer (BD Falcon), then washed with washing buffer. FITC-labeled ssDNA pool were incubated with 3 x 10^5 cells respectively in 200 μL of binding buffer containing 20% FBS on ice for 30 min. Cells were washed twice with 0.7 ml of binding buffer (with 0.1% NaN_2), and suspended in 0.3 ml of binding buffer (with 0.1% NaN_2). The fluorescence was determined with a FACScan cytometer (Becton Dickinson Immunocytometry systems, San Jose, CA) by counting 40000 events. The FITC-labeled unselected ssDNA library was used as negative control.

The binding affinity of aptamers was determined by incubating detached BNL 1ME A.7R.1 cells (3×10^5) with varying concentrations of FITC-labeled aptamer in 500 μL volume of binding buffer containing 20% FBS on ice for 30 min in the dark. Cells were then washed twice with 0.7 ml of the binding buffer with 0.1% sodium azide, suspended in 0.4 ml of binding buffer with 0.1% sodium azide and subjected to flow cytometric analysis within 30 min. The FITC-labeled unselected ssDNA library was used as negative control for the nonspecific binding. All the experiments for binding assay were repeated 2-4 times. The mean fluorescence intensity of target cells labeled by aptamers was used to calculate specific binding by subtracting the mean fluorescence intensity of non-specific binding produced by unselected library DNA. The equilibrium dissociation constants (K_d) of the fluorescent ligands were obtained by fitting the fluorescence intensity of binding (Y, Bmax) and the concentration of the ligands (X) to the equation: $Y=BmaxX/(K_d+X)$, using the SigmaPlot software (Jandel Scientific, San Rafael, Calif.).

Confocal Imaging of Cells Stained with Aptamer

For confocal imaging, the selected ssDNA pools (200 nM) or aptamers (25 nM) labeled with TMR or FITC incubated with cell monolayer in 35 mm Glass Bottom Culture Dish (Mat Tek Corp) in binding buffer containing 20% FBS on ice for 30 min. After washing, the dishes with cells in 1 mL binding buffer were placed above a 40x objective on the confocal microscope. The imaging of cells was performed with an Olympus FV500-IX81 confocal microscope (Olympus America Inc., Melville, NY). A 5 mW 543 nm He-Ne laser was the excitation for TMR, and a 5 mW 488 nm Ar+ laser was the excitation for FITC. The objective used for imaging was an Olympus LC Plan F1 40X/0.60 ph2 40x objective.

Mice Tumor Detection by Aptamers

Balb/cJ mice, 6-8 weeks old, were purchased from the Jackson Laboratory (Bar Harber, ME) and housed in the animal facility at the University of Florida with institutional regulatory approval (Institutional Animal Care and Use Committee). Balb/cJ mice were inoculated with either 1 x 10^7 *in vitro* propagated BNL 1ME A.7R.1 or BNL CL.2 cells, subcutaneously injected into each flank. When the tumors exceeded 1 cm in diameter, the tumors and normal livers were taken out. Some tumor and normal liver tissues were formalin fixed and embedded in paraffin. Five micron sections were cut from each paraffin block and stained with hematoxylin and eosin for microscopic examination. Some tumor and normal liver tissues were snap frozen in liquid nitrogen and stored at -80°C. Five micron sections were cut from frozen tissue and fixed by acetone for 15 min at room temperature and incubated with the unselected ssDNA library or aptamers (100 nM) labeled with FITC in binding buffer containing 20% FBS at 4°C for 1 h. After washing, the slides were imaged with a confocal microscope (20x

objective). The rest of tumor and liver tissues were put into a cell culture dish and cut into small pieces. The tissue fragments were resuspended with non-enzymatic cell dissociation solution (Cellgro) and filtered with a 40 μm Cell Strainer (BD Falcon), then washed three times with wash buffer. Then the isolated cells were incubated with FITC-labeled aptamers (50 nM) in 200 μL of binding buffer containing 20% FBS on ice for 30 min. Cells were washed twice with 1 ml of binding buffer (with 0.1% NaN_2), and suspended in 0.3 ml of binding buffer (with 0.1% NaN_2). The fluorescence was determined with a FACScan cytometer by counting 100 000 events. The FITC-labeled unselected ssDNA library (100 nM) was used as negative control.

Results

Liver Cancer Cell-SELEX

In liver cancer cell selection, we expanded the cell-SELEX strategy to solid tumor and adherent cell lines, BNL 1ME A.7R.1 and BNL CL.2. Additionally, the relationship of these two cell lines was very close. BNL CL.2 is a non-tumor, immortalized hepatocyte cell line derived from a Balb/cJ mouse liver. BNL 1ME A.7R.1 is a tumor cell line derived from BNL CL.2 by transformation with methylcholanthrene epoxide.[122,123] BNL CL.2 cells do not form tumors in Balb/cJ mice, while BNL 1ME A.7R.1 cells form tumors in Balb/cJ mice in two to three weeks. Morphologically, the difference between these two cell lines was considered to be minor. However, biologically, the two cell lines are significantly different: only BNL 1MEA7R.1 cells produce tumor when injected into the sygenic Balb/cJ mice. Using BNL 1ME A.7R.1 as target cell line and BNL CL.2 cell line as the negative control for counter-selection, we have generated aptamers for target molecules only present on BNL 1ME A.7R.1 cells surface. The aptamers would be

useful for diagnosis or therapy of this kind of cancer. In addition, this is an excellent model pair for the development of the cell-SELEX protocol for solid tumor samples.

In this selection, a single stranded DNA library that contained 45-mer random DNA sequences flanked by two 20-mer PCR primer sequences is used. After incubation with DNA pool and washing, the adherent cells were scraped off from the bottom of flask. Scraping was used to detach cells because it would not affect the binding of aptamers on cell membrane surfaces. The conventional detaching method by trypsin could not be used because it was demonstrated that trypsin could cleave the proteins on the cell surface to which aptamers bind.[78]

Monitoring the Progression of Aptamer Selection

The progress of the selection process was monitored using confocal imaging and flow cytometry. For cell-based SELEX, a flow cytometry assay is the best way to monitor the selection process because of the excellent reproducibility, a high degree of statistical precision due to the large number of cells measured, the quantitative nature of the analysis and the high speed. We have successfully applied flow cytometry to monitor the enrichment of aptamer selection process and to test the aptamer binding for suspension cells.[42,78] Here we explored the flow cytometry for adherent cell selection. Before incubation of the cells with DNA pool or the aptamer pool, we used non-enzyme cell dissociation solution (Cellgro) including EDTA to detach the adherent cells from the flask. After removing the dissociation solution, cells were resuspended in binding buffer and passed through a 40 μm strainer to remove the cell clusters which would block the flow cytometer. The cells can then be treated as suspension cells for flow cytometry

assay. For confocal imaging, cells were detected while still attached to the bottom of the dishes.

With increased numbers of selection cycles, the DNA probes with better binding affinity to the target cells were enriched in the first 5 rounds. Increases in fluorescence intensity on BNL 1ME A.7R.1 cells (target cells) were observed in flow cytometry analysis. However, there was no significant change in fluorescence intensity on BNL CL.2 cells (control cells) (Figure 2-2 A). These results indicate that the DNA probes specifically recognizing cell surface markers on BNL 1ME A.7R.1 cells were enriched. The specific binding of the selected pools to the target cells was also confirmed by confocal imaging (Figure 2-2 B). After incubation with the TMR dye-labeled aptamer pool, the BNL 1ME A.7R.1 cells showed bright fluorescence on the periphery of the cells, while the BNL CL.2 cells displayed no significant fluorescence. After 16 round of selection, the enriched aptamer pools were cloned and sequenced by the high-throughput genome sequencing method.

Identification of Selected Aptamers for Liver Cancer Cells

About 300 clones were sequenced in our experiments. After alignment, the sequences were found to be distributed into different families based on their sequence similarities, and many repeats were observed in each family. Eleven sequences were chosen from different sequence families for further characterization. These sequences become the candidates as aptamers for liver cancer. To confirm whether they are indeed aptamers for liver cancer, a series of experiments were done to confirm their target binding affinity and specificity.

The Selected Aptamers can Recognize Target Cells with High Specificity

The binding assay of these sequences was performed by flow cytometry (Figure 2-3). Seven aptamers (TLS1, TLS3, TLS4, TLS6, TLS7, TLS9 and TLS11) were found to have high affinity for BNL 1ME A.7R.1 cells with K_d in the nM range (Table 2-1) and did not show obvious binding to BNL CL.2 cells (Figure2-3 B). The K_d values were analogous to those of antibodies. The full length aptamers selected from this library are 85 mer sequences. Generally, not all the nucleotides are necessary for target binding. Thus, three of these aptamers were further optimized based on the predicted secondary structure.[61] The optimized aptamers TLS1c, TLS9a and TLS11a have the same or better binding affinity to their targets compared to the original full-length aptamers (TLS1, TLS9, TLS11) (Table 2-1). However, their length is greatly reduced; for example, the length of optimized aptamer TLS9a is less than half of the original sequence. The shorter sequences greatly increase the yield and decrease the cost of chemical synthesis, and are therefore preferred.

The specific cell recognition by the selected aptamers was further demonstrated by confocal imaging using FITC labeled aptamers. As shown in Figure 2-4, the BNL 1ME A.7R.1 cells presented very bright fluorescence (green) on the periphery of cells after incubation with aptamers, while the BNL CL.2 cells displayed no obvious fluorescence. None of BNL 1ME A.7R.1 and BNL CL.2 cells displayed any significant fluorescence after incubation with unselected DNA library. These results demonstrated that aptamers only recognized targets presenting on the surface of BNL 1ME A.7R.1 cells. It further implied that these aptamers would be potential molecular probes for liver cancer analysis.

The Selected Aptamers are Effective Molecular Probes for Liver Cancer in Mice

We tested whether the newly selected aptamers can recognize tumors grown inside a mouse. Total 5 Balb/cJ mice were injected with 10 million BNL 1ME A.7R.1 subcutaneously. All the mice inoculated with the cells formed tumors in two to three weeks (Figure 2-5). However, the five Balb/cJ mice inoculated with BNL CL.2 cells did not form tumors. The tumor size formed with IMEA cells ranges from 1.0 cm to 1.5 cm. Tumor tissues were removed and processed according to specific molecular analysis procedure developed in our pathology laboratory.

The tumor cell recognition by aptamers was demonstrated by both confocal imaging (Figure 2-6) and flow cytometry assay (Figure 2-7) using FITC labeled aptamers. As shown in Figure 2-6, the frozen tumor section gave bright green fluorescence after incubation with FITC labeled aptamer TLS11a compared with FITC labeled unselected DNA library, and no fluorescence signal was observed from frozen normal liver tissue sections stained with FITC labeled TLS11a or unselected library. The flow cytometry data (Figure 2-7) also demonstrated the specific binding ability of aptamers TLS9a and TLS11a to tumor cells; the cells isolated from tumor showed greatly higher fluorescence intensity after incubation with FITC labeled aptamer TLS9a and TLS11a, respectively compared to FITC labeled unselected DNA library. The isolated normal liver cells did not show obvious fluorescence enhancement after incubation with aptamers compared to unselected DNA library. These results clearly indicated that the selected aptamers were highly specific to the tumor cells and did not bind to the cells in normal liver tissue. They showed promise as specific molecular probes for liver cancer recognition and analysis.

To further test the specificity of these aptamers, FITC-labeled aptamers were incubated with different kinds of cells and then tested by flow cytometer. As shown in Table 2-2, all of the aptamers did not bind to human leukemia cells, lymphoma cells besides the control cells, BNL CL.2. Most of the aptamer except aptamers TLS1 and TLS11 did not bind to human lung cancer cell line H23, or the human liver cancer cell line, Huh7. This indicated that some of the aptamers are specific to the target cells, BNL 1ME A.7R.1 cells, and their targets are only highly expressed on BNL 1ME A.7R.1 cells. These aptamers could be important molecular probes for the recognition of biomarkers for liver cancer diagnosis and studies. Aptamer TLS1 slightly bound to H23 and Huh7. Aptamer TLS11 bound slightly to H23 and strongly to human liver cancer cell line, Huh7. Because aptamer TLS1 and TLS11 did not bind to cells in normal liver tissue and suspended tumor cells, such as leukemia and lymphoma, they would bind to the cell surface targets related to solid tumor. It indicated that their target molecules would provide useful information for explaining the mechanism of oncogenesis.

Discussion

Liver cancer is one of the most common malignancies in the world, and unfortunately there are few clinical options for patients who have this disease, because most patients are diagnosed at late stages. The urgent task for liver cancer research is to develop novel molecular approaches to diagnose this cancer early. Evidence supports that liver cancer undergoes multiple steps during its development [124-126]. During this process, there are genetic changes that affect the cell proliferation and apoptosis. Thus, the prevailing view is that biomarkers can be identified for liver cancer diagnosis. Recent work with cDNA microarray and proteomics indeed provide arrays of protein markers that are potentially applicable for liver cancer diagnosis and therapy [127-

[129]. However, the identification of a true biomarker for liver cancer studies is still a major difficulty.

In our study, we adopted a novel approach to identify biomarkers for liver cancer. Aptamer technology has been used for protein-protein interaction research and for molecular recognition. It is a robust technology to identify unknown targets. We hypothesized that aptamer binding principles can be applied for cancer biomarker identification. The study we did with human leukemia cells provided the proof of concept of aptamer technology. However, the technology was using flow cytometric analysis, which is feasible with suspension tumor cells. It was unknown whether the similar approach could be adopted for solid cancers, which usually attach to the culture surface. The current report provides convincing evidence of cell-SELEX as a tool to solid tumors.

For proof of concept, we decided to use murine cell lines, because of their availability in our laboratories. This pair of positive and negative cells provides significant advantages for our purposes in this study: the generation of aptamers that can be used to distinguish liver cancer cells. The BNL cell lines are a paired cell line derived from the same mouse; these two cell lines have a distinctive biological phenotype; one is a cancer cell line and the other is not. The MEAR cells can form a tumor in Balb/c mice within 3 weeks, which is an excellent model for validating the aptamer markers *in vivo*.

Our results clearly show that specific cancer cell-specific aptamers are identified (i.e., TLS9a and TLS11a in Figure 2-3). We found that the binding affinity is promising for potential diagnostic applications. We tested these aptamers using

immunofluorescence studies. The data suggested that they could specifically react with cancer cells, either in homogenous state or mixed with other cells (Figure 2-4 and Table 2-2).

Since one of the eventual applications of aptamers is in vivo diagnosis, we therefore injected BNL 1ME A.7R.1 cells into Balb/c mice. Using labeled aptamers, we found that these aptamers could only bind to tumor cells, not normal mouse hepatocytes. These results strongly support the potential of these aptamers for future *in vivo* applications.

The cell-SELEX process allows the selection of highly specific aptamers with high binding affinities without prior knowledge of any biomarkers or proteins on the cell surfaces. While it has been established that the understanding of the molecular nature of diseases is vital to medicine from detection to treatment of the disease, exploiting this has been undermined from an incomplete understanding of the biomolecular processes that cause the diseases. It is from these biomolecular processes that would allow detection, diagnosis, and treatment of the disease. The cell-SELEX process allows for aptamers to be selected from diseased cells in their native disease state. Thus, diseases can be detected and treated with aptamers without any knowledge of the molecular processes of the disease. This represents a shift in the paradigm of medical research in which new probes and techniques can be developed regardless of the level of knowledge or understanding of the disease.

Conclusion

In summary, our results demonstrate that cell-SELEX can produce a group of cell-specific aptamers for adherent cells. The selection process is reproducible, simple, and straightforward. Using the modified strategy for adherent cells, we have successfully

generated seven effective aptamers for the liver cancer cell line, BNL 1ME A.7R.1 with K_d's in the nanomolar range. Flow cytometry assays and confocal imaging show that the selected aptamers not only recognize the target liver cancer cells specifically, but also do not bind to its parent liver cells, BNL CL.2. Most of the selected aptamers also do not recognize other cell lines, such as human leukemia cell lines, lymphoma cell line, and lung cancer cell line. The cell-SELEX shows that the newly generated aptamers could be excellent molecular probes for liver cancer analysis and diagnosis. The close relationship between BNL 1ME A.7R.1 cells and BNL CL.2 cells indicated that cell-SELEX can be used to identify minor molecular level differences among cells. It further indicates that the target molecules would be specific biomarkers for this kind of liver cancer, and would provide useful information for explaining the mechanism of oncogenesis. Our study establishes cell-SELEX as a great tool for the generation of effective molecular probes for clinically meaningful analysis.

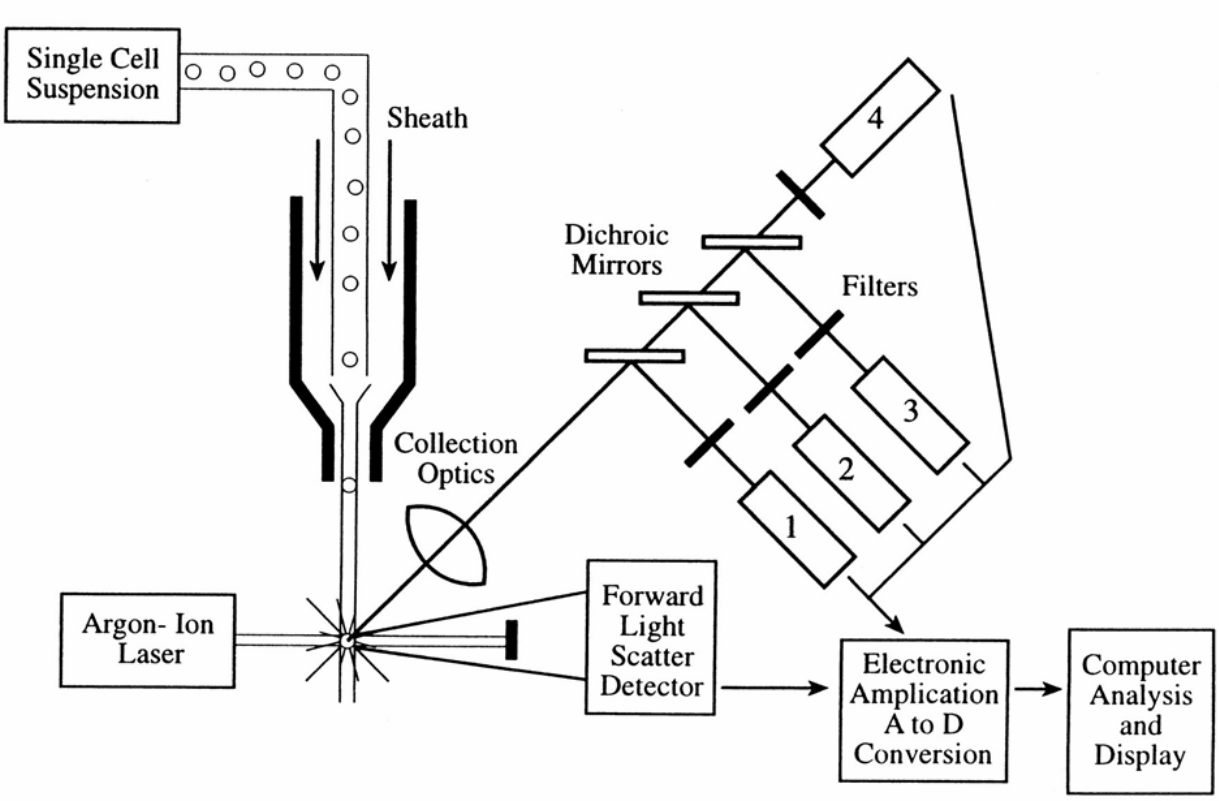

Figure 2-1. Schematic of a flow cytometer. A single cell suspension is hydrodynamically focused with sheath fluid to intersect an argon-ion laser. Signals are collected by a forward angle light scatter detector, a side-scatter detector (1), and multiple fluorescence emission detectors (2–4). The signals are amplified and converted to digital form for analysis and display on a computer screen.[121] (copyright permission acquired)

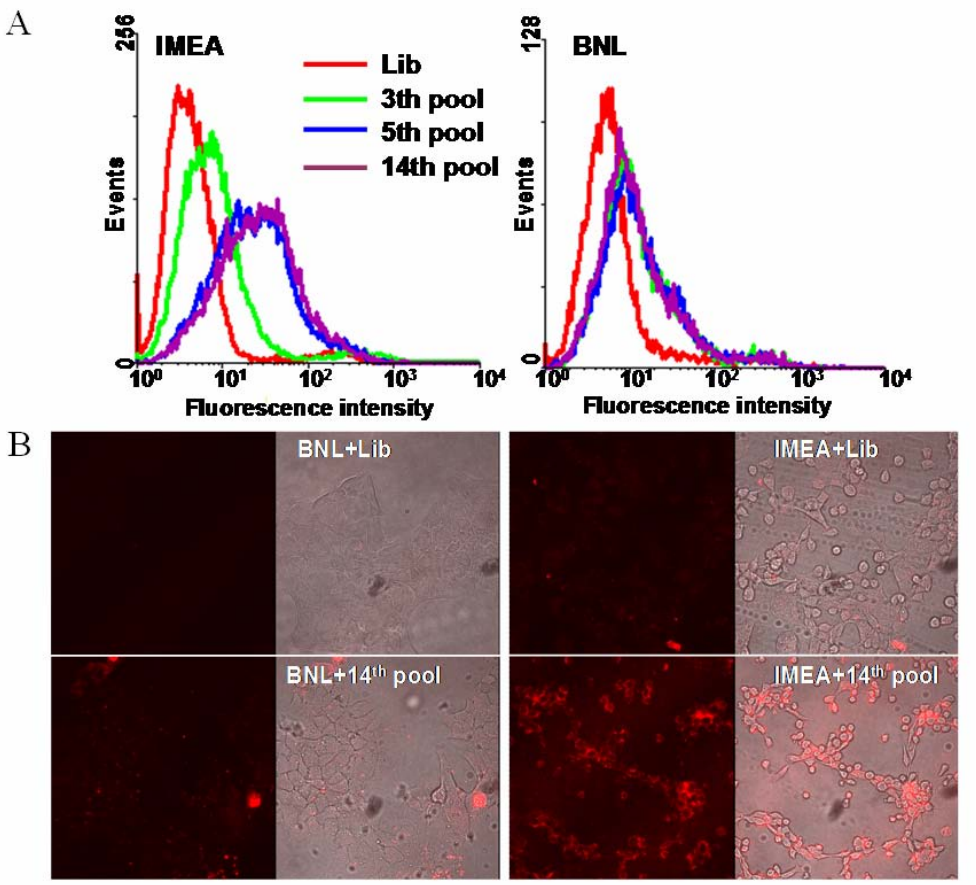

Figure 2-2. Binding assay of selected pool with BNL 1ME A.7R.1 and BNL CL.2 cells. A: Flow cytometry assay to monitor the binding of selected pool with BNL 1ME A.7R.1 cells (target cells) and BNL CL.2 cells (control cells). The red curve represents the background binding of unselected DNA library. For BNL 1ME A.7R.1 cells, there was an increase in binding capacity of the pool as the selection was progressing, while there was little change for the control BNL CL.2 cells. The final concentration of selected pool in binding buffer was 200 nM. B: Confocal imaging of cells stained by the 14^{th} round selected pool labeled with tetramethylrhodamine dye molecules. Top left: image of BNL CL.2 cells after incubated with DNA library; top right: image of BNL 1ME A.7R.1 cells after incubated with DNA library. Bottom left: image of BNL CL.2 cells after incubated with 14^{th} round selected pool; bottom right: image of BNL 1ME A.7R.1 cells after incubated with 14^{th} round selected pool. In each picture, left is the fluorescence image, right is the overlay of fluorescence image and optical image.

Table 2-1. Sequences and K_ds of selected aptamers for liver cancer.

Aptamers	Sequences*	K_ds (nM)
TLS1	ACGCTCGGATGCCACTACAGGAGTGATGGTTGTTATCT GGCCTCAGAGGTTCTCGGGTGTGGTCACTCATGGACGT GCTGGTGAC	10.34±0.96
TLS1c	ACAGGAGTGATGGTTGTTATCTGGCCTCAGAGGTTCTC GGGTGTGGTCACTCCTG	9.79±0.30
TLS3	ACGCTCGGATGCCACTACAGTGGGAATATTAGTACCGT TATTCGGACTCCGCCATGACAATCTGGCTCATGGACGT GCTGGTGAC	10.9±1.8
TLS4	ACGCTCGGATGCCACTACAGACGGTGGTCGTACACGG CCATTTTATTCCCGGAATATTTGTCAACCTCATGGACGT GCTGGTGAC	33.9±2.3
TLS6	ACGCTCGGATGCCACTACAGATACGGCCTGGGTCTTTA TTCGCCCCGAATATTTCTTAACGTCGGCTCATGGACGT GCTGGTGAC	157.0±16.9
TLS7	ACGCTCGGATGCCACTACAGTGCGCCCAAAGTTCCCAT ATTGCTTCCCTGTTGGTGAGTGCCGATCTCATGGACGT GCTGGTGAC	68.1±7.6
TLS9a	AGTCCATTTTATTCCTGAATATTTGTTAACCTCATGGAC	7.38±0.28
TLS11a	ACAGCATCCCCATGTGAACAATCGCATTGTGATTGTTAC GGTTTCCGCCTCATGGACGTGCTG	4.51±0.39

* The fixed regions of original aptamer are denoted in underline

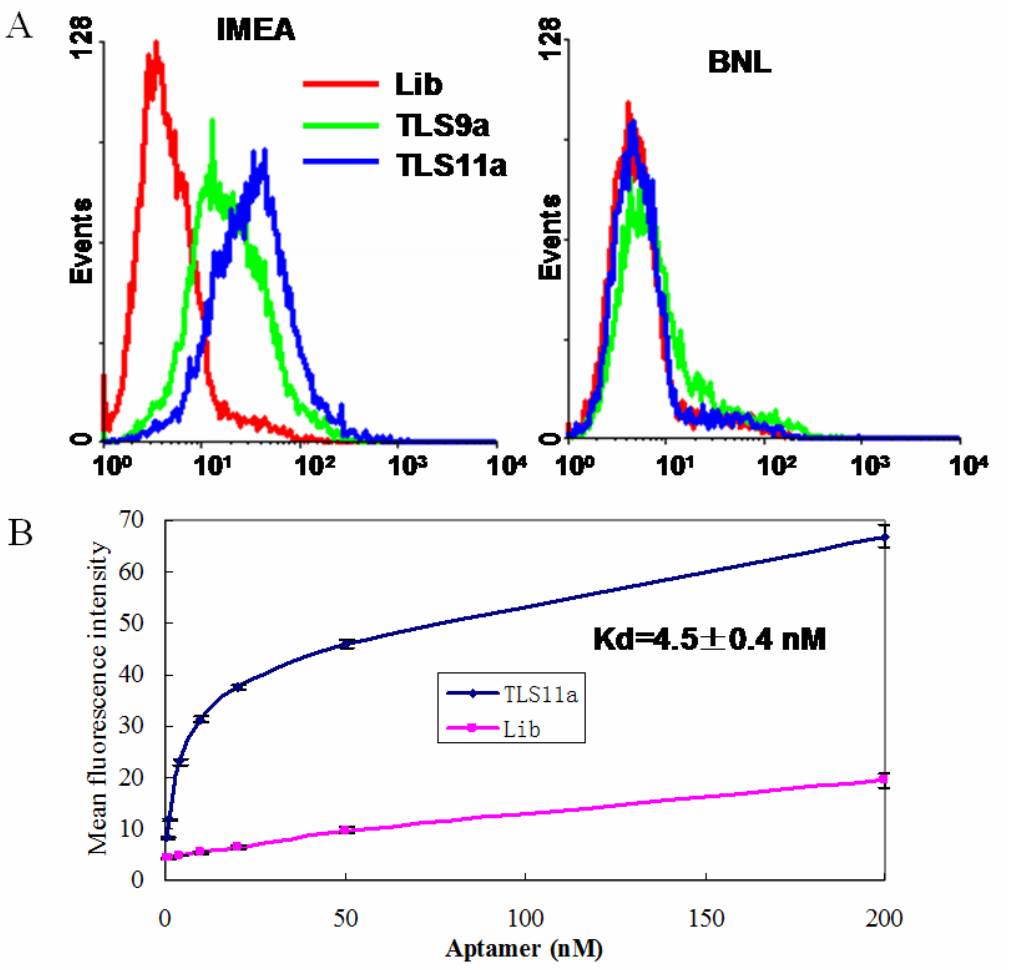

Figure 2-3. A. Flow cytometry assay for the binding of the FITC-labeled sequence aptamer TLS9a and TLS11a with BNL 1ME A.7R.1 cells (target cells) and BNL CL.2 cells (control cells). The red curve represents the background binding of unselected DNA library. The concentration of the aptamers in the binding buffer was 20 nM. B: Using flow cytometry to determine the binding affinity of the FITC-labeled aptamer sequence TLS11a to BNL 1ME A.7R.1 cells. The nonspecific binding was measured by using FITC-labeled unselected library DNA.

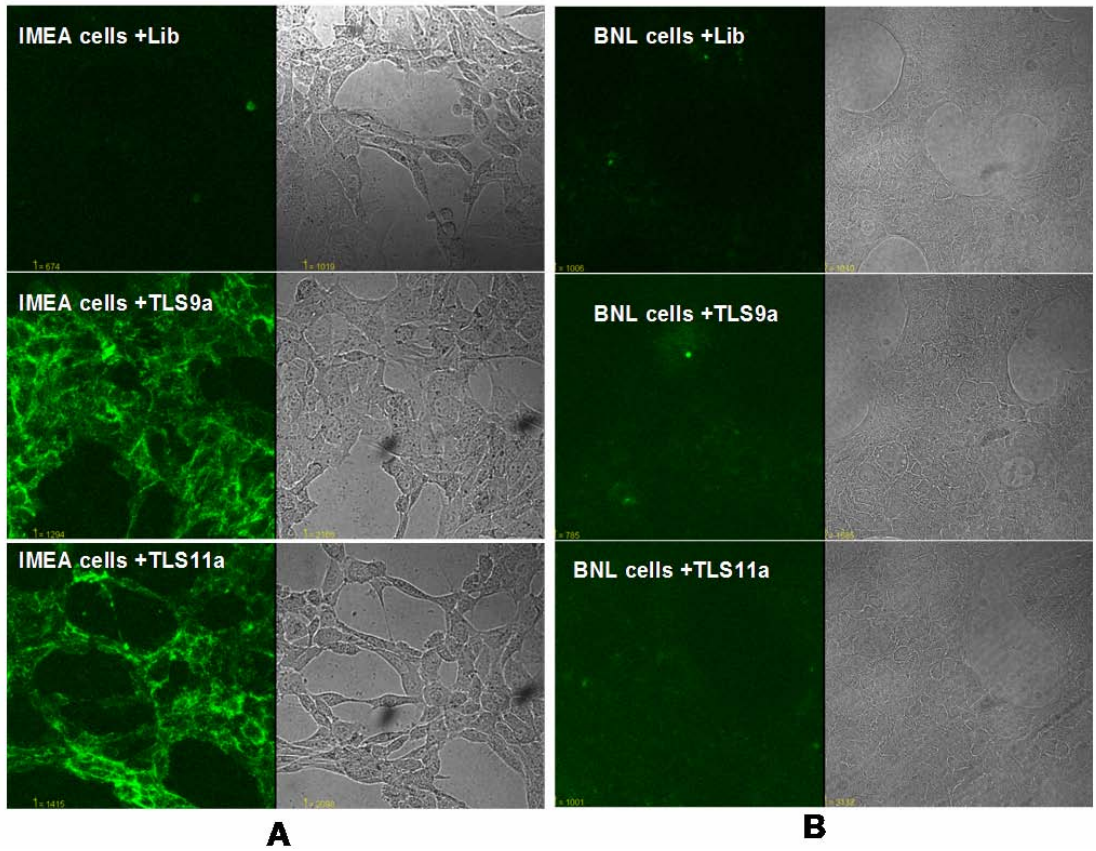

Figure 2-4. Fluorescence confocal images and optical images of (A) BNL 1ME A.7R.1 cells and (B) BNL CL.2 cells stained by unselected library (top), aptamers TLS9a (middle) and TLS11a (bottom) labeled with FITC. In each picture, Left is the fluorescence images and Right is the optical images for BNL 1ME A.7R.1 cells and BNL CL.2 cells respectively.

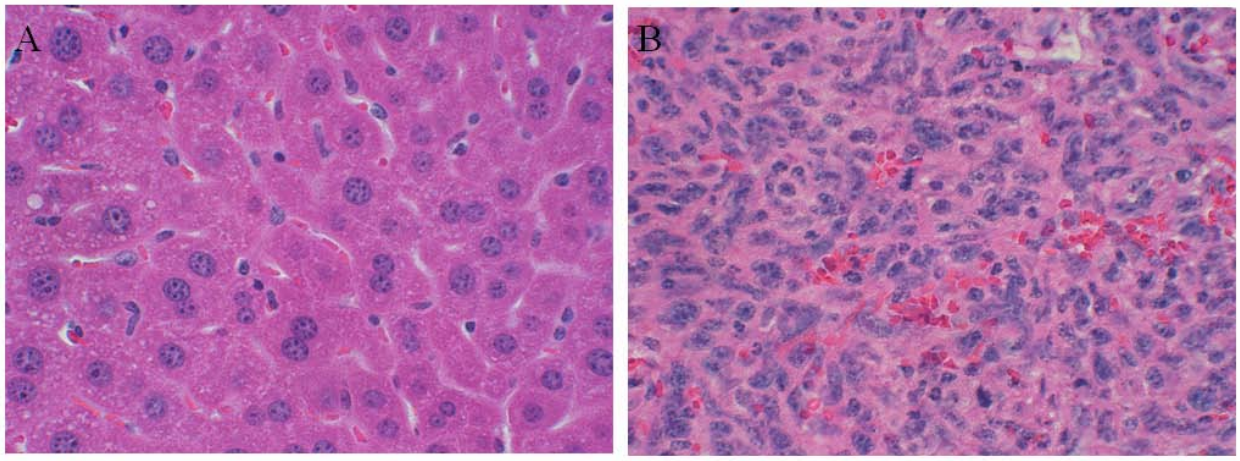

Figure 2-5. Microscopic examination of the formation of tumors. Formalin fixed normal (A) liver tissues and (B) tumor tissue embedded in paraffin were stained with hematoxylin and eosin.

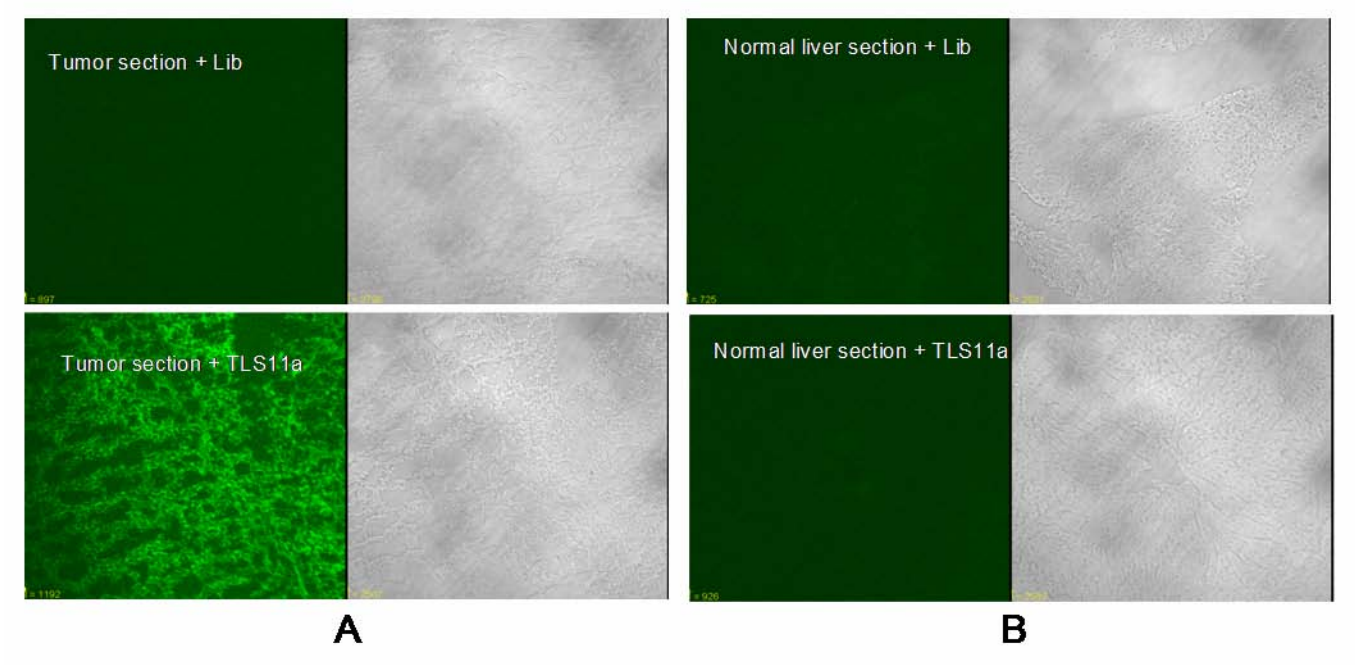

Figure 2-6. Fluorescence confocal images and optical images of (A) frozen tumor sections and (B) frozen normal liver sections stained by unselected library (top), aptamers TLS11a (bottom) labeled with FITC. In each picture, Left is the fluorescence images and Right is the optical images respectively.

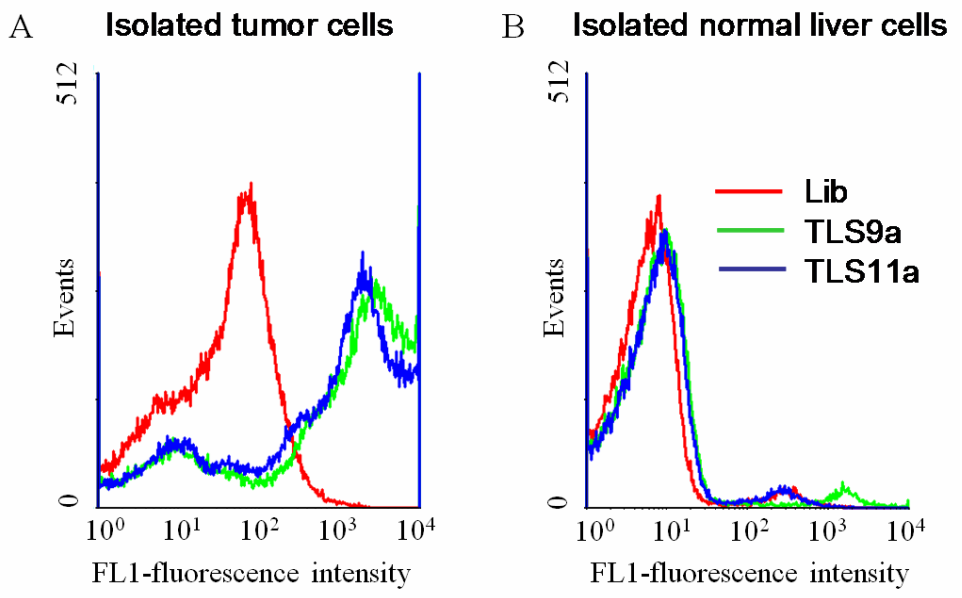

Figure 2-7. Flow cytometry assay for the binding of the FITC-labeled sequence aptamer TLS9a and TLS11a (50 nM) with isolated (A) tumor cells and (B) normal liver cells. The red curve represents the background binding of unselected DNA library (50 nM).

Table 2-2. Aptamers binding to different kinds of cell lines

Cell Line	TLS1	TLS3	TLS4	TLS6	TLS7	TLS9	TLS11
BNL 1ME A.7R.1 (Mouse)	++++	++	++	++	++	+++	++++
BNL CL.2 (Mouse)	-	-	-	-	-	-	-
CCRF-CEM(leukemia, Human)	-	-	-	-	-	-	-
Ramos(Lymphoma, Human)	-	-	-	-	-	-	-
Jurkat(leukemia, Human)	-	-	-	-	-	-	-
K562 (leukemia, Human)	-	-	-	-	-	-	-
H23(lung cancer, Human)	+	-	-	-	-	-	+
Huh7(Liver cancer, Human)	+	-	-	-	-	-	++

A threshold based on fluorescence intensity of FITC in the flow cytometry analysis was chosen so that 95 percent of cells incubated with the FITC-labeled unselected DNA library would have fluorescence intensity below it. After binding with FITC-labeled aptamer, the percentage of the cells with fluorescence above the set threshold was used to evaluate the binding capacity of the aptamer to the cells. -: <10% +: 10-35%, ++: 35-60%, +++: 60-85%, ++++: >85%; the final concentration of aptamer in binding buffer is 100 nM.

CHAPTER 3
TARGETING DELIVERY OF CHEMOTHERAPY AGENTS BY A CANCER SPECIFIC APTAMER

Introduction

The major problems associated with traditional cancer chemotherapy are caused by side effects when the drugs non specifically target normal cells, often killing them. Nontargeted chemotherapy agents can and often do cause life-threatening toxicity effects for patients undergoing chemotherapy treatment. Patients are given the highest dose of these nontargeted drugs which can be tolerated. To overcome this problem and achieve specific drug delivery, our group and other investigators have used antibodies[130,131] or aptamers[89,93,95,98,132,133] to design ligand-linked drug conjugates for targeted-delivery applications.

Aptamers are single-stranded oligonucleotides which can specifically bind to small molecules,[134] peptides and proteins.[135] Aptamers not only provide the advantages of antibodies, such as high specificity and affinity, but they also have low immunogenicity, and are stable and easy to synthesize and modify. Recently, a process called cell-SELEX (systematic evolution of ligands by exponential enrichment) has been developed to generate aptamers for specific recognition of target cancer cells, including T-cell acute lymphoblastic leukemia (T-cell ALL), small-cell lung cancers, liver cancers and virus-infected cells. [41-43,49,57,58,78] These aptamers are highly specific for different types of tumor cells and have excellent binding affinities. Because aptamers provide specificity at the molecular level, it is believed that aptamer-drug conjugates may enhance the efficiency of drug delivery and decrease systemic toxicity.

Hepatocellular carcinoma (HCC) is recognized as one of the most common and deadly cancers in the world. Currently, treatments for early liver cancer have relied on

liver transplantation and surgical resection. Traditional chemotherapy has not been efficient on liver cancer patients and the traditional chemotherapeutic agents are not specific for liver tumor cells, leading to toxic side effects. In Chapter 2, we reported the development of a series of specific aptamers based on a mouse model.[41] One of these aptamers can also specifically recognize human liver cancer cells. This chapter details the use of this aptamer for the targeted delivery of Doxorubicin (Dox) to liver cancer cells.

Doxorubicin (Dox), a topoisomerase inhibitor, is a widely used drug for the treatment of liver cancer, but its efficacy is impeded by toxic side effects. This problem can be overcome by conjugating Dox into an aptamer probe. Dox is known to intercalate into the DNA strand due to the presence of flat aromatic rings in this molecule. Recent research has shown that Doxorubicin can intercalate into aptamer A10 to provide specific killing efficiency to prostate cancer cells.[93,97]

Aptamer TLS11a was previously selected by cell-SELEX against the BNL 1ME A.7R.1 (MEAR) mouse hepatoma cell line[41] and described in chapter 2 It was chosen for this application because it showed great binding affinity for LH86 established from a patient with liver cancer.[136] In order to achieve greater intercalation efficiency, a long GC tail was added to TLS11a to form a modified aptamer, TLS11a-GC. Through the interaction, the ratio between Doxorubicin and TLS11a-GC was 25:1, so the delivery efficiency of Doxorubicin was much higher compared to the original TLS11a. Also, *in vitro* and *in vivo* experiments showed TLS11a-GC-Dox conjugates have much better specific killing efficiency for target cancer cells compared to free Dox and control aptamer-Dox conjugates.

Materials and Methodology

Cell Culture and Reagents

The liver cancer cell line, LH86, was derived from resected well-differentiated hepatocellular carcinoma tissue with adequate patient consent. Tumor tissue was first rinsed with phosphate-buffered saline (PBS) and minced into small pieces. The tissue fragments were then digested with liver digestion medium (Invitrogen, Carlsbad, CA). Single tumor cells were cultured in Dulbecco's modified Eagle medium (DMEM) with 10 ng/mL human epithelial growth factor (EGF). One clone survived in a long-term culture, this clone became the LH86 cell line.[136] LH86 cells were cultured in DMEM supplemented with 10% fetal bovine serum (FBS) (heat inactivated) and 100 IU/mL penicillin-streptomycin at 37ºC in a humid atmosphere with 5% CO_2.

Doxorubicin hydrochloride (Dox) was purchased from Fisher Scientific (Houston, TX, USA). All reagents for DNA synthesis were purchased from Glen Research. Unless otherwise noted, reactants, buffers and solvents were obtained commercially from Fisher Scientific.

Conjugation of Aptamer-Dox

The sequences of aptamer TLS11a, a control sequence TD05, modified aptamer TLS11A-GC and modified control sequence TD05-GC are shown in table 3-1. All DNA aptamers were synthesized on an ABI3400 DNA/RNA synthesizer (Applied Biosystems, Foster City, CA, USA). The completed sequences were then deprotected in AMA (ammonium hydroxide/40% aqueous methylamine 1:1) at 65ºC for 30 min and further purified by reversed-phase HPLC (ProStar, Varian, Walnut Creek, CA, USA) on a C-18 column. To make aptamer-Dox conjugates, TLS11a-GC or TD05-GC was mixed with

Doxorubicin in binding buffer (PBS containing 5 mM $MgCl_2$, 4.5 mg/mL glucose, 0.1 mg/mL yeast tRNA, 1 mg/mL BSA) or DMEM media at 1:25 aptamer:Dox ratio.

Determination of Aptamer Affinity

The binding affinity of aptamer TLS11a was determined using flow cytometry. The LH86 cells were detached from dishes using nonenzymatic cell dissociation solution (Cellgro) and then washed with washing buffer (PBS containing 5 mM $MgCl_2$, 4.5 mg/mL glucose). The binding affinity of TLS11a was determined by incubating LH86 cells (10^5 cells) on ice for 30 min with a series of concentrations of biotin-labeled TLS11a in binding buffer (100 mL). Cells were then washed twice with washing buffer (1.0 mL) and suspended in fluorescein-labeled streptavidin (0.1 mL) for further incubation (15 min on ice). Before flow cytometric analysis, cells were washed with washing buffer twice and suspended in washing buffer (0.2 mL). The mean fluorescence intensity of cells was used to calculate the equilibrium dissociation constant (K_d) of TLS11a and LH86 cell interaction by fitting a plot of fluorescence intensity (F) on the concentration of the biotin-labeled TLS11a (L) to the following equation:

$$F = Bmax[L]/(Kd + [L])$$

Where F, Bmax, [L] and K_d represent fluorescence intensity, the maximum fluorescence intensity, the dissociation constant and the concentration of biotin-labeled TLS11a, respectively. The binding assay experiments were repeated at least three times.

To monitor the binding affinity of TLS11-GC, a competition experiment was carried out. Briefly, 200 nM TLS11a-GC was incubated with LH86 cells for 20 min on ice, and then 1 μM biotin-labeled TLS11a was added for 15 min further incubation. Cells were then washed twice with washing buffer (1.0 mL) and suspended in fluorescein-labeled streptavidin (0.1 mL) for further incubation (15 min on ice). Before flow cytometric

analysis, cells were washed with washing buffer twice and suspended in washing buffer (0.2 mL).

Confocal Microscopy of Cultured Cells

The binding of TLS11a with LH86 cells was then assessed by confocal microscopy. Here, LH86 cells were seeded in a 35-mm Petri dish, 10 mm microwell (MatTek Corporation) and cultured overnight. The cells showing more than 60% confluence were carefully washed and then incubated with the biotin labeled TLS11a or control TD05 at a final concentration of 200 nM. After incubation at 4ºC for 30 min, cells were carefully washed before further incubation with a 1:200 dilution (optimized) of streptavidin conjugated Alexafluor 633 (Invitrogen) for 15 min. Excess probes were removed by washing off and the signal was detected by confocal microscopy (FV500-IX81 confocal microscope, Olympus America Inc., Melville, NY), using a 40x oil immersion objective (NA=1.40, Olympus, Melville, NY). A 633 nm laser line was used for excitation and the emitted light was passed through a LP650 filter prior to detection.

For the internalization study, a co-localization experiment was carried out. As described above, LH86 cells were first incubated with biotin labeled TLS11a or TD05 and then future incubated with a 1:400 dilution (optimized) of streptavidin conjugated PE-Cy5.5 (Invitrogen). After washing, DMEM media with 1:1000 dilution of LysoSensor™ Green DND-189 (Invitrogen) was added to the dishes. After incubation at 37ºC for 2 h, cells were washed twice with washing buffer, and the fluorescence signal was detected by confocal microscopy. A 488 nm laser line was used for excitation and the emitted light was passed through a LP515 filter prior to detection.

Protease Assay

Extracellular membrane proteins are common targets of cell-SELEX as demonstrated by many cell-SELEX schemes. In this work, protease assays was performed to determine the type of surface molecules that the aptamers bind. LH86 cells were dissociated with non-enzymatic dissociation solution. The cells were washed twice with washing buffer and incubated with trypsin (Cellgro) solution (0.05% trypsin/0.53 mM EDTA in HBSS) for 10 min at 37ºC. After incubation, ice cold washing buffer containing 20% FBS was added to halt the protease activity. Cells were quickly centrifuged at 1000 rpm for 5 min and washed twice with washing buffer. The cell pellets were incubated with aptamers in a binding buffer, and then the signal was detected by flow cytometry.

Monitoring of Complex Formation by Fluorescence

Physical conjugates between aptamer (TLS11a or TD05) and Doxorubicin were prepared at a 1:28 molar ratio of aptamer to Doxorubicin (10 μM) in binding buffer, and fluorescence was monitored at 500-720 nm (1.5 mm slit) on a Fluorolog-Tau-3 Spectrofluorometer (Jobin Yvon) with excitation at 480 nm.

Assessment of Cellular Uptake of Dox by Confocal Microscopy

The cellular uptake of Dox was assessed by confocal microscopy. LH86 cells were seeded in a 35 mm Petri dish, 10 mm microwell (MatTek Corporation) and cultured overnight. The cells showing more than 60% confluence were carefully washed and then incubated with Dox or aptamer-Dox conjugates in DMEM media (without FBS) at 37ºC for 1 h. The concentration of Dox in all samples was kept constant at 7.5 μM. After washing once using media, fresh media was added to the dishes for further incubation at 37 ºC.for 3 h; then, the dishes with cells were placed above the 40× objective of an

Olympus FV500-IX81 confocal microscope (Olympus America Inc., Melville, NY). A 5-mW, 488-nm Ar+ laser was the used for excitation of Dox. The objective used for imaging was an Olympus LC Plan F1 40X/0.60 PH2 40× objective.

MTS Cell Viability Assay

Chemosensitivity of LH86 to Dox or aptamer-Dox conjugates was determined using the CellTiter 96 cell proliferation assay (Promega, Madison, WI, USA). Briefly, a 100 µL aliquot of LH86 cells (5×10^4 cells/mL) were seeded in 96 well plates (n=3) and allowed to grow overnight. They were then treated for 1 h with 100 µL of one of the following: 1) control aptamer TD05-GC; 2) aptamer TLS11a-GC; 3) Dox; 4) TD05-GC-Dox physical conjugate (25:1 Doxorubicin to TD05-GC mole ratio); or 5) TLS11a-GC-Dox physical conjugate (25:1 Doxorubicin to TLS11a mole ratio). The cells were washed, and further incubated in fresh media for a total of 48 hrs. For cytotoxicity measurements, media was removed from each well. Then CellTiter reagent (20 µL) and media (100 µL) were added to each well and incubated for 3 h. Using a plate reader (Tecan Safire microplate reader, AG, Switzerland), the absorption was recorded at 490 nm. The percentage of cell viability was determined by comparing Dox and aptamer-Dox conjugate-treated cells with the untreated control.

Hoechst 33258 Staining for Apoptotic Cells

Cell apoptosis was determined by nucleus morphology change. LH86 cells in exponential growth were placed in a 48-well plate at a final concentration of 1.5×10^4 cells per well. After 12 h, cells were treated with different concentrations of TD05-GC-Dox physical conjugate (25:1 Doxorubicin to TD05-GC mole ratio) or TLS11a-GC-Dox physical conjugate (25:1 Doxorubicin to TLS11a mole ratio) for 1 hour, washed, and further incubated in fresh media for a total of 48 hrs. Subsequently, cells were washed

twice with PBS, and stained with Hoechst 33258 staining solution according to the manufacturer's instructions. After incubation at 37 ºC for 10 min, cell nucleus fragmentation/condensation was detected by fluorescence microscopy. Apoptotic cell death was assessed by calculating the number of apoptotic cells with condensed nuclei in six to eight randomly selected areas. The results presented below represent three independent experiments.

Western Blotting Analysis

Cells were harvested and washed twice with phosphate saline buffer. The cell pellets were resuspended in lysis buffer, containing Nonidet P-40 (10 mM (4-(2-hydroxyethyl)-1-piperazineethanesulfonic acid (HEPES), pH 7.4, 2 mM ethylene glycol tetraacetic acid (EGTA), 0.5% Nonidet P-40, 1mM NaF, 1 mM $NaVO_4$, 1 mM phenylmethylsulfonyl fluoride, 1 mM dithiothreitol, 50 µg/ml trypsin inhibitor, 10 µg/ml aprotinin, and leupeptin) and incubated on ice for 30 min. After centrifugation at 12000×g at 4ºC for 15 min, the supernatant was transferred to a fresh tube, and the protein concentration was determined. Equivalent samples (20 µg of protein) were subjected to SDS-PAGE on 12% gels. The proteins were transferred onto nitrocellulose membranes and probed with the indicated primary antibodies (cleaved caspase-3 antibody, CellSignaling), followed by the appropriate secondary antibodies conjugated with horseradish peroxidase (HRP, Santa Cruz Biotechnology, Inc.). Immunoreactive bands were detected using enhanced chemiluminescence (ECL, Pierce). The molecular sizes of the proteins detected were determined by comparison with prestained protein markers (Bio-Rad). All band densities were calculated using ImageJ software.

In vivo Experiments of Dox-TS11a Conjugates

The NOD. Cg-Prkdc (scid) IL2 mice were purchased from the Jackson Laboratory (Bar Harber, ME) and housed in the animal facility at the University of Florida with institutional regulatory approval (Institutional Animal Care and Use Committee). Forty NOD. Cg-Prkdc (scid) IL2 mice were subcutaneously injected with 7×10^6 *in vitro* propagated LH86 cells. When the tumors could be easily seen and measured, mice were divided into four groups: (1) group 1, untreated; (2) group 2, treated with free Dox; (3) group 3, treated with TLS11a-GC-DOX complex; (4) group 4, treated with TD05-GC-DOX complex. The Dox dosage was kept the same in groups 2, 3 and 4 at 2 mg/kg. All treatments continued for 12 days. Drugs were injected through tail vein on days 1, 2, 3, 4, 5, 9, 10, 11, and all samples were collected on day 12. The tumor size for each mouse was measured every other day. Heart, lung, liver, kidney and tumor of each mouse were collected on day 12 and fixed using 10% formalin for 24 h at room temperature, and then hematoxylin and eosin staining (H&E staining) was carried out.

Results

Binding Affinity of Aptamer TLS11a

Aptamer TLS11a (Figure 3-1 A) was generated against the BNL 1ME A.7R.1 (MEAR) mouse hepatoma cell line[41] and showed strong binding affinity (K_d= 4.51±0.39 nM). [41] The LH86 cell line was established from a patient with liver cancer.[136] When TLS11a was used to test LH86 cells, obvious binding ability was observed (Figure 3-1 B). Also, human normal liver cells, Hu1082, were tested using TLS11a and no significant binding was observed (Figure 3-1 C). In Figure 1 the green histogram shows the background binding (control aptamer, TD05), and the red fluorescence intensities show the binding of TLS11a with target and control cells. Compared to the control

aptamer, there is a significant difference between the binding strength of TLS11a to LH86 and to Hu1082 cells. There is no probe that has been previously reported to differentiate between liver cancer cells and human normal liver cells. Also, the K_d of TLS11a to LH86 was 7.16 ± 0.59 nM (Figure 3-2) compared to 4.51 ± 0.39 nM to BNL 1ME A.7R.1.[41]

Immunohistological imaging and fluorescence microscopy have been widely used in the study of solid tumors, so we also assessed whether TLS11a can be used for tumor imaging with LH86, the positive cell line. In this study, we performed binding assays in culture dishes with cell confluency of over 60%. After washing, the signal was detected with streptavidin-alexafluor 633. Figure 3-1D shows the confocal images of LH86 detected with TLS11a and a control sequence, TD05. There was significant signal strength of TLS11a compared with negative control, and the signal pattern shows that the aptamers bind to the surface of the cells.

Preliminary Determination of Aptamer Target Molecule

It is usually assumed that aptamers selected against cell lines bind to cell membrane proteins. This has been demonstrated in most of the SELEX protocols involving tumor cell lines.[76,77] In order to investigate the target molecule of TLS11a, we performed a protease assay, in which LH86 cells were treated with trypsin for 10 min at 37ºC. After the incubation period, the protease activity was stopped with the addition of ice cold PBS containing 20% FBS. The cells were quickly washed twice by centrifugation and then incubated with the aptamers. As shown in Figure 3-3, TLS11a lost recognition for trypsin treated cells. The fluorescence signals reduced to the background indicating that the treatment of the cells with the proteases caused

digestion of the target protein, showing that the target molecule of TLS11a is a membrane protein.

An internalization assay was then performed to see if TLS11a can be internalized when it binds to the target. LH86 cells were first incubated with biotin labeled TLS11a or TD05 and then further incubated with streptavidin conjugated PE-Cy5.5. The binding event was observed by confocal microscopy (Figure 3-1 D). TLS11a bound the outer margins of the cell indicating that it is binding to molecules on the cell surface. Then the buffer was removed and culture medium with of LysoSensor™ Green DND-189 (λ_{exc}=443 nm, λ_{em}=505 nm) was added to the cells and incubated at 37ºC for two hours. The LysoSensor dyes, which act as fluorescent pH indicators, are acidotropic probes that appear to accumulate in acidic organelles (lysosome) as the result of protonation. This protonation also relieves the fluorescence quenching of the dye by its weak base side chain, resulting in an increase in fluorescence intensity. So LysoSensor served as an indicator of the lysosome location in the cells. As shown in Figure 3-4, there was clear internalization of the aptamer. The TLS11a signal was inside the cells rather than on the outer margins and it co-located with LysoSensor. The control sequence did not show any signal in both 4ºC and 37ºC assays. The results suggest that TLS11a may be binding to a protein that can be internalized.

Conjugation of Aptamer-Dox Complex

Dox is known to intercalate within the DNA strand due to the presence of flat aromatic rings, and it preferentially binds to double-stranded 5'-GC-3' or 5'-CG-3' sequences.[137,138]. The secondary structure of TLS11a, predicted by NUPACK software (http://www.nupack.org/), is shown in Figure 3-1. According to the structure, there are two 5'-GC-3' or 5'-CG-3' sequences in the TLS11a sequence, so that one TLS11a

sequence could intercalate a maximum of two Doxorubicin molecules. In order to intercalate more Doxorubicin molecules, a long GC tail was added to the 5' end of TLS11a to generate a modified aptamer, TLS11a-GC (Figure 3-5). Because of the long GC tail, TLS11a-GC forms a dimer structure. Nupack calculation indicated that one TLS11a-GC dimer can intercalate up to 56 Doxorubicin molecules to produce a TLS11a-GC to Doxorubicin ratio of 1:28. A control aptamer sequence, TD05, was also modified with a long GC tail to make the same aptamer to Dxorubicin ratio (Figure 3-5). Even though the TLS1a-GC and TD05-GC dimers can intercalate up to 28 Dox per aptamer, in these experiments the ratio between aptamer and Doxorubicin was kept at 1:25.

It is well known that Dox has fluorescence properties, but the intercalation of Dox into DNA aptamer quenches the fluorescence of Dox because of the formation of charge-transfer complexes between the DNA bases and the anthracycline ring.[139-141] To examine whether such interaction occurs with modified TLS11a-GC and TD05-GC aptamers, fluorescence was acquired for Dox in the absence and in the presence of one of the aptamers (Figure 3-6). The solution of free Dox had the highest fluorescence signal compared to the black group (binding buffer). When modified aptamer (TLS11a-GC or TD05-GC) was added to Dox solution at 1:28 ratio and mixed well, the fluorescence dramatically decreased almost to the background level, indicating that the intercalation of Dox into DNA aptamer is feasible and rapid. Even after the aptamer-Dox complex solution was kept at room temperature for 3 h, the fluorescence stayed the same, indicating that the aptamer-Dox complex is very stable.

Characterization of Aptamer-Dox Complexes

The binding affinity of TLS11a-GC was determined by a competition assay. After incubating with unlabeled TLS11a-GC, the binding sites on LH86 cells were completely occupied. Then all cells were further incubated with dye-labeled TLS11a. Because all binding sites on the cell membrane were occupied by unlabeled TLS11a-GC, dye-labeled TLS11a could not bind to LH86 cells, and after washing, no fluorescence signal was detected (Figure 3-7 A). At the same time, a competition experiment between TD05-GC and dye labeled TLS11a was carried out. Because TD05-GC did not bind to LH86, the binding sites were available for interaction with dye-labeled TLS11a, resulting in a high fluorescence signal (Figure 3-7 B). The flow cytometry data clearly showed that, after modification with the long GC tail, TLS11a-GC could still bind to LH86 cells, while TD05-GC could not bind to LH86.

Dox internalization and release was investigated using confocal microscopy. After 1 h incubation with Dox or aptamer-Dox conjugates, cells were further incubated for 3 h at 37ºC before imaging. Figure 3-8 showed that cells treated with free Dox had the most Dox in their nuclei, while the nuclei for cells treated with TLS11a-GC-Dox conjugates also contained Dox. However, the nuclei of cells treated with TD05-GC-Dox conjugates contained almost no Dox. This experiment confirmed that TLS11a-GC-Dox conjugates had specific binding affinity to LH86 cells compared to TD05-GC-Dox conjugates. Furthermore, Dox could be released from TLS11a-GC-Dox conjugates after internalization and could enter the nucleus.

Cell Toxicity of Aptamer-Dox Conjugates

The cell viability of LH86 treated with either TLS11a-GC-Dox, TD05-GC-Dox, Doxorubicin, TLS11a-GC, or TD05-GC was tested and compared to that of untreated

cells (Figure 3-9 A). The Dox concentration in TLS11a-GC-Dox, TD05-GC-Dox, and free Dox was kept at 7.5 μM, and the ratio of Doxorubicin to aptamer was 25:1. The aptamer concentration in the TLS11a-GC, TD05-GC, TLS11a-GC-Dox, and TD05-GC-Dox groups was kept at 300 nM. Cell viability was tested by MTS assay, which is a colorimetric method for measuring the activity of enzymes that reduce MTS (3-(4,5-dimethylthiazol-2-yl)-5-(3-carboxymethoxyphenyl)-2-(4-sulfophenyl)-2H-tetrazolium, a yellow color), in the presence of phenazine methosulfate (PMS), to produce a formazan product (a purple color) that has an absorbance maximum at 490-500 nm.[142] The main application of MTS is to assess the cell viability and proliferation. From the data shown in Figure 3-9, TLS11a-GC and TD05-GC had no significant effect on cell viability. And it is obvious that treatment with TLS11a-GC-Dox conjugates decreased cell viability. The efficiency of cell toxicity was Dox > TLS11a-GC-Dox > TD05-GC-Dox. Even though the cell toxicity of TLS11a-GC-Dox was less than that of free Dox, the toxicity effect of TD05-GC-Dox was much poorer. Further experiments using Hu1229 human normal liver cells (Figure 3-9 B) showed that free Dox had significant toxicity, while TLS11a-GC-Dox and TD05-GC-Dox had similar and very limited toxicity. These data demonstrate the specific toxicity of TLS11a-GC-Dox to target cells only, achieved because of the specificity of aptamer TLS11a-GC to LH86 cells.

Cell apoptosis was investigated using Hoechst 33258 (λ_{exc}=350 nm and λ_{em}=461 nm) staining (Figure 3-10 A). Hoechst 33258 is a fluorescent stain for labeling DNA in live or fixed cells. From the fluorescence images, when the Dox concentration was 60 μM, there were more apoptotic and dead cells in the TLS11a-GC-Dox group (35.1%) than in the TD05-GC-Dox group (13.7%), further indication of the specificity of aptamer-

Dox conjugates. In additions, caspase 3 activation was monitored using western blot (Figure 3-10 B). The caspase 3 protein is a member of the cysteine-aspartic acid protease (caspase) family. Caspase 3 plays an important role in cell apoptosis and cleaved caspase 3 indicates the activation of caspase 3. Caspase-3 is activated in the apoptotic cell both by extrinsic (death ligand) and intrinsic (mitochondrial) pathways.[143,144] From the data shown, when the Dox concentration was 60 μM, the band density of cleaved caspase 3 in cells treated with TLS11a-GC-Dox was 3.3 times higher than in cells treated with TD05-GC-Dox.

***In vivo* Studies**

Forty NOD Cg-Prikdc (sccd) IL2 mice were treated as described in the experimental section. The tumor size of each mouse was measured every other day, and the average tumor volume was calculated (Figure 3-11 A). The data shows that free Dox, TLS11a-GC-DOX complex and TD05-GC-DOX complex all had significant tumor inhibition compared to the untreated group. And TLS11a-GC-DOX complex had the most efficient effect compared to free Dox and TD05-GC-DOX, indicating that TLS11a-GC-Dox conjugates targeted the tumor cells and achieved higher local Dox concentration in the tumor site compared to free Dox and TD05-GC-Dox. Also, tumors of each mouse were collected and fixed using 10% formalin for 24 h. Then all samples were sent to the molecular pathology core lab for hematoxylin and eosin staining (H&E staining). H&E is the most widely used staining method in histology, hemalum stains the cell nuclei blue and eosin colors other structures various shades of red, pink and orange. From the H&E stained slides, the TLS11a-GC-DOX complex treated tumor (Figure 3-11 B, right) showed significant tumor cell necrosis compared to the untreated tumor (Figure 3-11 B, left).

Discussion

TLS11a was generated using mouse liver cancer cells, but it also binds human liver cancer cells with high affinity. Meanwhile, it is the first aptamer to be identified as specific for human liver cancer cells. Our results showed that the target molecule of TLS11a is very likely a membrane protein which can be internalized into cells. These results indicate TLS11a may be a useful aptamer for targeted drug delivery in liver cancer treatment.

Dox plays a very important role in liver cancer treatment, and it is one of the most utilized anticancer drugs worldwide. Dox inhibits cell proliferation through intercalation of DNA in the cell's nucleus, and subsequent inhibition of topoisomerase II. Several reports have demonstrated that free Dox is membrane permeable and can be uptaken by cells through passive diffusion, rapidly transported to the nuclei, where it binds to chromosomal DNA.[145] As it is readly and non-specifically internalized it is toxic to all proliferating cells, including normal cells. This toxicity limits the therapeutic activity of Dox in clinical use. By making use of modification of a specific liver cancer aptamer and the intercalation properties of Dox, we generated an easy, rapid, and efficient method to target delivery of Dox to cancer cells. During *in vitro* experiments, we showed TLS11a-GC targets LH86 cells, and not normal human liver cells. Futhermore, we demonstrated the specific toxicity of TLS11a-GC-Dox complex to target cells, compared to normal liver cells, thereby limiting its toxicity only to target cells. This targeting was achieved through the specific binding affinity of the TLS11a aptamer. During MTS assay, although TLS11a-GC-Dox achieved good cell toxicity compared to control TD05-GC-Dox, less toxicity was observed in the TLS11a-GC-Dox group than in the free Dox group. Also, less internalization and release of Dox in the TLS11a-GC-Dox group than in the free

Dox group was observed using confocal microscopy. Dox itself is a small molecule and it can be rapidly uptaken by cells through a passive diffusion mechanism. Within 15 min, cells treated with free Dox show an intense red fluorescence in the nuclear region indicating that the uptake speed is very rapid.[145] However, once Dox was intercalated into the DNA aptamer to form a much larger molecule, the cell uptake of the aptamer-Dox complex was mainly dependent on the aptamer and its cell membrane target. And the internalization of aptamer required more time (about 2 h) than free Dox, thus slowing down the internalization of aptamer-Dox complex and the release of Dox from the complex. Therefore, less toxicity was observed in the TLS11a-GC-Dox group than in the free Dox group during *in vitro* experiments.

By contrast, during *in vivo* experiments, although TLS11a-GC-Dox had decreased cell internalization speed compared to free Dox. TLS11a-GC-Dox increased the local concentration of Dox very much compared to free Dox, because of the target recognition by TLS11a aptamer. Hence, higher tumor inhibition efficacy was achieved in the TLS11a-GC-Dox treated mouse group.

Conclusion

In summary, by making use of the ability of anthracycline drugs to intercalate between bases of nucleotides, a new design to modify aptamer TLS11a to TLS11a-GC and to make Dox and TLS11a-GC conjugates was investigated. The specificity and efficacy of this conjugate to serve as a drug-delivery platform was further demonstrated *in vitro* and *in vivo*. Our data showed that the modified aptamer retains its specificity and can load much more Dox than the unmodified aptamer. Also, the aptamer-Dox conjugates are stable in cell culture medium and can differentially target LH86 cells. The specificity of this system was further demonstrated by treatment of human normal liver

cells, which lack the aptamer binding target. The aptamer-Dox conjugate prevents the nonspecific uptake of Dox and decreases cellular toxicity to the non-target cells. Furthermore, the *in vivo* experiment showed better tumor inhibition by the TLS11a-GC-Dox group compared to all other control groups, indicating the successful delivery of Dox by the modified aptamer. This targeting specificity assured a higher local Dox concentration in the tumor. In addition, aptamer-Dox conjugates are smaller than antibody-based drug delivery systems, presumably allowing faster penetration and fewer immunoreactions. We anticipate that the design of aptamer modification and aptamer-Dox conjugation platform technology based on the intercalation of anthracyclines may be utilized in distinct ways to develop novel targeted therapeutic modalities for more effective cancer chemotherapy.

Table 3-1. Different aptamer sequences

Aptamer	Sequence
TLS11a	ACAGCATCCCCATGTGAACAATCGCATTGTGATTGTTACGGTTTCCG CCTCATGGACGTGCTG
TD05	CACCGGGAGGATAGTTCGGTGGCTGTTCAGGGTCTCCTCCCGGTG
TLS11a-GC	CGCGCGCGCGCGCGCGCGCGCGCGCGCGCGCGCGCGCGCGCGC GCGCGCGCGCGCGCGACAGCATCCCCATGTGAACAATCGCATTGT GATTGTTACGGTTTCCGCCTCATGGACGTGCT G
TD05-GC	*CGCGCGCGCGCGCGCGCGCGCGCGCGCGCGCGCGCGCGCGC GCGCGCGCGCGCGCGCGAACACCGTGGAGGATAGTTCGGTGGCT GTTCAGGGTCTCCTCCCGGTG*

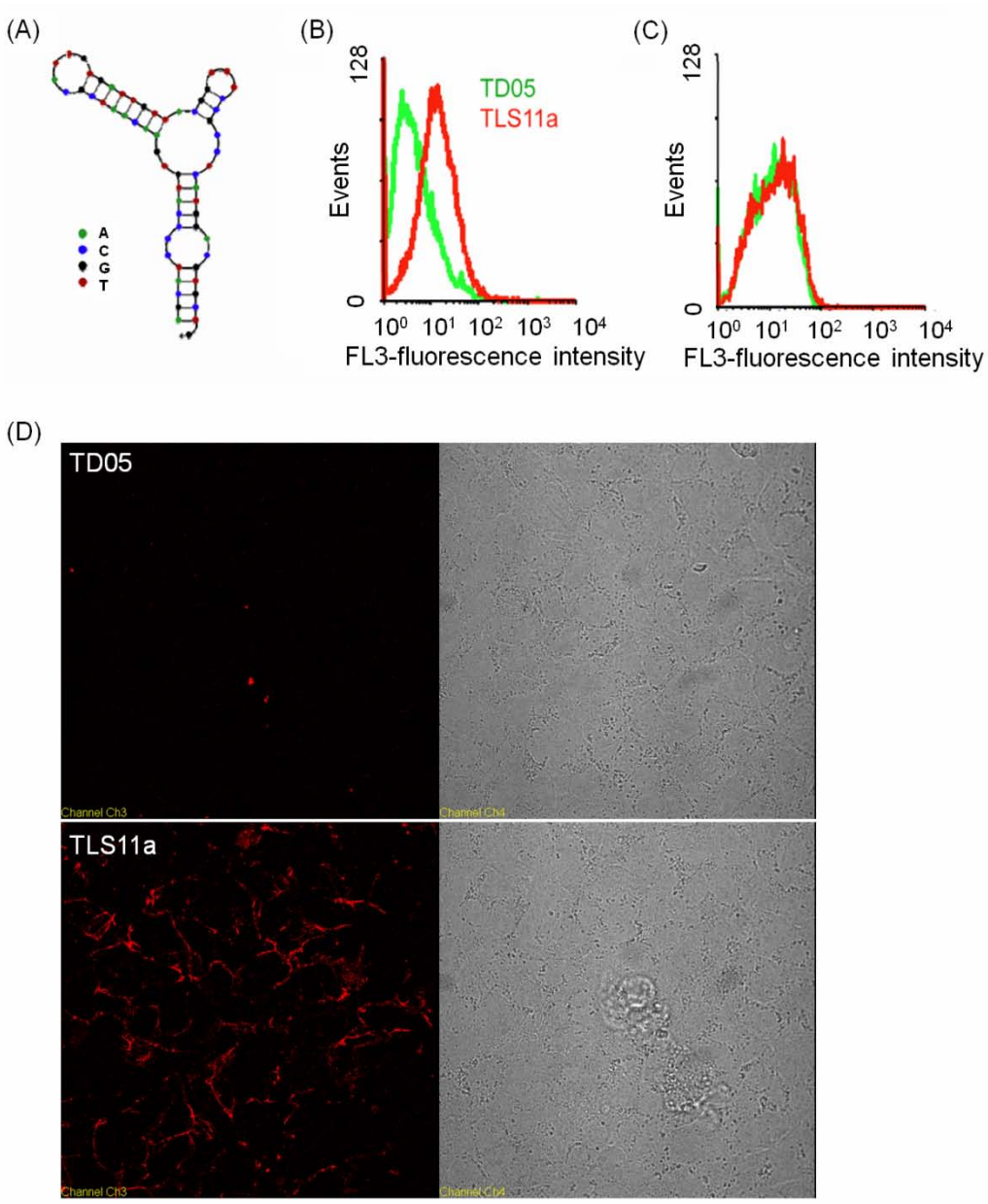

Figure 3-1. (A) The secondary structure of aptamer TLS11a and its binding ability to (B) LH86 and (C) human normal liver cells, Hu1082. The green histogram shows the background binding (control aptamer, TD05), and the red fluorescence intensities show the binding of TLS11a with target and control cells. All probes were labeled with Phycoerythrin-Cy5.5. (D) Confocal images of aptamer staining with cultured LH86 cells. Cells were incubated with aptamer conjugated with biotin and the binding event was observed with AlexaFluor 633 conjugated streptavidin. Non-binding sequence TD05 showed the background binding. Aptamers show significant binding over the background signal.

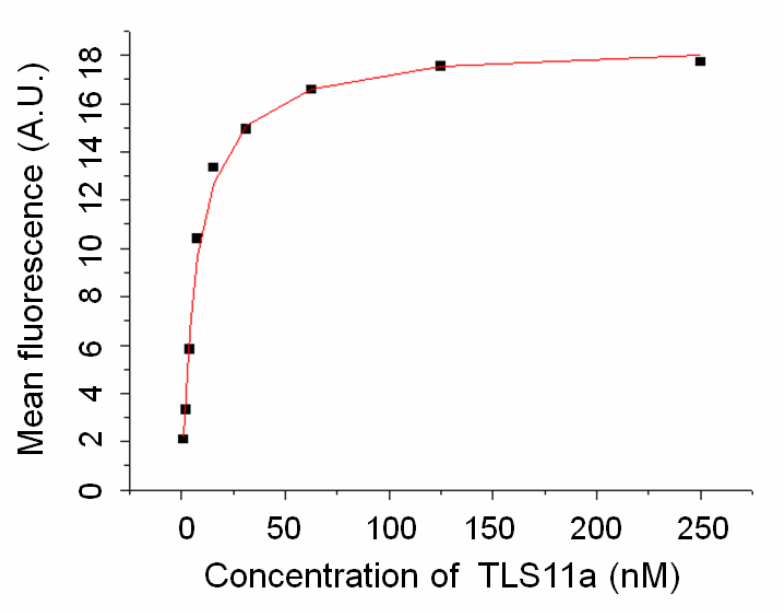

Figure 3-2. Representative binding curve of TLS11a aptamer with LH86 cells. Cells were incubated with varying concentrations of Biotin-labeled TLS11a aptamer in duplicate. The florescence signal was detected with streptavidin-PE-cy5.5. The mean fluorescence intensity of the unselected library (background binding) at each concentration was subtracted from the mean fluorescence intensity of the corresponding aptamer. The actual fluorescence intensity was fitted using Origin to determine the apparent K_d.

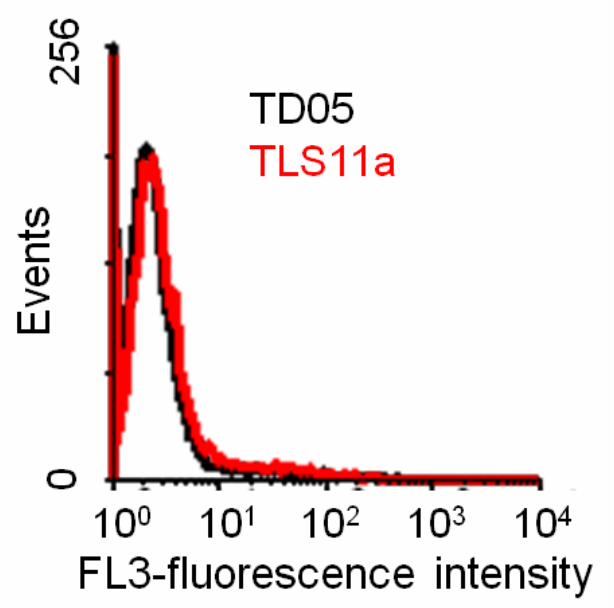

Figure 3-3. Preliminary determination of the type of cell surface molecules which bind to TLS11a. Cells were treated with trypsin for 10 min and then incubated with aptamer.

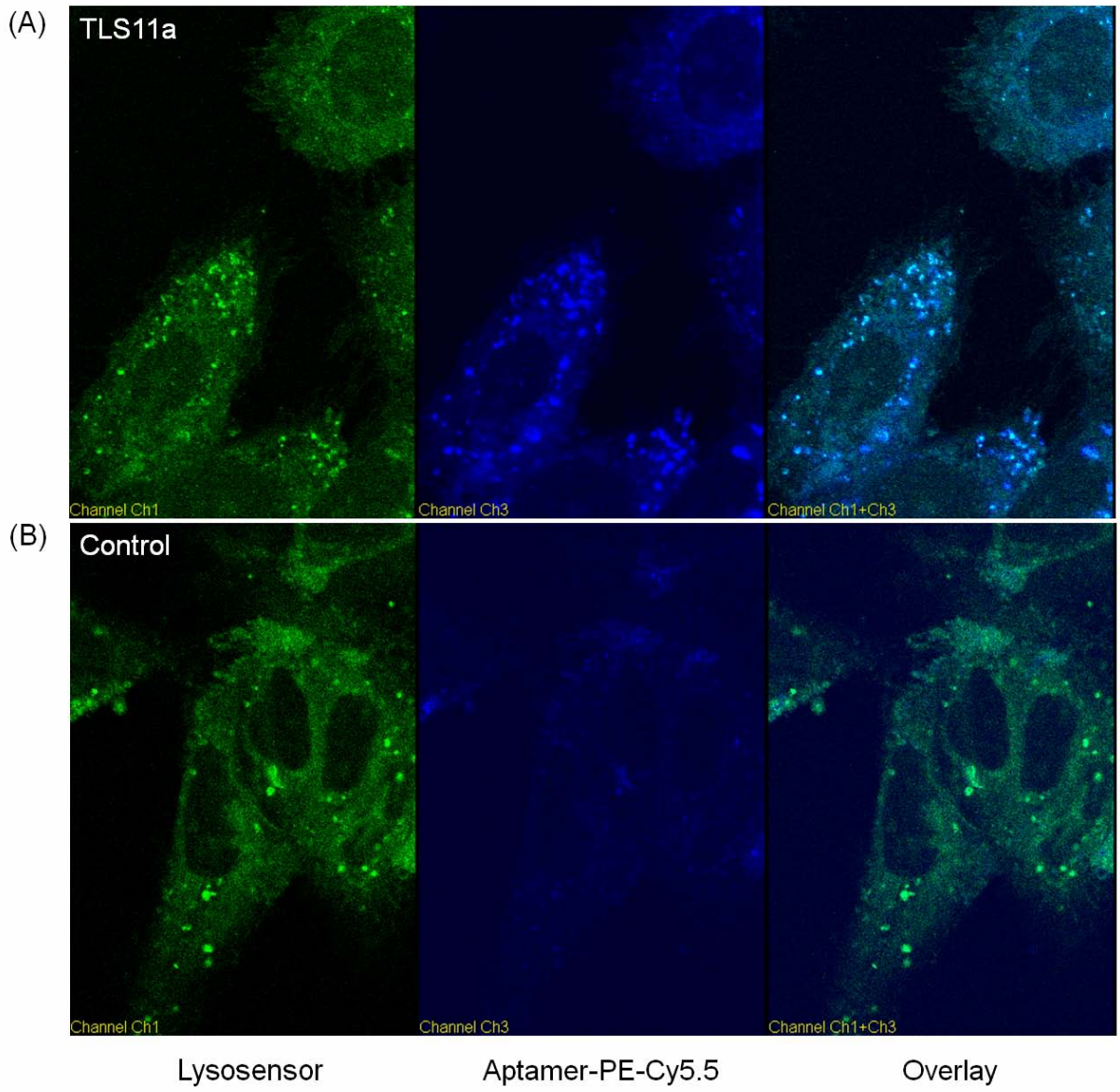

Figure 3-4. Co-localization of (A) TLS11a or (B) control TD05 and Lysosensor in endosomes after two hour incubation at 37ºC.

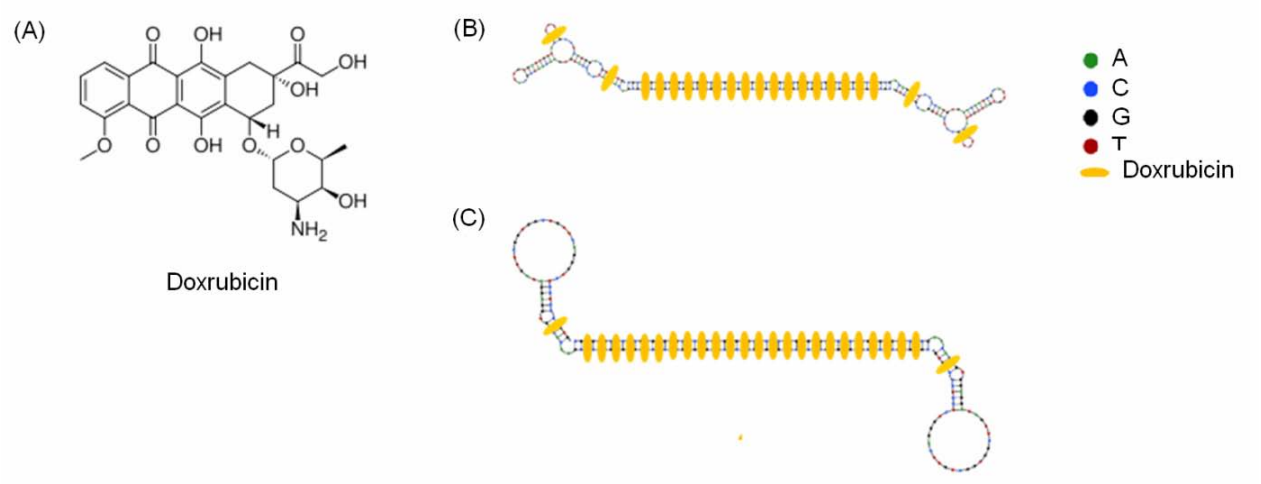

Figure 3-5. The intercalation of Dox into GC-modified aptamers to form physical conjugates. (A) Structure of Doxrubicin; (B) Structure of TLS11a-GC-Dox. (C)Structure of TD05-GC-Dox.

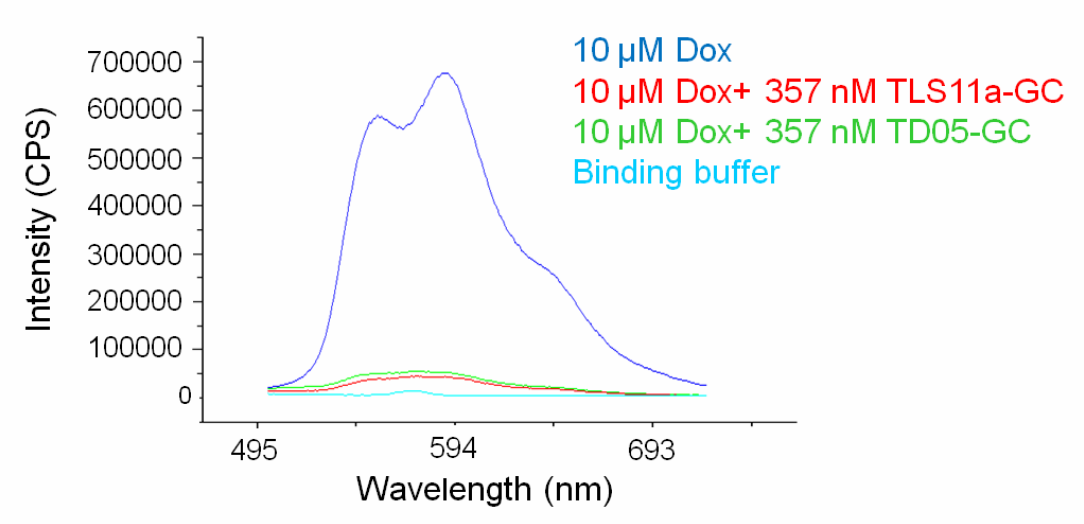

Figure 3-6. Fluorescence spectra of doxorubicin solution (10 µM) (dark blue) with modified TLS11a-GC (red) or TD05-GC (green). The background fluorescence was obtained in binding buffer sample (light blue).

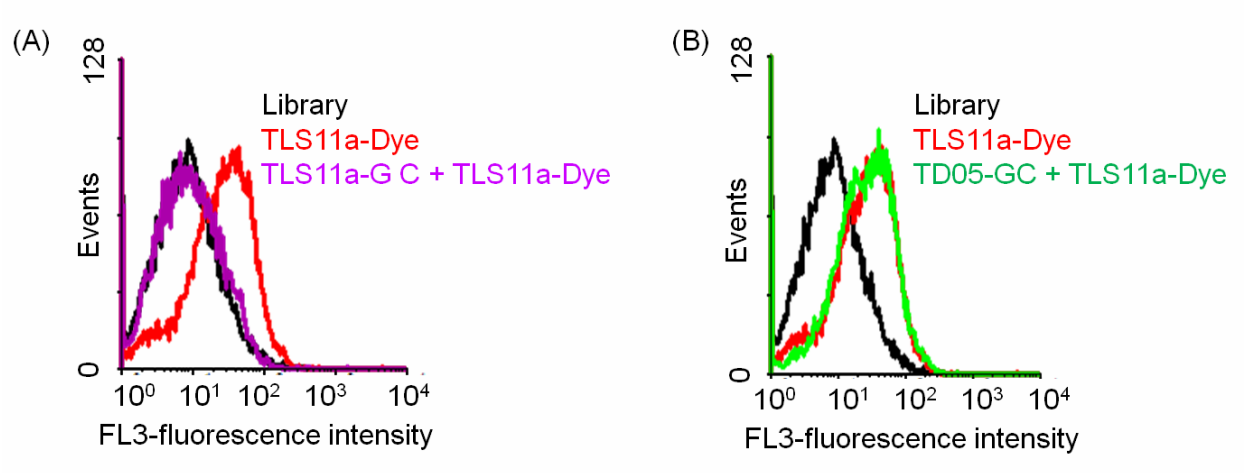

Figure 3-7. The binding affinity of (A) TLS11a-GC or (B) TD05-GC to LH86 cells monitored using flow cytometry. A competition experiment was carried out. Unlabeled TLS11a-GC or TD05-GC was first incubated with LH86 cells, followed by biotin labeled TLS11a. Then cells were further incubated with streptavidin-PE-cy5.5. The binding buffer and unselected DNA library were used as negative controls. The fluorescence signal is from Phycoerythrin-Cy5.5. The black histogram shows the background binding.

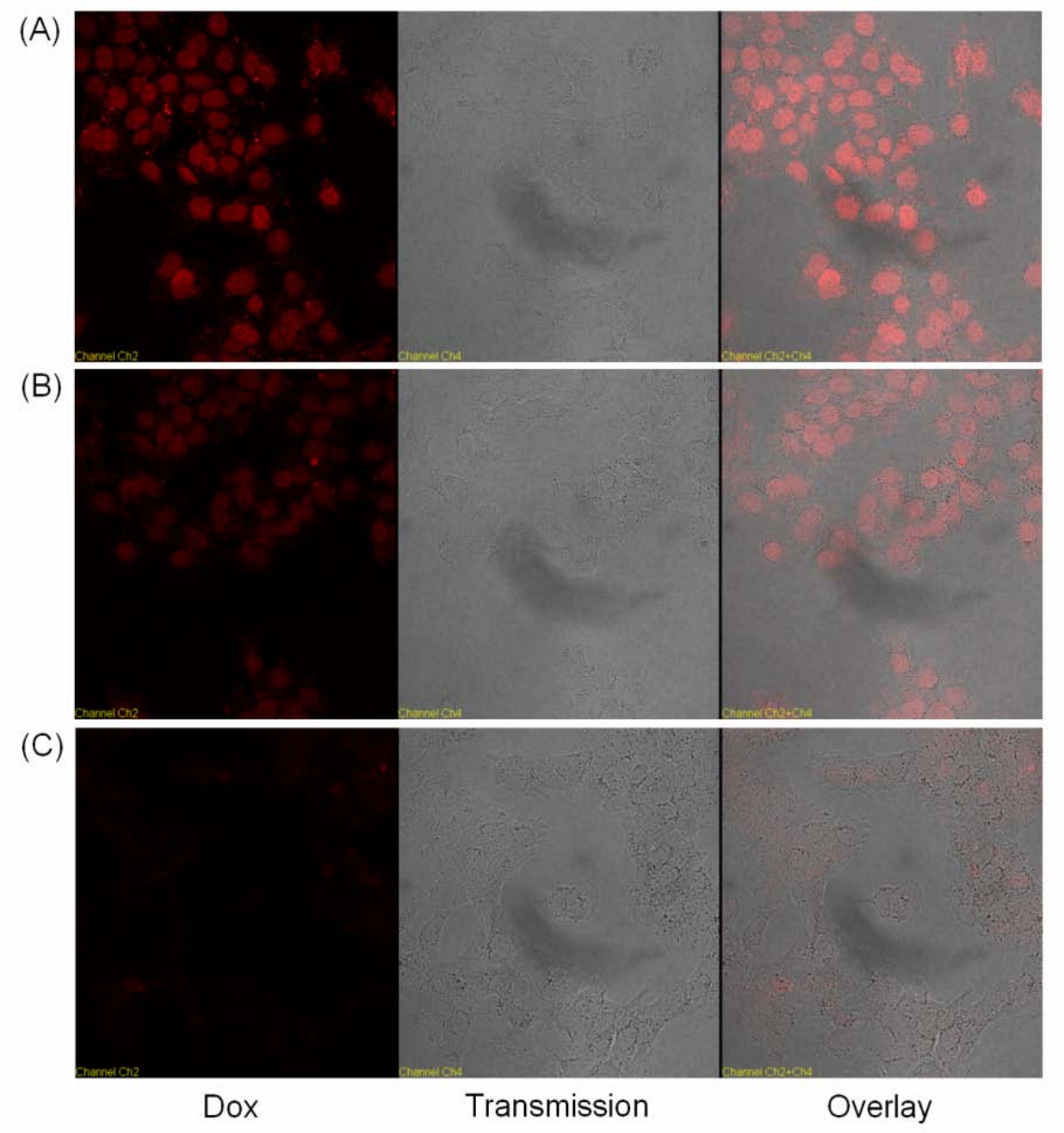

Figure 3-8. Internalization of (A) Dox, (B) TLS11a-gc-Dox, and (C) TD05-GC-Dox observed by confocal microscopy.

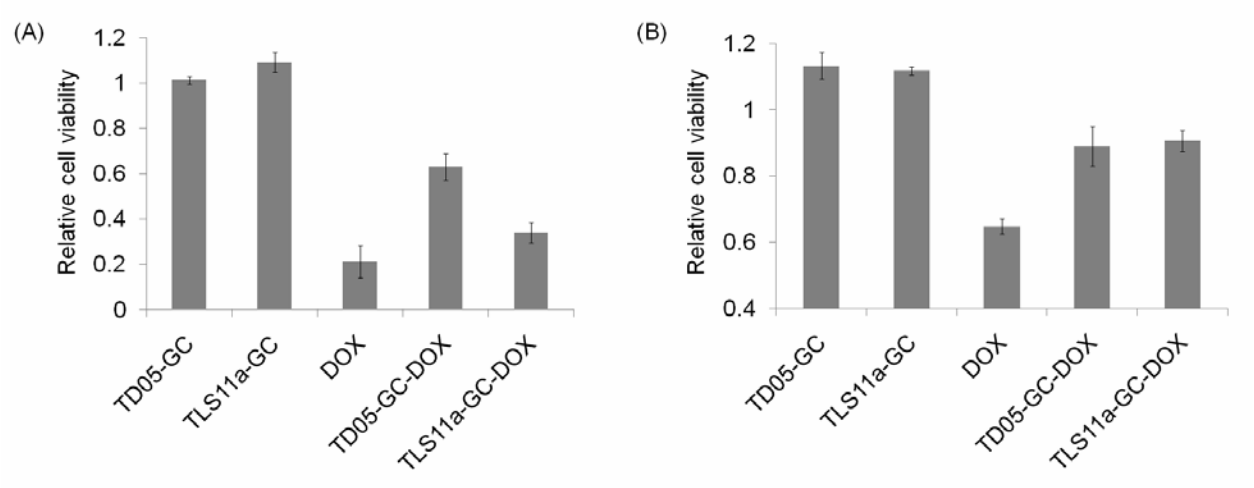

Figure 3-9. Relative cell viability of cells treated with either TLS11a-GC, TD05-GC, free Doxorubicin, TLS11a-GC-Dox or TD05-GC-Dox. (A) Relative cell viability of LH86 (target cell line); (B) Relative cell viability of Hu1229 (human normal liver cells).

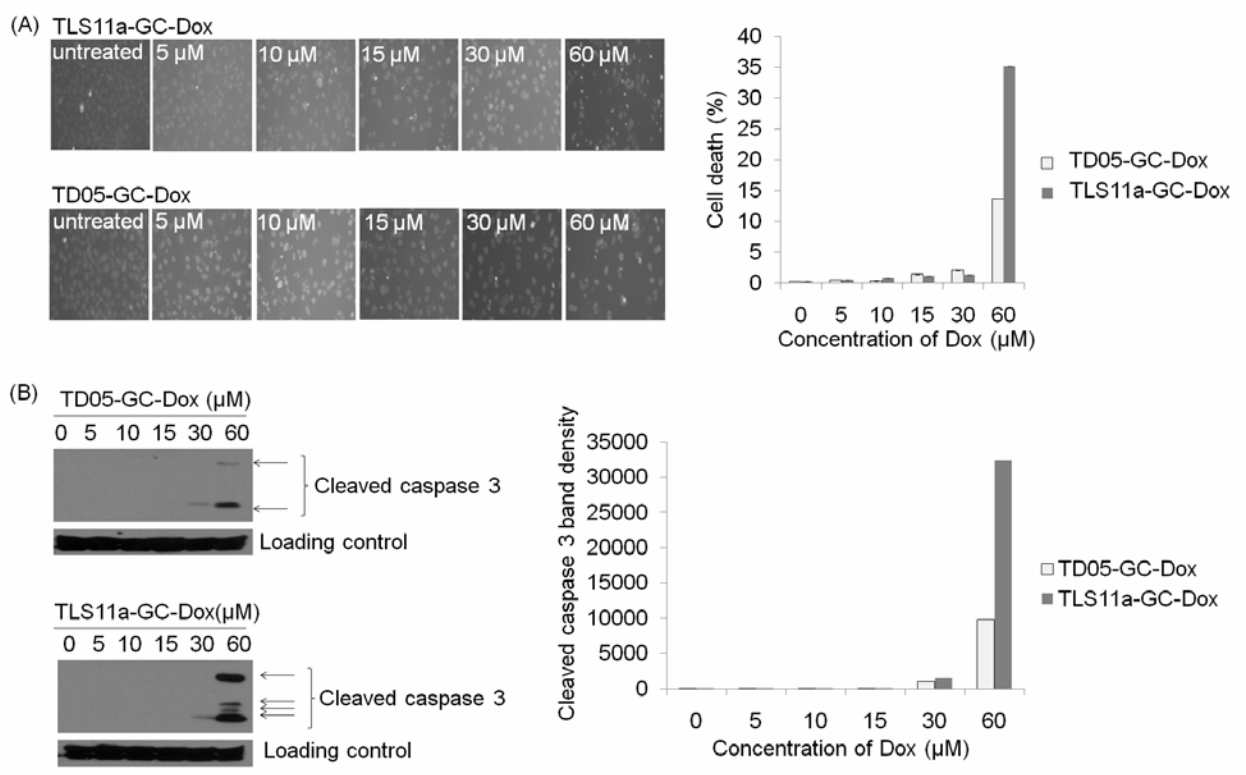

Figure 3-10. Apoptosis of cells treated with either TLS11a-GC, TD05-GC, free Doxorubicin, TLS11a-GC-Dox or TD05-GC-Dox. (A) Hoechst 33258 staining for apoptotic and dead LH86 cells treated with a series of concentrations of TLS11a-gc-Dox or TD05-GC-Dox; (B) Western blot results for cleaved caspase 3 in LH86 cells treated with a series of concentrations of TLS11a-gc-Dox or TD05-GC-Dox.

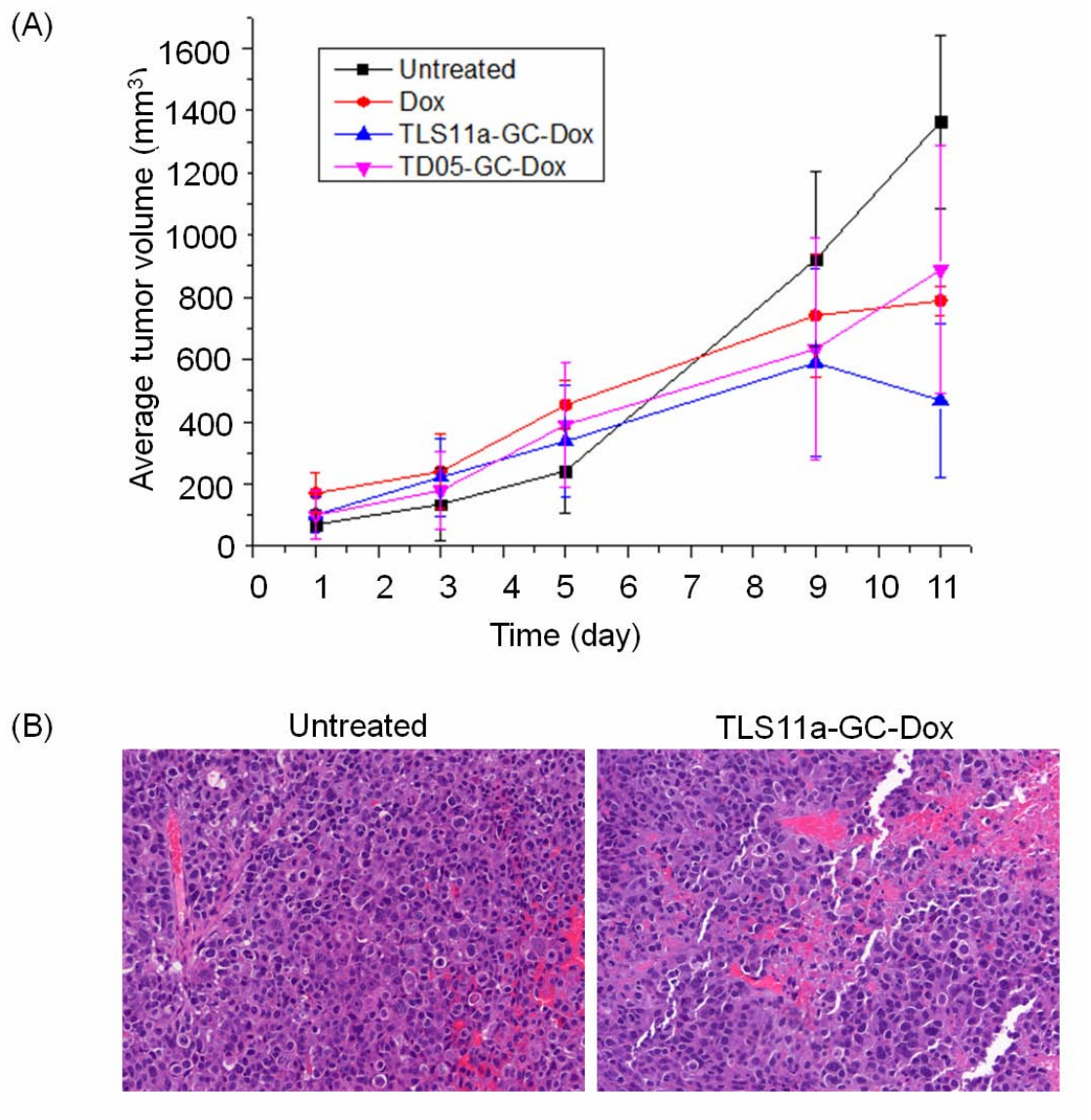

Figure 3-11. Tumor inhibition of the aptamer-Dox complex in mice model. (A) Average tumor volume of mice treated with either nothing (black), Doxrobicin (red), TLS11a-GC-Dox (blue), or TD05-GC-Dox (purple); (B) Microscopy images of H&E stained tumor tissue slides.

CHAPTER 4
SILENCING OF PTK7 IN COLON CANCER CELLS: CASPASE-10-DEPENDENT APOPTOSIS VIA MITOCHONDRIAL PATHWAY

Introduction

Receptor tyrosine kinases (RTKs) compose a class of transmembrane signaling proteins that transmit extracellular signals to the interior of the cell. Misregulation of RTKs plays an important role in the development and/or progression of many forms of cancer.[146] Protein tyrosine kinase-7 (PTK7), which is also known as colon carcinoma kinase-4 (CCK4), is a relatively new and little studied member of the RTK superfamily. It contains an extracellular domain with seven immunoglobulin-like loops, a transmembrane domain, and a catalytically inactive tyrosine kinase domain.[147,148] However, as a result of an ancient and well conserved amino acid substitution within the catalytic domain, PTK7 is a pseudokinase without detectable catalytic tyrosine kinase activity.[146,149] It was originally identified as a gene-expressed in colon cancer-derived cell line, but not in human adult colon tissues.[147] In contrast, high levels of PTK7 expression are seen in fetal mouse colons.[146,147,149] The expression of PTK7 is up-regulated in many common human cancers, including colon cancer, lung cancer, gastric cancer and acute myeloid leukemia.[76,147,150-153] Recently, PTK7 was identified as a novel regulator of non-canonical WNT or planar cell polarity (PCP) signaling.[154,155] PTK7 also appears to play an important role in tube formation, migration, invasion of endothelia and angiogenesis in HUVEC cells.[156] However, the functional role of PTK7 in cell proliferation and apoptosis remains unclear. Our lab became interested in PTK7 when it was identified as the target molecule of the aptamer sgc8.[76] Aptamer sgc8 was identified through Cell-SELEX procedure against T cell acute lymphoblastic leukemia

(ALL) cell line, CCRF-CEM, since then it has been shown that sgc8 can effectively be used as a molecular probes for recognition of neoplastic cells in patient samples.[40]

Apototosis is programmed cell death, typically mediated by a family of cysteine proteases known as caspases.[157] Caspases are synthesized as inactive proenzymes with either a long (caspase-8, -9 and -10) or a short (caspase-3, -6 and -7) prodomain.[158,159] These latter proteases are called “executioner” or “effector” caspases, and their activation leads to programmed cleavage of a series of essential intracellular proteins leading to cell death.[160] Two main apoptosis pathways have been identified and the mechanism of apoptosisis shown in Figure 4-1.[161] The intrinsic pathway (mitochondria pathway) involves a decrease in mitochondrial membrane potential and release of cytochrome *c*[162] which activates caspase-9 through the apoptosome. Then, caspase-9 initiates a proteolytic caspase cascade that kills the cells. The extrinsic pathway (death receptor pathway) involves the tumor necrosis factor (TNF) receptor superfamily. In response to TNF ligand binding, these membrane receptors recruit adapter molecules and activate caspase-8/10 in the death-inducing signaling complex (DISC). Activated caspase-8/10 either directly activates downstream effector caspases, such as caspase-3, or connects to the intrinsic pathway through cleavage of BCL-2 Interacting Domain (Bid) to truncated Bid (tBid).[163]

The caspase-10 gene is linked to the caspase-8 gene at the human chromosome locus 2q33-34.[164] While, the physiological functions of caspase-10 remain poorly understood, it is thought to play a role in the death receptor pathway. Recently caspase-10 was also reported to be activated downstream of the mitochondria in cytotoxic drug-induced apoptosis of tumor cells.[165] Acquired inactivating mutations of caspase-10 have

been identified in tumor cells from patients with solid tumors.[166-168] Recently, caspase-10 was shown to play a role in apoptosis induced by paclitaxel, an anticancer drug, through a Fas-Associated protein with Death Domain (FADD) -dependent mechanism.[169]

The term RNA interference (RNAi) was first used by Fire *et al.* [170] in their work on *Caenorhabditis elegans*. RNAi is a cellular mechanism which helps to control which genes are active and how active they are. RNAi is an RNA-dependent gene silencing process controlled by the RNA-induced silencing complex (RISC). There are two types of small RNA molecular, microRNA (miRNA) and small interfering RNA (siRNA), which are central to RNAi. miRNAs are genomically encoded approximately 21-nucleotide-long non-coding RNAs which regulate gene expression, particularly during development.[171,172] miRNAs typically have incomplete base pairing to a target and inhibit the translation of many different mRNAs with similar sequences. In contrast, siRNAs (21-25 nucleotides in length) are artificial, typically base-pair perfectly and trigger the degradation of single specific mRNA.[170,173] The siRNA structure and the mechanism of RNAi induced by siRNA is shown in Figure 4-2. In the first step, the ribonuclease enzyme Dicer cleaves long double-stranded RNA (dsRNA) molecules to produce 21-25 base pairs-long siRNAs with a few unpaired overhang bases on each end.[174-176] Studies suggest this length maximizes target-gene specificity and minimizes non-specific effects.[177] These siRNAs are incorporated into a multiprotein RNA-inducing silencing complex (RISC). After integration into the RISC, siRNAs are unwound, leaving the antisense strand to guide RISC to its homologous target mRNA for endonucleolytic cleavage,preventing mRNA from being used as a translation template.[178] It has been

demonstrated that siRNAs can silence cognate gene expression via the RNAi pathway in mammalian cells.[179] The properties of RNAi, including stringent target-gene specificity and simplicity of design and testing,[180] have greatly widened the potential for mechanistic studies of proteins, as well as for therapeutic approaches to treat diseases, including cancer.[181,182]

In this study, a siRNA targeting human PTK7 mRNA was used for maximal inhibition of PTK7 expression in order to probe the role of PTK7 in apoptosis and proliferation. Knocking down PTK7 in HCT 116 cells inhibited cell proliferation and induced apoptosis. Furthermore, this apoptosis was characterized by decreased mitochondrial membrane potential and activation of caspase-9 and -10. Addition of a caspase-10 inhibitor totally blocked this apoptosis, suggesting that caspase-10 may play a critical role in PTK7-knockdown-induced apoptosis downstream of mitochondria. Therefore, these observations may indicate a role for PTK7 in cell proliferation and cell apoptosis.

Materials and Methodology

Materials

McCoy's 5A media were purchased from ATCC; fetal bovine serum (FBS) (heat inactivated) was purchased from GIBCO, and penicillin-streptomycin was purchased from Cellgro. HiPerFect transfection reagent, HP-validated siRNA specific for PTK7, named PTK7 siRNA (sense: 5'- CGGGATGATGTCACTGGAGAA-3'), and a nonspecific siRNA were purchased from Qiagen. Micro-FastTrack 2.0 Kit was purchased from Invitrogen. A colorimetric bromodeoxyuridine (BrdU) kit was from BD Pharmingen. IScript One-Step RT-PCR Kit with SYBR Green was from Biorad. Protease inhibitor cocktail (mixture of 4-(2-aminoethyl)benzenesulfonyl fluoride (AEBSF), E-64, bestatin,

leupeptin, aprotinin, and sodium EDTA) and 0.4% trypan blue were from Sigma. The protein assay kit was from Bio-Rad. Antibodies against caspase-9 and β-actin were from Cell Signaling Technology. Anti caspase-10 antibody was purchased from Millipore. Antibody against PTK7 was from Abnova. Goat anti-mouse IgG HRP-conjugated secondary antibody and goat anti-rabbit IgG HRP-conjugated secondary antibody were purchased from Cell Signaling Technology. Vybrant Apoptosis Assay Kit #2, 4× NuPAGE LDS sample buffer, 4-12% NuPAGE Bis-Tris gels, 20× NuPAGE MOPS SDS running buffer, and 20× NuPAGE transfer buffer were from Invitrogen. Immobilon-P transfer membrane was from Millipore. SuperSignal West Dura Extended-Duration Substrate and Restore plus Western blot Stripping buffer were from Thermo Scientific. X-ray films were from ISCBioExpress. JC-1 (5,5',6,6'-tetrachloro-1,1',3,3'-tetraethylbenzimidazolylcarbocyanine iodide) was purchased from Anaspec**.** Caspase-9 inhibitor (Z-LEHD-FMK), caspase-3 inhibitor (Z-DEVD-FMK), caspase-8 inhibitor (Z-IETD-FMK), caspase-family inhibitor (Z-VAD-FMK), caspase-1 inhibitor (Z-YVAD-FMK), caspase-10 inhibitor (Z-AEVD-FMK) and caspase-2 inhibitor (Z-VDVAD-FMK) were purchased from BioVision. Caspase-10 Fluorometric Protease Assay Kit was from Millipore.

Cell Culture

HCT 116 (colon carcinoma) cells were obtained from ATCC (Manassas, VA) and maintained in culture at 37 °C and 5% CO_2. p53-null HCT 116 cells were provided by Dr. Bert Vogelstein (The Johns Hopkins Kimmel Cancer Center). Cells were cultured in McCoy's 5A medium supplemented with 10% fetal bovine serum (FBS) (heat inactivated) and 100 IU/mL penicillin-streptomycin. Cells were split at regular intervals and were not allowed to overgrow.

Transfection of siRNA

HCT 116 cells were transfected with siRNA by HiPerFect transfection reagent. On day 1, cells in exponential growth phase were harvested and suspended in growth medium. Cells were divided into four groups and were treated with PTK7 siRNA, a nonspecific siRNA as negative control, HiPerFect vehicle only, or were left untreated. For each transfection, a 500 μL cell suspension was transfected with 25 nM siRNA using 4 μL transfection reagent in 24-well plates. Cells were kept in normal culture conditions and collected 2, 3 or 4 days after transfection for analysis.

Flow Cytometry Analysis

During our study, after transfection with siRNAs as described above, cells were detached using nonenzymatic cell dissociation solution (Cellgro), washed twice in PBS, and counted using a hemocytometer. Aliquots of $5x10^5$ cells were incubated with excess phycoerythrin (PE)-labeled anti-PTK7 in 200 μL of binding buffer (PBS containing 5 mM $MgCl_2$, 4.5 mg/mL glucose, 0.1 mg/mL yeast tRNA, 1 mg/mL BSA and 20% FBS) on ice for 30 min. Cells were then washed twice with 1 mL of binding buffer and suspended in 0.3 mL of binding buffer. The fluorescence was determined with a FACScan cytometer (Becton Dickinson Immunocytometry Systems, San Jose, CA). PE-labeled anti-IgG was used as a negative control.

Quantitative RT-PCR

Total mRNA from cells treated with various siRNAs was extracted with Micro-FastTrack 2.0 Kit according to the manufacturer's instructions. In eukaryotic organisms, most mRNA molecules are polyadenylated at the 3' end. Here, in order to separate mRNA from the majority of the RNA found in the cells, affinity binding to oligo(dT) cellulose was used. Briefly, DNA and proteins were removed from samples, and mRNA

bound to oligo(dT) cellulose under high salt conditions. After removing rRNA by washing using a low salt buffer, mRNA was eluted with a very low ionic strength buffer. Isolated mRNA was kept at -80ºC. To determine the concentration of the eluted mRNA, samples were diluted by adding Elution Buffer from the kit. Elution Buffer was used to blank the spectrophotometer at 260 nm. And then the absorbances of diluted samples were read at 260 nm. The following formula was used to determine RNA concentration:

$$[\mathrm{RNA}] = (\mathrm{A260})\left(0.04\ \mu\frac{\mathrm{g}}{\mu\mathrm{L}}\right)\mathrm{D}$$

Where, [RNA], A260 and D represent RNA concentration, absorbance at 260 nm and the dilution factor, respectively.

Real-time PCR was performed on mRNA (50 ng) with iScript One-Step RT-PCR Kit using SYBR Green with a Biorad iCycler. All reactions were performed in a 50-µL volume in triplicate. Primers for human PTK7 were purchased from Qiagen (QT00015568). The PCR preparation was shown in Table 4-1.RT-PCR procedure parameters were as follows: 50 °C for 30 min, 5 min of Taq activation at 95 °C, followed by 45 cycles of PCR: 95 °C × 30 s, 57 °C × 60 s, and 72°C × 60 s. The relative amount of target mRNA was normalized to GAPDH mRNA. Specificity was verified by melting curve analysis.

Cell Number Detection by Trypan Blue Exclusion Assay

For four days after treatment, cell suspensions were prepared by detaching cell from a dish using nonenzymatic solution and resuspending them in 1 mL media. To 25 µL of the cell suspension, 25 µL of 0.4% trypan blue was added, and cells were counted using a hemocytometer. Trypan blue is a diazo dye which cannot be absorbed by viable

cells, but can traverse the membrane in a dead cell. So trypan blue stains only dead cells blue under a microscope.

Proliferation Assay

Cell proliferation was studied using a colorimetric bromodeoxyuridine (BrdU) kit according to the manufacturer's instructions. First, cells were transfected with siRNA. After 48 h of treatment, 10 µM BrdU solution was added to the medium. The media was discarded after 2 h, and cells were fixed and permeabilized with BD Cytofix/Cytoperm Buffer for 30 min at room temperature. After removing Cytofix/Cytoperm Buffer, cells were incubated with 100 µL of diluted DNase (diluted to 300 µg/mL in PBS) for 1 hour at 37°C to expose incorporated BrdU. Cells were then resuspended in 50 µL of BD Perm/Wash Buffer containing diluted FITC-labeled anti-BrdU and incubated for 20 minutes at room temperature. Finally, cells were incubated with 20 µL of the 7-Aminoactinomycin D (7-AAD) solution which is a fluorescent chemical compound with a strong affinity for DNA. 7-AAD cannot pass through intact cell membranes, but in this experiment, the cell membrane had been permeabilized, so 7-AAD stained whole cell population. Samples were analyzed by flow cytometry. Means and standard errors of at least three replicates of each experiment were calculated. Significance was determined by t-test; a p value≤0.05 is indicated by an asterisk.

Annexin V/Propidium Iodide Double-Staining Assay

Annexin V/propidium iodide (PI) double-staining was performed using the Invitrogen Vybrant Apoptosis Assay Kit #2. Cells were washed twice in ice-cold PBS buffer and centrifuged at 900 rpm for 3 min. The pellets were resuspended in binding buffer at a density of 10^6 cells/mL. A sample solution (100 µL) was double-stained with 5 µL Annexin V/Alexa Fluor 488 and 2 µL 100 µg/mL PI. After incubation at room

temperature for 15 min, 400 µL of binding buffer was added, and cells were analyzed by flow cytometry.

Western Blot Analyses

Western blot is a widely used analytical technique for detecting specific proteins in a given sample such as tissue homogenate and cell lysate. Gel electrophoresis was used to separate proteins by the length of the polypeptide (denaturing conditions) or by the 3-D structure of the protein (native/ non-denaturing conditions). All proteins are then transferred to a nitrocellulose or PVDF membrane, where antibodies specific to the target protein was used to probe the proteins.[183,184]

In our study, Western blot was carried out to detect PTK7 expression, caspase 9, 10 and Bid activation. Briefly, after HCT 116 cells were transfected with PTK7 siRNA for 12 h, 24 h, 30 h, and 48 h, whole cells were harvested and washed twice with ice-cold PBS. Then cells were lysed in radioimmunoprecipitation buffer (150 mM NaCl, 1% Triton X-100, 1% sodium deoxycholate, 0.1% sodium dodecyl sulfate (SDS), 50 mM Tris-HCl, pH 7.5, and 2 mM EDTA) in the presence of proteinase inhibitor cocktail for 20 min on ice. Lysates were centrifuged at 14,000 rpm for 20 min at 4°C, and the protein content in the supernatant was measured using the Bio-Rad protein assay. Fifty micrograms of supernatant proteins were mixed with 4× NuPAGE LDS sample buffer and heated at 70°C for 10 min. The proteins were separated on 4-12% NuPAGE Bis-Tris gels with 1× NuPAGE MOPS SDS running buffer and then electrotransferred onto a PVDF transfer membrane with NuPAGE transfer buffer at 50 V for 1 h. The membranes were blocked with 5% nonfat dry milk in PBS buffer containing 0.2% Tween 20 (PBST) for 2 h at room temperature. The membranes were probed with primary antibodies in PBST containing 5% nonfat dry milk overnight at 4°C. After three successive washings

with PBST for 10 min, the membranes were incubated with horseradish peroxidase-conjugated goat anti-mouse IgG antibody or goat anti-rabbit IgG antibody in PBST containing 5% nonfat dry milk for 1 h at room temperature. After three successive washings with PBST for 10 min, the proteins signals were developed with a SuperSignal West Dura Extended Duration Substrate kit and transferred from the membrane to X-ray films. Protein loading was normalized by probing the same membrane with anti-actin antibody. For β-actin detection, previously used membranes were soaked in Restore Plus Western Blot Stripping Buffer at room temperature for 30 min and hybridized with anti-β actin.

Measurement of Mitochondrial Membrane Potential

Dye JC-1 (5,5',6,6'-tetrachloro-1,1',3,3'- tetraethylbenzimidazolylcarbocyanine iodide) was used to determine mitochondrial membrane potential ($\Delta\Psi_m$), the loss of which is regarded as a crucial step in the apoptosis pathway. HCT 116 cells were transfected with siRNA for 48 h or 72 h, after which the cells were washed with cold PBS and stained by incubating with 2 μM JC-1 for 20 min at 37°C. Then, the mitochondrial membrane potential was detected by fluorescence microscopy and flow cytometry at 590 nm.

Caspase-10 Activity Measurement

Caspase-10 activity was measured using the Caspase-10 Fluorometic Protease Assay Kit. Briefly, cells were transfected with PTK7 siRNA, and after 24 h or 48 h cells were harvested. Two million cells were resuspended in chilled lysis buffer and incubated on ice for 10 min. Then, 50 μL of 2× Reaction Buffer and 5 μL of the 1 mM AEVD-AFC substrate (50 μM final concentration) were added to each sample. After incubation at 37°C for 2 h, samples were analyzed using a microplate reader equipped with a 400 nm

excitation filter and a 505 nm emission filter. Means and standard errors of at least three replicates of each experiment were calculated. Significance was determined by t-test, a p value≤0.05 is indicated by an asterisk.

Results

Inhibition of PTK7 Expression by PTK7 siRNA

Expression of PTK7 in HCT 116, human colon carcinoma cells, was investigated by flow cytometry (Figure 4-3 A, untreated) and Western blot (Figure 4-3 B, 0 h). Comparing the fluorescence signal of PE-labeled anti-PTK7 to PE-labeled anti-mouse IgG clearly shows that PTK7 is expressed in HCT 116 cells.

Inhibition of PTK7 protein expression

Expression of PTK7 was knocked down using PTK7-targeted siRNA and the flow cytometry results for the targeted cells were compared to those exposed to vehicle only, nonspecific siRNA or untreated as shown in Figure 4-3 A. After 48 hours, the peak of anti-PTK7-PE in HCT 116 transfected with PTK7 siRNA shifted back to the peak of the background control protein, anti-IgG-PE, indicating that the PTK7 expression level in HCT 116 cells transfected with PTK7 siRNA greatly decreased. At the same time, there was no corresponding shift in the control siRNA or vehicle-treated groups, indicating that neither the HiPerFect transfection reagent nor the nonspecific siRNA affected PTK7 expression. When PTK7 expression was probed after 12 h, 24 h, 30 h and 48 h of transfection using Western blot (Figure 4-3 B), the results clearly showed that the level of PTK7 expression decreased after 48 h of transfection.

Inhibition of PTK7 mRNA expression

In addition, total mRNA was extracted from the untreated, vehicle, nonspecific siRNA, and PTK7 siRNA groups. mRNA is a molecule of RNA which is transcribed from

a DNA template, and carries coding information protein synthesis. In eukaryotic organisms, most mRNA molecules are polyadenylated at the 3' end. The poly(A) tail and the protein bound to it aid in protecting mRNA from degradation by exonucleases. Here, in order to separate mRNA from the majority of the RNA from cell lysate, oligo(dT) cellulose was used to bind to the poly(A) tail and isolate mRNA. After mRNA isolation, quantitative RT-PCR was performed to access the PTK mRNA level in different groups. Basically, the RNA strand was first reverse transcribed into its complementary DNA (cDNA) using reverse transcriptase, and the resulting cDNA was amplified using real-time PCR. SYBR Green I is an asymmetrical cyanine dye[185] which can binds to DNA and the resulting DNA-dye-complex absorbs blue light (λ_{max} = 488 nm) and emits green light (λ_{max} = 522 nm). So SYBR Green I was used as a dye for the quantification of double stranded real-time PCR.[186] At the same time, GAPDH, as a house keeping gene, was measured in the same sample and the amount of PTK7 mRNA was normalized to it. As shown in Figure 4-4, PTK7 siRNA induced 75-80% reduction of PTK7 mRNA in HCT 116 cells. These results indicated that both PTK7 protein and mRNA expression levels were greatly decreased by PTK7 siRNA. This proved the function and efficiency of PTK7 siRNA and provided a solid basis for our study of PTK7's functional role.

Viability of PTK7 siRNA-Treated HCT 116 Cells

The effect of PTK7 suppression on the viability of HCT 116 cells was investigated by counting the total number of live cells every day after transfection. Trypan blue, as a diazo dye which cannot be absorbed by viable cells, but can traverse the membrane in a dead cell, was used to count the live cells number. Under a microscope, trypan blue can color dead cells blue, but live cells are excluded from staining. As shown in Figure

4-5, the number of live HCT 116 cells transfected with PTK7 siRNA was shown to be significantly lower than untreated groups on day 4. This finding demonstrated a significant inhibition of cell viability in the HCT 116 cells treated with PTK7 siRNA. To confirm that the decrease of cell viability resulted from suppression of PTK7, the same assays were carried out with HCT 116 cells transfected with nonspecific siRNA or treated only with vehicle. The results showed that the PTK7 siRNA-treated sample contained the smallest number of cells. Although vehicle-treated and nonspecific siRNA-treated cells had smaller cell numbers than untreated cells, there were significantly fewer cells in the PTK7 siRNA-treated sample.

Proliferation of PTK7 siRNA-Treated HCT 116 Cells

To ascertain the effect of suppression of PTK7 on HCT 116 cell proliferation, a BrdU incorporation experiment was performed to measure DNA synthesis. BrdU is an analog of the deoxythymidine which can be incorporated into newly synthesized DNA by cells entering and progressing through the S (DNA synthesis) phase of the cell cycle. And then dye-labeled BrdU antibody can determine the amount of BrdU incorporation. After 48 h of transfection, cells were seeded in 24-well culture plates and were incubated with 10 μM BrdU for 2 h. Cells were then fixed, and BrdU incorporation was detected using a FITC-labeled anti-BrdU antibody (Figure 4-6). Silencing of PTK7 significantly inhibited BrdU incorporation in HCT 116 cells, suggesting a direct effect of PTK7 protein on HCT 116 cell proliferation.

Increase of Apoptosis of PTK7 siRNA-Treated HCT 116 Cells

An Annexin V/PI staining experiment was carried out to study the possibility that knocking down PTK7 could affect the apoptosis of HCT 116 cells. Phosphatidylserine (PS) is located in the inner leaflet of the cell membrane in healthy cells. During

apoptosis, PS becomes translocated to the outer surface of the cell membrane, and Alex 488 labeled Annexin V recognizes the PS on the outer. Propidium iodide (PI) is an intercalating agent and a fluorescent molecule which can be used to stain DNA. PI is membrane impermeant and generally excluded from viable cells so PI is commonly used for identifying dead cells in a population. The results in Figure 4-7 show that the PTK7 siRNA group showed significant increase in apoptotic cells on day 3 and 4 compared with untreated, vehicle, and nonspecific siRNA control groups.

Changes in Mitochondrial Membrane Potential and Activation of Caspase-9

A variety of signalling pathways may be involved in apoptosis, and the mitochondria play a major role in apoptosis signalling. Mitochondrial dysfunction causes mitochondrial membrane potential decrease and the release of cytochrome *c* which activates caspase-9, in turn fueling apoptosis. Dye JC-1 (5,5',6,6'-tetrachloro-1,1',3,3'-tetraethylbenzimidazolylcarbocyanine iodide) was used to determine mitochondrial membrane potential ($\Delta\Psi_m$), the loss of which is regarded as a crucial step in the apoptosis pathway. In healthy cells, intact mitochondria have a negative charge, which allows JC-1 dye with delocalized positive charge to enter the mitochondrial matrix and accumulate there. When the critical concentration is exceeded, JC-1 forms J-aggregates, and cells become fluorescent red (FL2). In apoptotic cells, the mitochondrial membrane potential collapses, and JC-1 cannot accumulate within the mitochondria. In these apoptotic cells, JC-1 remains in the cytoplasm in a green fluorescent monomeric form (FL1).

To study the mechanism through which knocking down PTK7 induces apoptosis in HCT 116 cells, the effect of knocking down PTK7 on $\Delta\Psi_m$ was determined by fluorescence microscopy (Figure 4-8 A) and flow cytometry (Figure 4-8 B). After cells

were transfected with siRNA or control as described above and incubated for 48 h or 72 h, the decrease of $\Delta\Psi_m$ in HCT 116 cells transfected with PTK7 siRNA was observed. After 72 h of transfection, the percentage of cells with intact mitochondria was 90%, 87% and 88% for cells in the untreated, vehicle and nonspecific siRNA groups, respectively. However, only 35% of total cells in the PTK7 siRNA group had intact mitochondria. This trend was seen even at 48 h when only 58% cells had intact mitochondria. These data suggested that mitochondrial dysfunction was involved in the apoptosis induced by PTK7 knockdown.

Caspase-9 are first synthesized as inactive pro-caspase-9 (47 kD) and activated during apoptosis through mitochondrial pathway. Mitochondrial membrane potential decrease causes release of cytochrome *c* which turns inactive pro-caspase-9 into active caspase-9 (37 Kd and 17 kD). Caspase-9 activation was detected by Western blot after HCT 116 cells were transfected with PTK7 siRNA and cultured for 12 h, 24h, 30 h, and 48 h, respectively. As shown in Figure 4-9, caspase-9 was activated and involved in the apoptosis induced by PTK7 knockdown.

Role of Caspase-10 in PTK7-Knockdown-Induced Apoptosis

To determine whether caspases mediate the apoptosis induced by knock down of PTK7, cells were pretreated with a pancaspase inhibitor or one of several single-caspase-specific inhibitors which are short peptides and can bind to the active sites of caspases to inhibit the function of caspases. Rescue of the cells from apoptosis would mean that the inhibited caspase was implicated in PTK7-deficient cell death. After pre-incubation of the HCT 116 cells with 20 μM pancaspase-family inhibitor at 37°C for 3 h, the cells were transfected with siRNA for 48 h. After incubation for 48 h, cell viability was tested using Annexin V/PI (Figure 4-10 A). Cells pre-incubated with pancaspase-

family inhibitor showed good cell viability (80±13%) after transfection with PTK7 siRNA, within uncertainty of the cell viability of the nonspecific siRNA group (83±7.5%). Meanwhile, cells directly transfected with PTK7 siRNA had significantly lower cell viability (36±12%). Pancaspase-family inhibitor blocked all caspase activity and also blocked apoptosis induced by knock down of PTK7, indicating that the apoptosis induced by knockdown of PTK7 is caspase-dependent.

To investigate which caspase plays the critical role in this apoptosis, HCT 116 cells were pre-treated with caspase-9 inhibitor (Z-LEHD-FMK), caspase-3 inhibitor (Z-DEVD-FMK), caspase-8 inhibitor (Z-IETD-FMK), caspase-family inhibitor (Z-VAD-FMK), caspase-1 inhibitor (Z-YVAD-FMK), caspase-10 inhibitor (Z-AEVD-FMK), caspase-2 inhibitor (Z-VDVAD-FMK), or DMSO vehicle at 37°C for 3 h, followed by transfection with PTK7 siRNA. After incubation for 48 h, cell viability was tested by Annexin V/PI using flow cytometry. Fluoromethyl ketone (FMK)-derivatized peptides acted as effective irreversible inhibitors. As shown in Figure 4-10 B, inhibition of caspase-10 blocked apoptosis, with 79±3% of cells viable. This meant that caspse-10 may play a critical role in the apoptotic pathway induced by knock down of PTK7.

To confirm the activation of caspase-10 in apoptosis induced by PTK7 knockdown, procaspase-10 (59 kD) protein levels in cell lysates transfected with PTK7 siRNA were examined using Western blot (Figure 4-11 A). Procaspase-10 decreased after 12 h of transfection and increased after 30 h of transfection. Also, as the linkage between intrinsic pathway and extrinsic pathway, the cleavage of Bid (22 kD) to tBid (15 kD) was investigated, and there was no obvious tBid, indicating that there was no signal transfer from the extrinsic pathway to the intrinsic pathway. In another experiment, PTK7

expression in HCT 116 was initially suggested using PTK7 siRNA, resulting in apoptosis in these cells. The ability of cell lysates to cleave the peptide substrates (AEVD-AFC) was tested as an indicator of caspase-10 activity. AEVD-AFC emits blue light (lmax=400 nm); upon cleavage of the substrate by caspase-10, free AFC emits a yellow-green fluorescence (lmax=505 nm), which can be quantified using a fluorescence microtiter platereader. Comparison of the fluorescence of AFC from PTK7 siRNA treated sample with an untreated control allows determination of the fold increase in AEVD-dependent caspase-10 activity. The results in Figure 4-11 B show significant increase in caspase 10 activity in cells treated with PTK7 siRNA.

p53 involvement in PTK7-knockdown-induced Apoptosis

The protein p53 is a proven a tumor suppressor protein in humans[187], and HCT 116 cells express wide-type p53.[188,189] In order to study the involvement of p53 in the apoptosis induced by PTK7 knockdown, p53-null HCT 116 was used as the second cell line to carry out PTK7 knockdown and other related experiments. First, the PTK7 expression level with or without siRNA treatment was monitored by flow cytometry (Figure. 4-12 A). The p53-null HCT 116 cells express a high amount of PTK7 on the cell membrane, but after 48 hours of PTK7 siRNA transfection, the peak for anti-PTK7-PE in p53-null HCT 116 shifted back to the peak of the background control protein, anti-IgG-PE. This indicated that the PTK7 expression level in p53-null HCT 116 cells transfected with PTK7 siRNA was greatly decreased. Next, the number of live p53-null HCT 116 cells transfected with PTK7 siRNA was shown to be significantly different from that of untreated groups on day 4, demonstrating a significant inhibition of cell viability in p53-null HCT 116 cells by treating with PTK7 siRNA (Figure 4-12 B). And in the BrdU incorporation experiment, silencing of PTK7 significantly inhibited BrdU incorporation in

p53-null HCT 116 cells, suggesting a direct effect of PTK7 protein on cell proliferation (Figure 4-12 C). On the other hand, the Annexin V/PI staining experiment showed that the PTK7 siRNA-treated p53-null HCT 116 showed significant increase in apoptotic and dead cells on day 4 compared with untreated, vehicle, and nonspecific siRNA control groups (Figure 4-12 D).

The apoptosis induced by PTK7 knockdown has been shown to be caspase-10 dependent in wild type HCT 116. So the apoptosis pathway in p53-null HCT 116 induced by PTK7 knockdown was further investigated. JC-1 experiment was monitored by both fluorescence microscopy (Figure 4-13 A) and flow cytometry (Figure 4-13 B). Clearly, mitochondrial membrane potential decreased in p53-null HCT 116 cells treated with PTK7 siRNA. At the same time, a caspase inhibitor experiment was carried out using p53-null HCT 116 cells. As shown in Figure 4-13 C, pancaspase inhibitor or caspase-10 inhibitor treatment inhibited the apoptosis induced by PTK7 knockdown compared to all other inhibitors, which indicated the apoptosis in p53-null HCT 116 cells induced by PTK7 knockdown was also caspased-10 dependent.

Discussion

The present work demonstrates that RNAi suppression of PTK7 induces caspase-10-dependent apoptosis in colon cancer cells. Small interfering RNA is a very popular reverse genetic tool, allowing researchers to identify the role of a protein by inhibiting gene expression through sequence-specific degradation of target mRNA. This study showed that siRNA efficiently suppressed PTK7 expression at the level of both mRNA and protein. A nonspecific siRNA was used as a negative control to confirm that suppression of PTK7 was the result of the specific silencing effect of PTK7 siRNA.

After confirming suppression of PTK7 by siRNA, we then considered whether the inhibition of PTK7 would affect cell viability and proliferation. Trypan Blue Exclusion Assay showed that the number of live HCT 116 cells transfected with PTK7 siRNA was remarkably less than that of the control groups on day 4. Compared to nonspecific siRNA group as negative control, it was clear that suppression of PTK7 accounted for the inhibition of cell viability. To assess the effect of PTK7 knockdown on HCT 116 cell proliferation, a BrdU incorporation experiment was performed to measure DNA synthesis. Interestingly, PTK7 silencing significantly inhibited BrdU incorporation in HCT 116 cells, indicating that knock down of PTK7 expression had a direct effect on HCT 116 cell growth. In fact, PTK7 has been identified as a gene expressed in primary colon carcinoma, and overexpression of PTK7 is often found in colon carcinoma cells. Furthermore, knock down of PTK7 induced cell apoptosis, verified through Annexin V/PI stain. After knock down of PTK7, ratios of apoptotic HCT 116 cells revealed by Annexin V/PI stain, which showed a large increase of percentage of apoptotic HCT 116 cells. These results provide evidence that suppression of PTK7 can significantly increase the occurrence of apoptosis in HCT 116 cells, and that an excess of PTK7 can be associated with resistance of cancer cells to induction of cell death.

The results further demonstrated that knock down of PTK7 caused a large decrease in mitochondrial membrane potential of HCT 116 cells, suggesting that mitochondria dysfunction maybe involved in this apoptosis and that the mitochondrial pathway to cell death may play an important role in apoptosis induced by knock down of PTK7. Caspase-9 was also activated after PTK7 siRNA treatment. At the same time, apoptosis inhibition experiments showed that caspase-10 also plays a critical role in

apoptosis induced by knock down of PTK7. Interestingly, caspase-8 inhibitor had no effect on this apoptosis at all, even though it has always been thought that caspase-8 and caspase-10 play identical roles in the extrinsic pathway to cell death. Western blot was used to examine the procaspase-8, -10 and active caspase-8 levels in PTK7 siRNA-treated cells. Procaspase-10 level changes were significant, but active caspase-8 was not detectable. Additionally, Bid/t-Bid level changes were examined, and no t-Bid was found (Figure 4-11 A), indicating that there was no signal transfer from the extrinsic pathway to the intrinsic pathway. Thus, the extrinsic pathway was not involved as reported by Filomenko P. et al.[165].

Furthermore, p53-null HCT 116 cells were used to study the involvement of p53 in the apoptosis induced by PTK7 knockdown. When treated with PTK7 siRNA, cell proliferation decreased and apoptosis increased in p53-null HCT 116 cells. Also, mitochondria were involved in the apoptosis, which was caspase-10 dependent. When comparing the results between wild type HCT 116 and p53-null HCT 116, PTK7 knockdown had less effect on cell proliferation and apoptosis in p53-null HCT 116 cells, but the apoptosis induced by PTK7 knockdown was caspase-10 dependent in both cell lines. Therefore, the effect of PTK7 knockdown on cell apoptosis was p53 related but not dependent.

Altogether, the results show that the knock down of PTK7 in HCT 116 cells induces cell apoptosis and affects cell proliferation. Also, caspase-10 activation plays a critical role in the caspase cascade downstream of mitochondria after knock down of PTK7.

Conclusion

In conclusion, suppression of PTK7 significantly increases apoptosis and inhibits cell proliferation in HCT 116 cells, indicating that PTK7 may play an important role in maintaining cancer cell viability. Apoptosis induced by knockdown of PTK7 was caspase-10-dependent, and caspase-10 activation was downstream of mitochondrial damage. Therefore, the use of PTK7 siRNA, or other methods that counteract PTK7 function, may be valuable in the development of anticancer therapeutic agents.

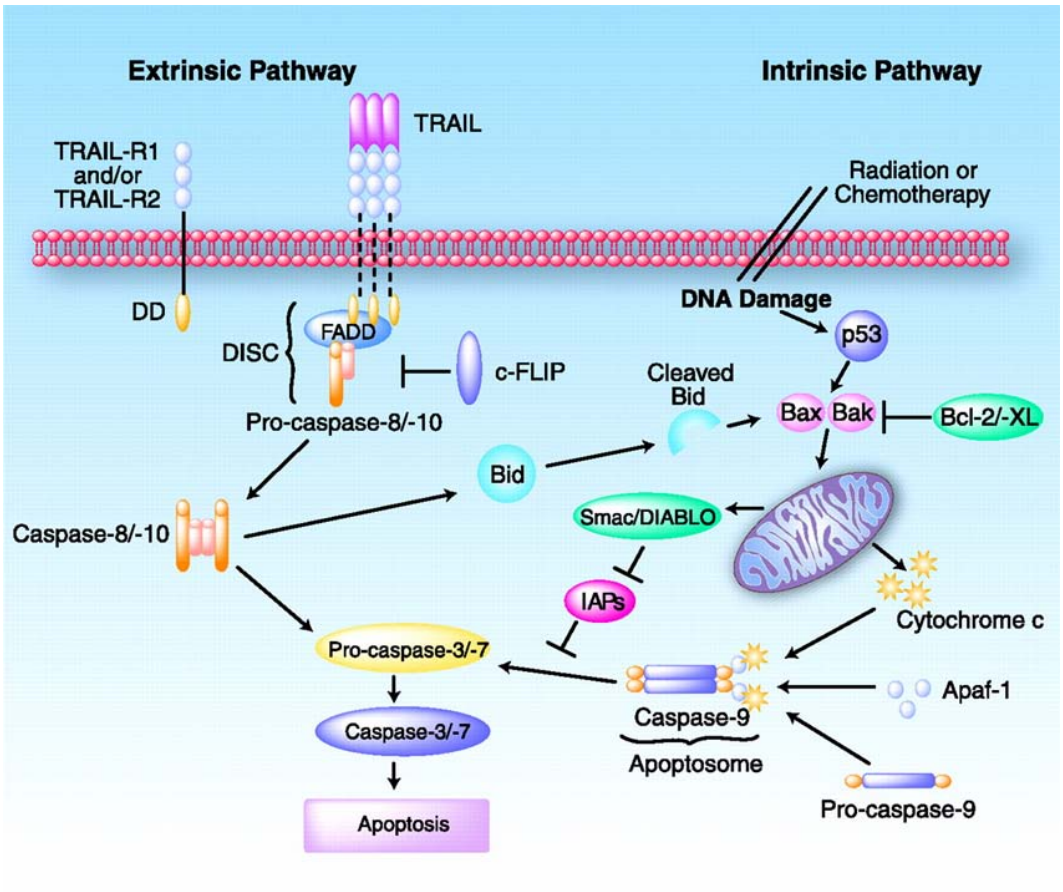

Figure 4-1. Crosstalk between apoptosis signaling pathways following activation of death receptors. Death receptors trigger the cell-intrinsic pathway by activation of caspase-8 and caspase-10. Cleaved BID interacts with Bax and Bak, which in turn, activate caspase-9 and caspase-3, resulting in apoptosis induction through the cell-extrinsic pathway.[161] (copyright permission acquired)

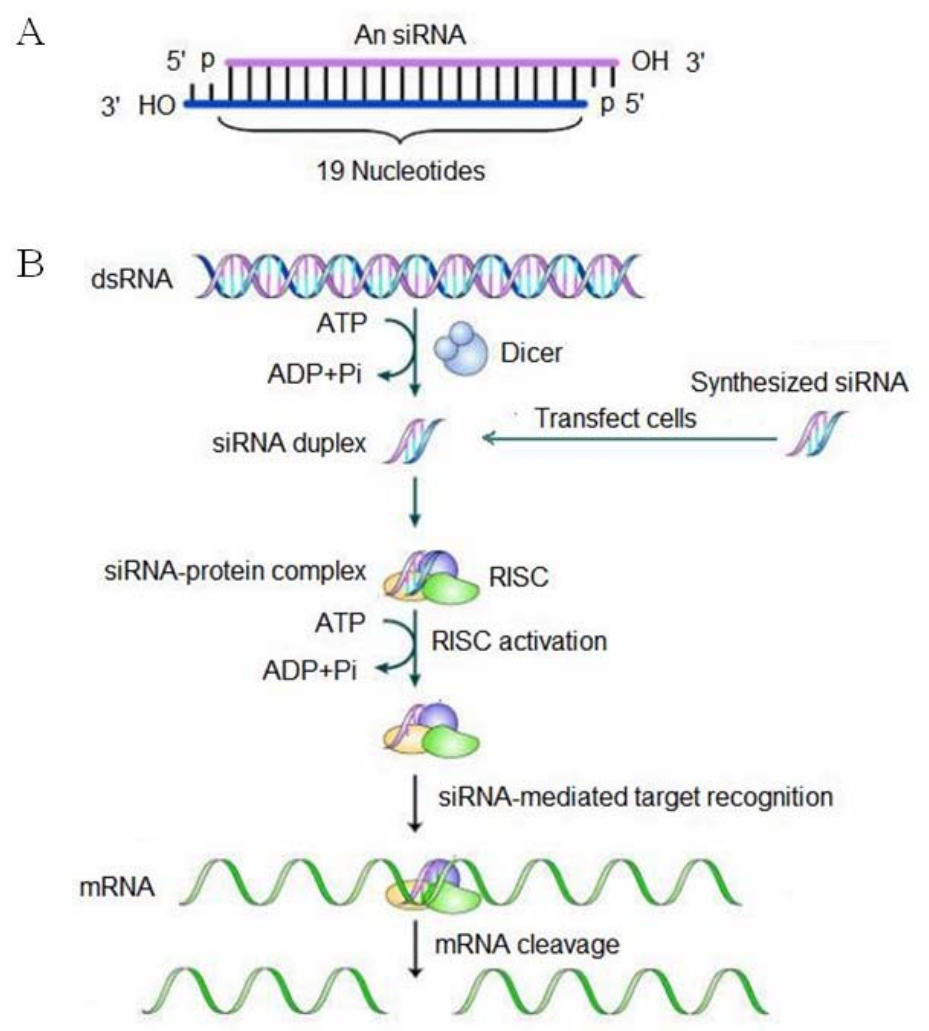

Figure 4-2. (A) Short interfering (si)RNAs. Molecular hallmarks of an siRNA include 5' phosphorylated ends, a 19-nucleotide (nt) duplexed region and 2-nt unpaired and unphosphorylated 3' ends that are characteristic of RNase III cleavage products.[190] (B) The siRNA pathway. Long double-stranded (ds)RNA is cleaved by the RNase III family member, Dicer, into siRNAs in an ATP-dependent reaction104. These siRNAs are then incorporated into the RNA-inducing silencing complex (RISC). Although the uptake of siRNAs by RISC is independent of ATP, the unwinding of the siRNA duplex requires ATP. Once unwound, the single-stranded antisense strand guides RISC to messenger RNA that has a complementary sequence, which results in the endonucleolytic cleavage of the target mRNA.[191] (copyright permission acquired)

Table 4-1. RT-PCR preparation

Component	Volume per reaction
2X SYBR® Green RT-PCR Reaction Mix	25 µL
PTK7 Forward primer (10 µM)	1.5 µL
PTK7 Reverse primer (10 µM)	1.5 µL
Nuclease-free H_2O	X µL
RNA template (50 ng mRNA)	X µL
RNA template (1 pg to 100 ng total RNA)	1 µL
Total Volume	50 µL

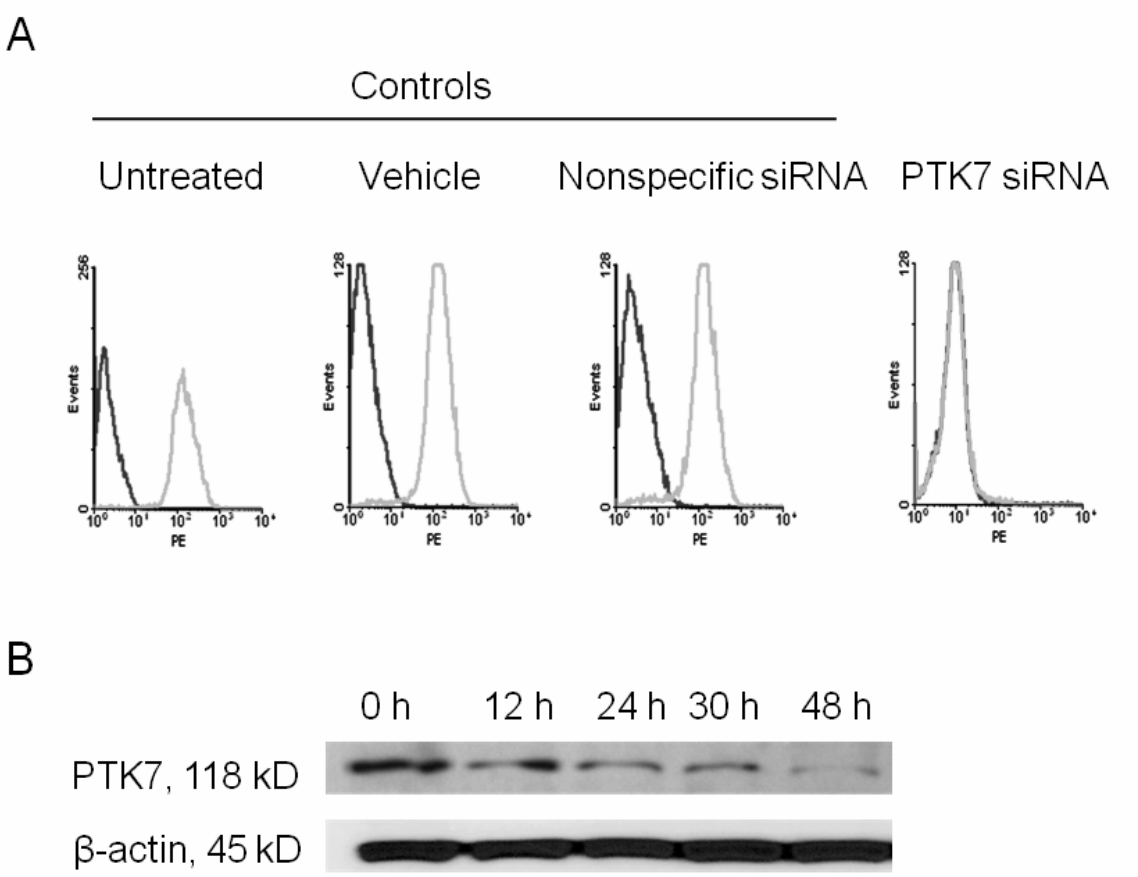

Figure 4-3. PTK7 expression in HCT 116 cells after treatment with vehicle, nonspecific siRNA and PTK7 siRNA. (A) Flow cytometry assay for the binding of the PE-labeled anti-PTK7 with HCT 116 cells (Grey curves). The black curves represent the background binding of anti-IgG-PE. The concentration of the antibody in the binding buffer was 2 µg/µL. (B) Western blot analysis of PTK7 in HCT 116 cells transfected by PTK7 siRNAs. The membrane was stripped and reprobed by β-actin antibody as a loading control.

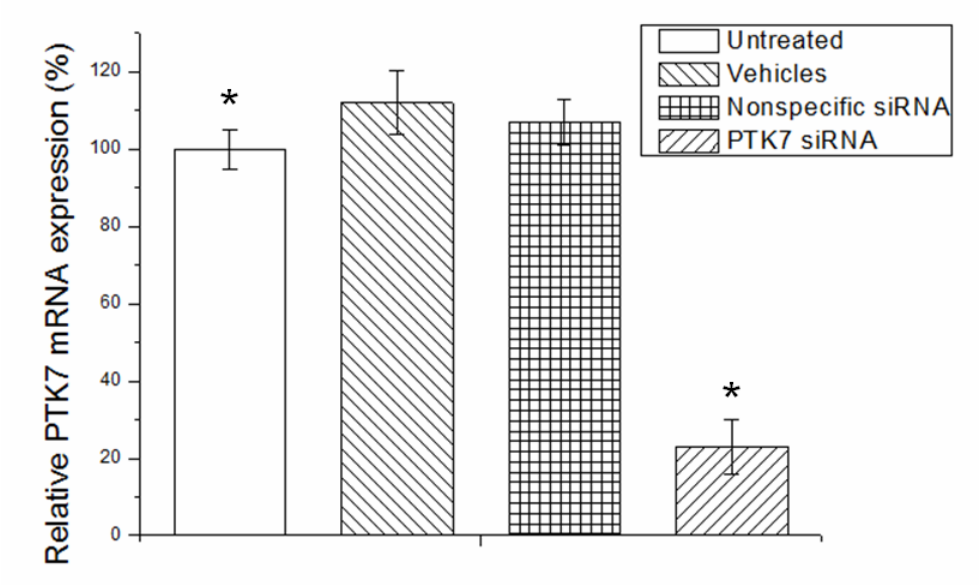

Figure 4-4. Suppression of PTK7 mRNA expression in HCT 116 cells by PTK7 siRNAs. Cells were harvested after 48 h of treatment. RT-PCR was performed using gene-specific primers. The amount of PTK7 mRNA expression was normalized to the untreated group. Data are mean±s.d. of three independent experiments. *Student's t-test: $P<0.05$.

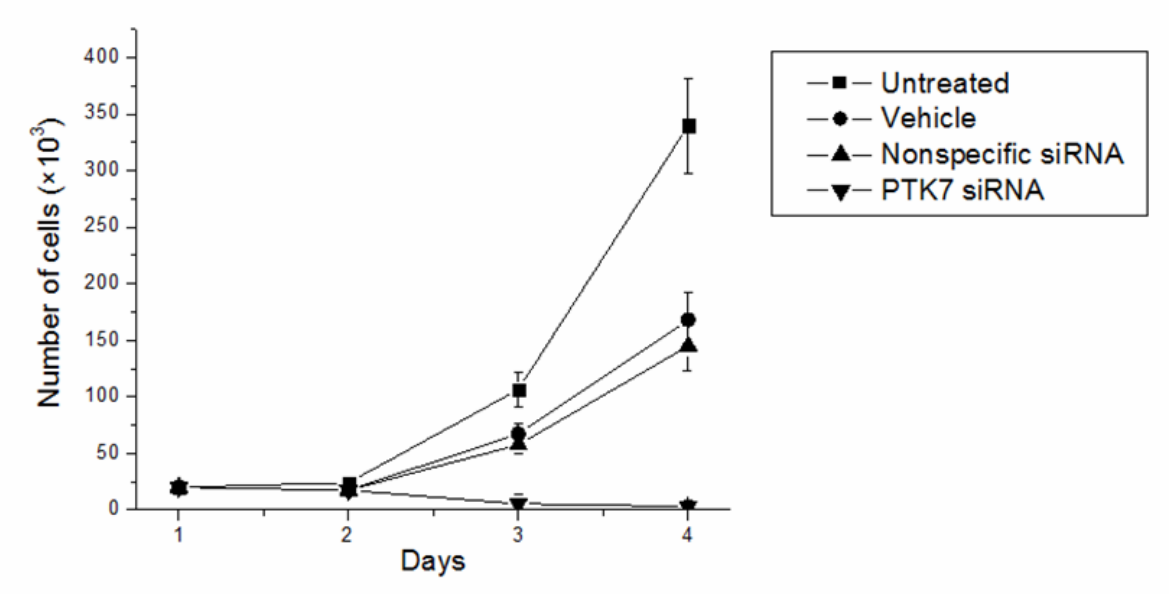

Figure 4-5. Cell viability in HCT 116 cells after treatment with vehicle, nonspecific siRNA and PTK7 siRNA. Data are mean±s.d. of three independent experiments. The number of live cells was counted daily for 4 days using Trypan blue

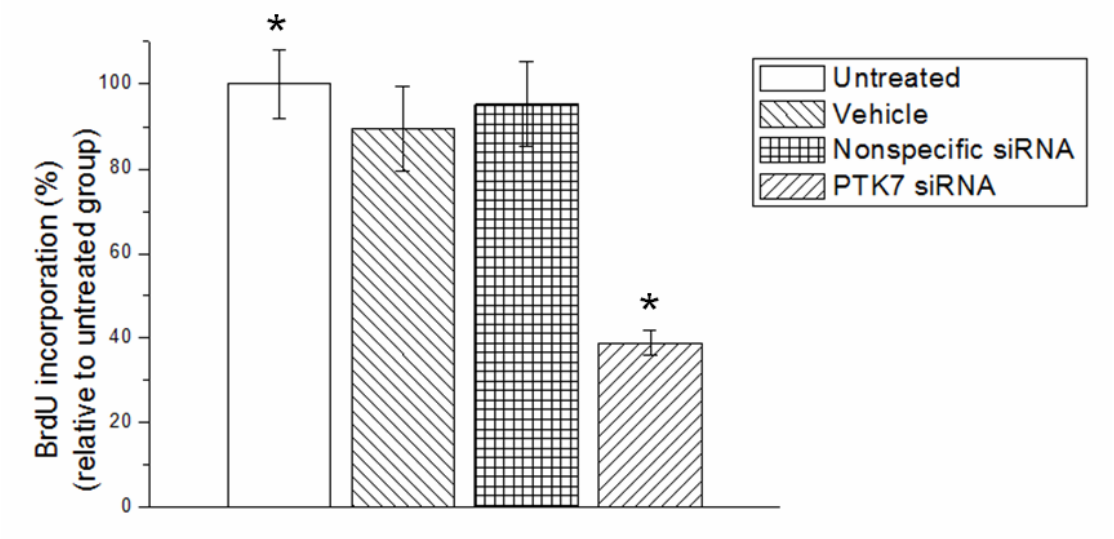

Figure 4-6. BrdU incorporation relative to untreated cells detected by flow cytometry. Cells were incubated with 10 μM BrdU for 2 h after 48 h of treatment. Data are mean±s.d. of three independent experiments. *Student's t-test: P<0.05.

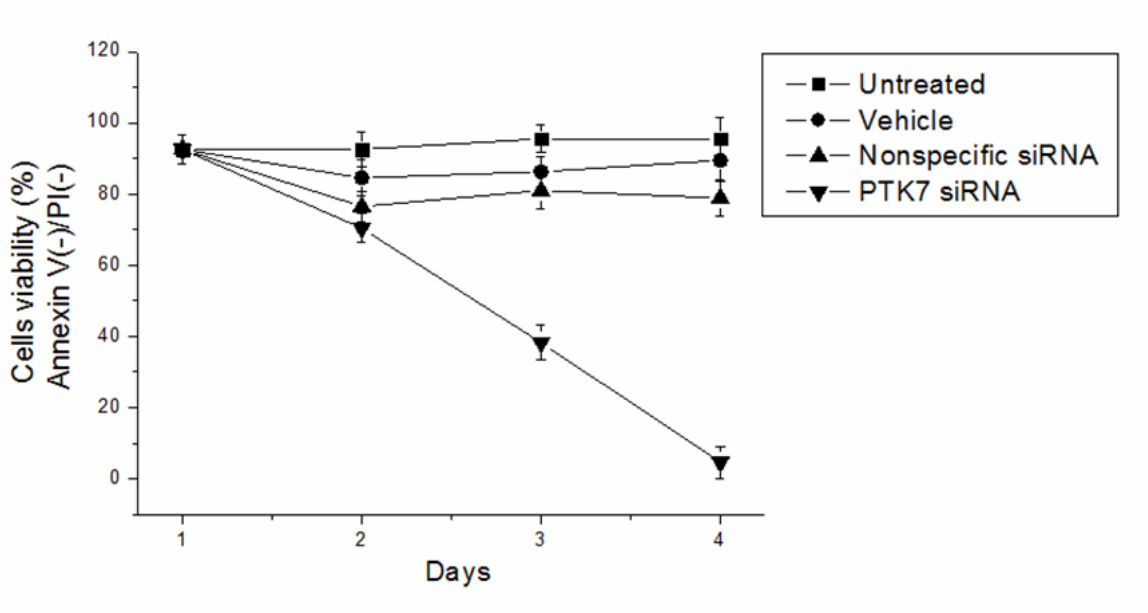

Figure 4-7. Apoptosis occurrence in HCT 116 cells detected by Annexin V/PI stain on days 1-4 after transfection. Cells stained negative for both Annexin V and PI were considered healthy.

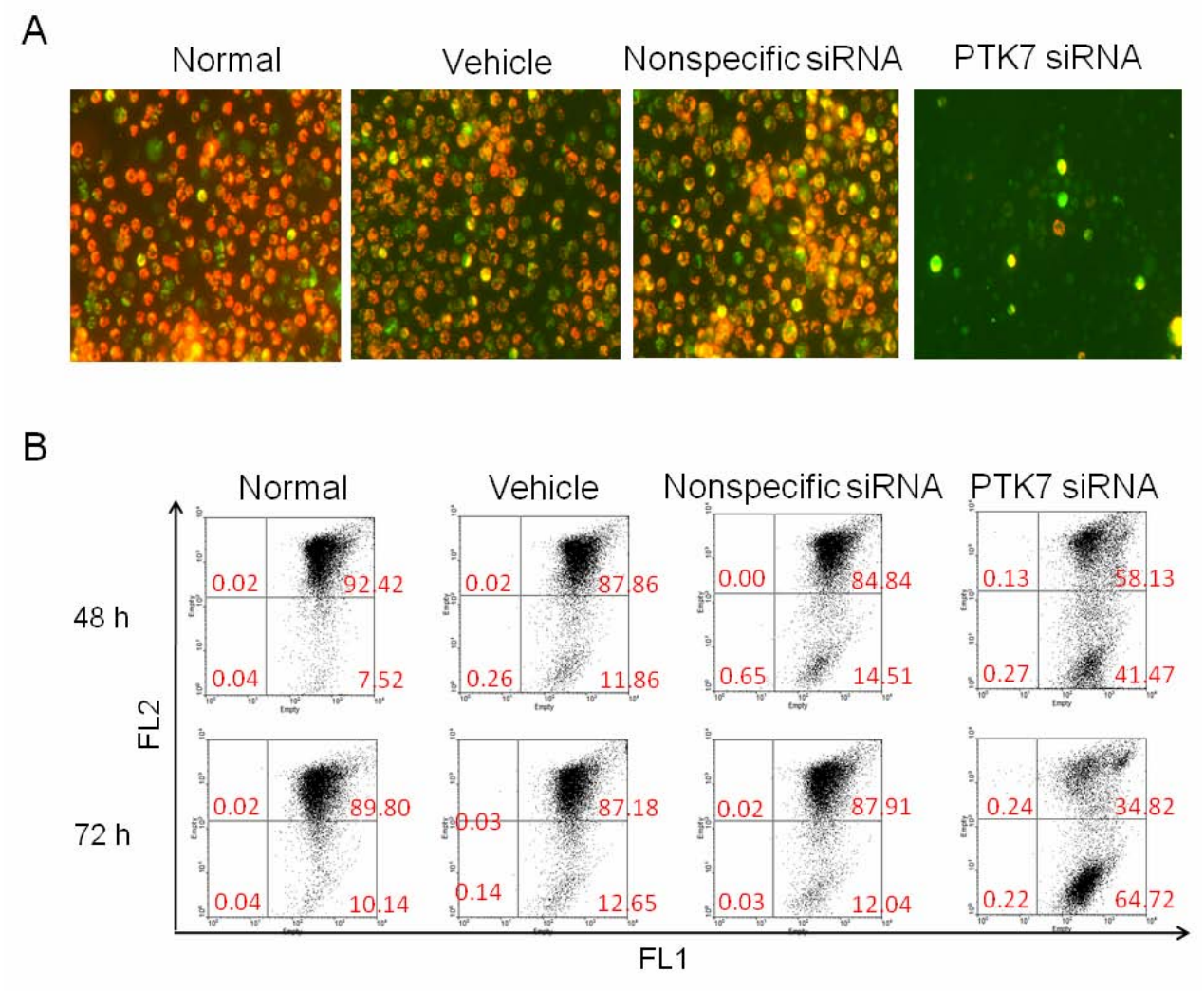

Figure 4-8. Involvement of mitochondrial pathway in apoptosis induced by PTK7 scilencing. (A) Fluorescence microscope detection of mitochondrial membrane potential in treated HCT 116 cells. (B) Flow cytometry detection of mitochondrial membrane potential in treated HCT 116 cells.

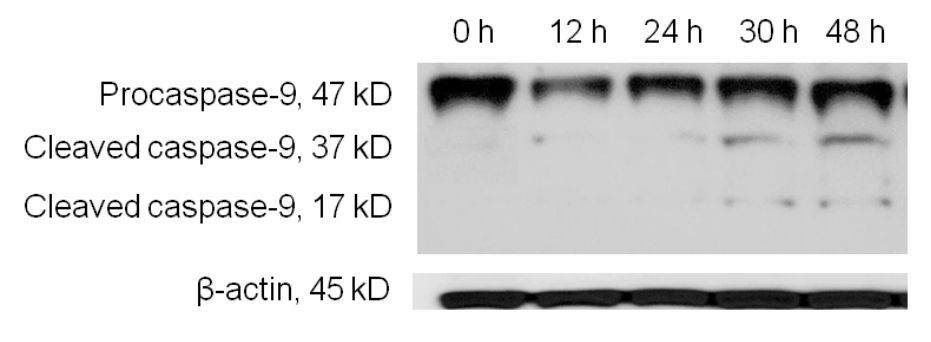

Figure 4-9. Activation of caspase-9 involved in apoptosis induced by knocking down PTK7. The membrane was stripped and reprobed by β-actin antibody, as a loading control.

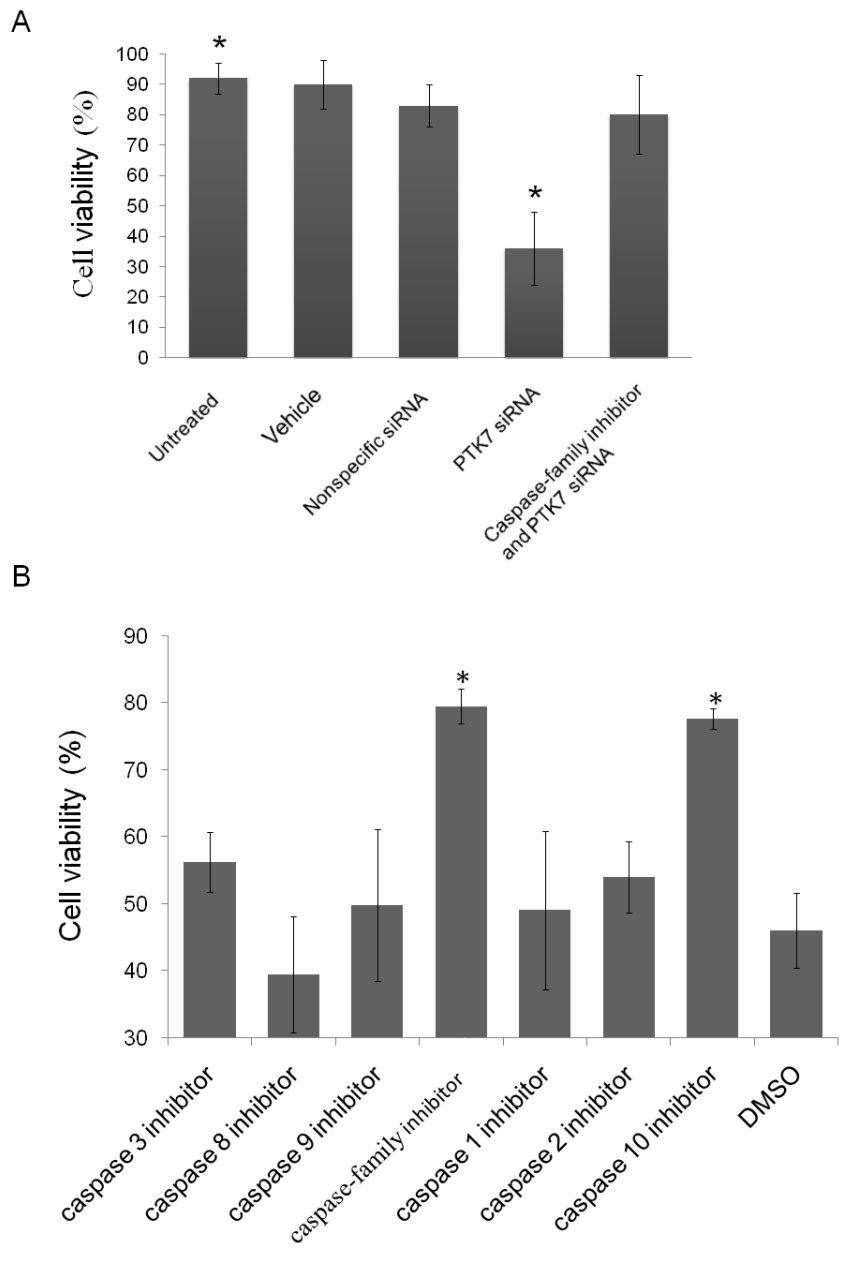

Figure 4-10. Cell viability after incubation with caspase inhibitors prior to transfection of PTK7 siRNA. (A) Apoptosis induced by knocking down PTK7 was caspase-dependent. Data are mean±s.d. of three independent experiments. (B) Caspase-10 inhibitor totally blocked the apoptosis induced by knock down of PTK7. Data: mean±s.d. of three independent experiments, *Student's t-test: $P<0.05$.

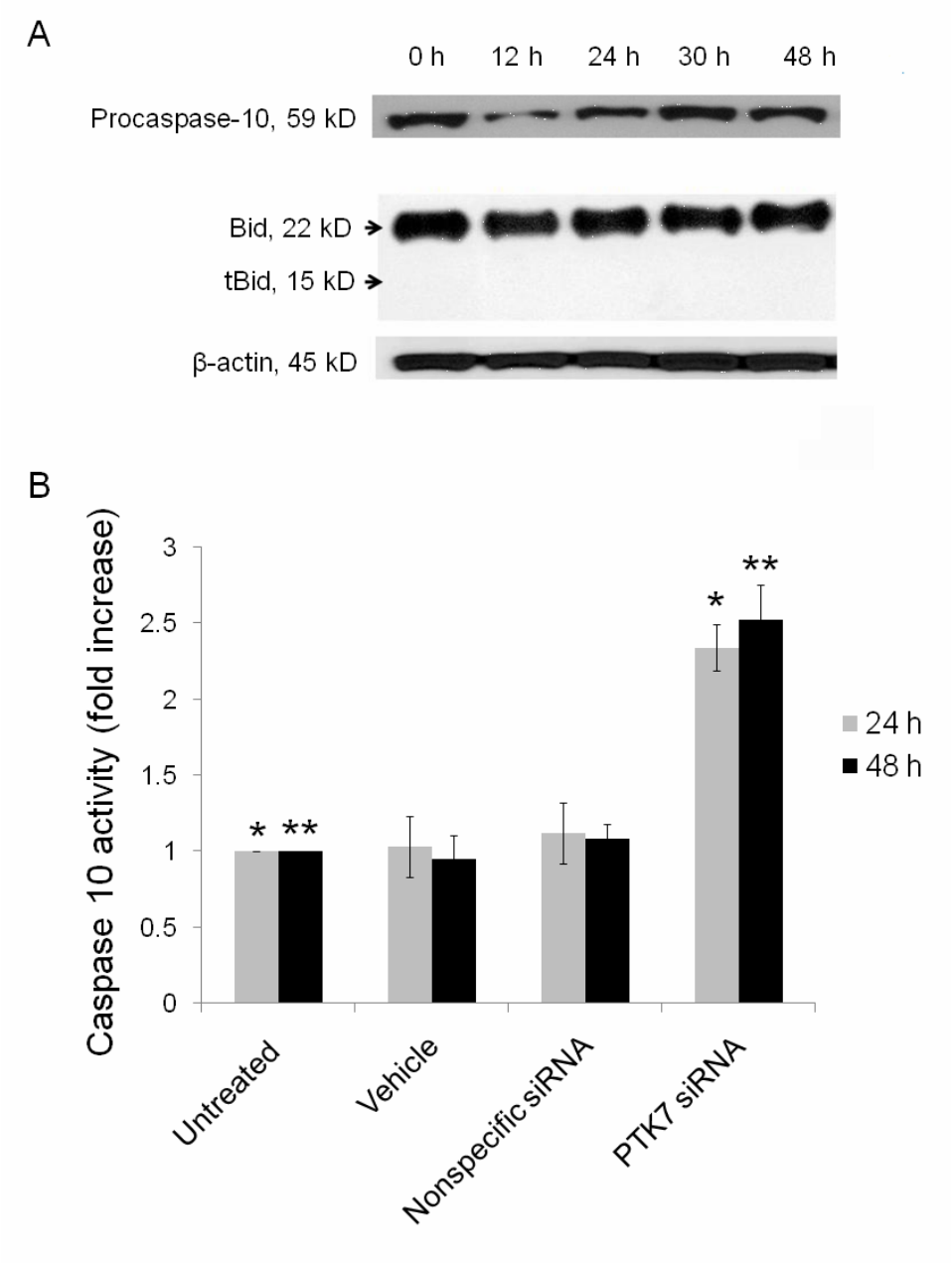

Figure 4-11. The activation of caspase-10 in apoptosis induced by knocking down of PTK7. (A) Western blot analysis of procaspase-10 and Bid in HCT 116 cells transfected by PTK7 siRNAs. The membrane was stripped and reprobed by β-actin antibody, as a loading control. (B) Caspase-10 activity in HCT 116 cells: untreated and treated with vehicle, nonspecific siRNA and siRNA. Results were given as ratios to caspase-10 activity in untreated cells. Data are mean±s.d. of three independent experiments. *Student's t-test: $P<0.05$.

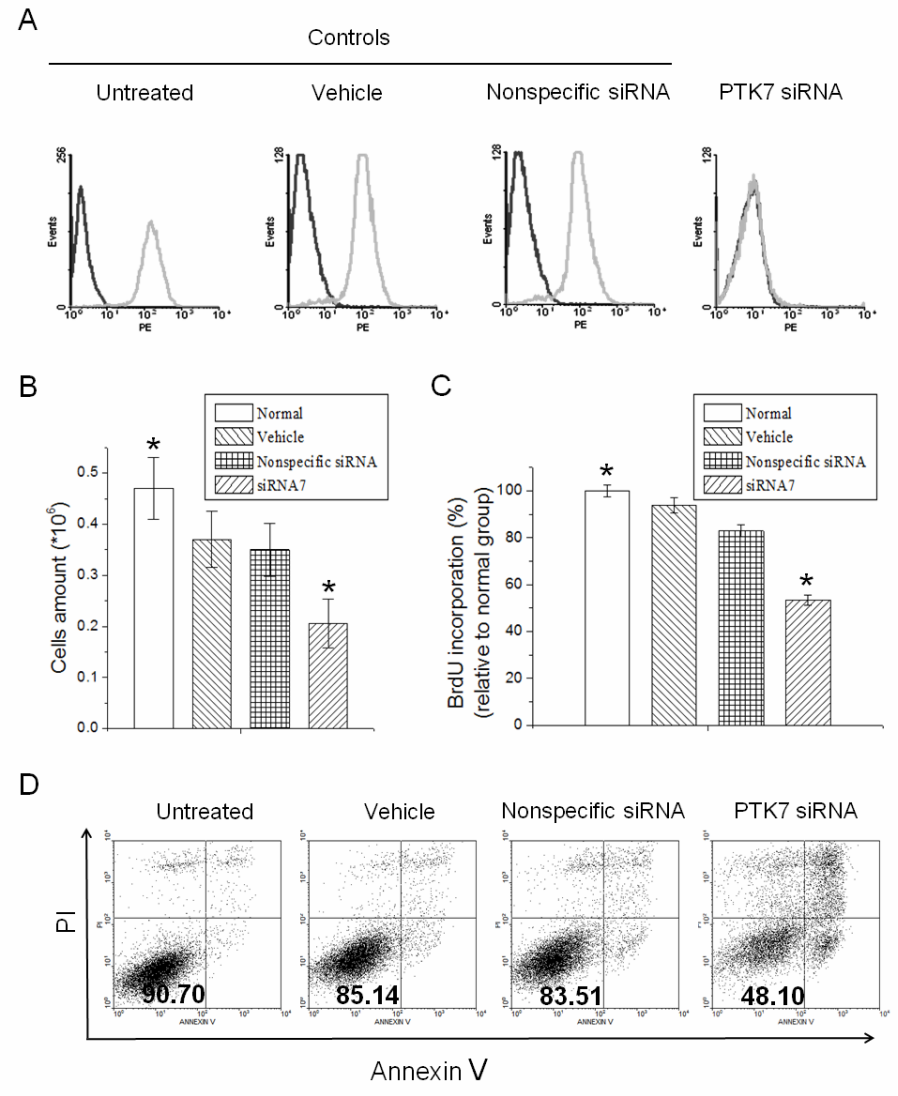

Figure 4-12. PTK7 expression and cell apoptosis induced by knocking down of PTK7 in p53-null HCT 116 cells. (A) Flow cytometry assay for the binding of the PE-labeled anti-PTK7 with p53-null HCT 116 cells (Grey curves). The black curves represent the background binding of anti-IgG-PE. The concentration of the antibody in the binding buffer was 2 μg/μL. (B) The number of live p53-null HCT 116 cells was counted on day 4 after treatment with vehicle, nonspecific siRNA and PTK7 siRNA. Data are mean±s.d. of three independent experiments. *Student's t-test: $P<0.05$. (C) BrdU incorporation relative to untreated cells detected by flow cytometry. p53-null HCT 116 Cells were incubated with 10 μM BrdU for 2 h after 48 h of treatment. The amount of BrdU incorporation was normalized to the untreated group. Data are mean±s.d. of three independent experiments. *Student's t-test: $P<0.05$. (D) Apoptosis occurrence in p53-null HCT 116 cells detected by Annexin V/PI stain on days 4 after transfection. Cells stained negative for both Annexin V and PI were considered healthy and percentage was shown in the Figure.

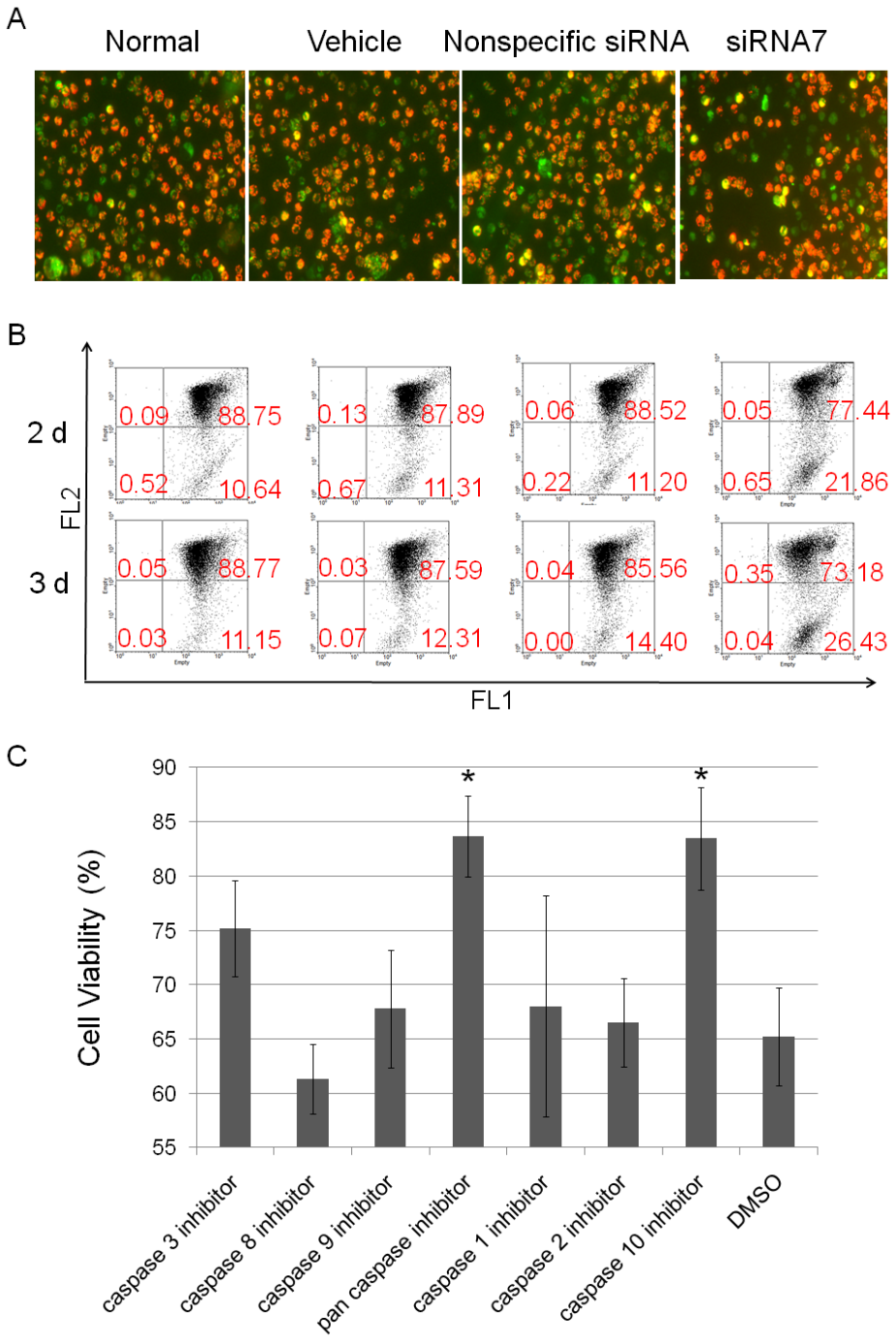

Figure 4-13. Mitochondria and caspase-10 involvement in the apoptosis induced by knocking down of PTK7 in p53-null HCT 116 cells. (A) Fluorescence microscope detection of mitochondrial membrane potential in treated p53-null HCT 116 cells. (B) Flow cytometry detection of mitochondrial membrane potential in treated p53-null HCT 116 cells. (C) Cell viability after incubation with caspase inhibitors prior to transfaction of PTK7 siRNA. Caspase-10 inhibitor totally blocked the apoptosis induced by knock down of PTK7. Data: mean±s.d. of three independent experiments, *Student's t-test: $P<0.05$.

CHAPTER 5
SUMMARY AND FUTURE PLAN

Currently cancer classification, monitoring, diagnosis, and therapy are a major driver of research in the world. Considering all the properties and advantages of aptamers, they will be an unparalleled tool in cancer-related research. In this dissertation, we have successfully developed a panel of useful high affinity aptamers for liver cancer cells, achieved targeted drug delivery using a modified aptamer, and discovered the functional role of a biomarker in cancer cell apoptosis and proliferation.

In Chapter 2, we demonstrated that cell-SELEX could produce a group of cell-specific aptamers for adherent cells. The selection process is reproducible, simple, and straightforward, and seven effective aptamers have been successfully generated for a live liver cancer cell line with K_ds in the nM range. Flow cytometry assays and confocal imaging show that the selected aptamers not only recognize the target liver cancer cells specifically, but also do not bind to its parent liver cells, BNL CL.2. The close relationship between BNL 1ME A.7R.1 cells and BNL CL.2 cells indicates that cell-SELEX can be used to identify minor molecular level differences among cells. The cell-SELEX shows that the newly generated aptamers could be excellent molecular probes for liver cancer analysis and diagnosis. It further indicates that the target molecules could be specific biomarkers for this kind of liver cancer, and would provide useful information for explaining the mechanism of oncogenesis.

In Chapter 3, a targeted drug delivery platform was investigated. By making use of the ability of anthracycline drugs to intercalate between bases of nucleotides, a TLS11a-GC-Dox conjugate was made, and the specificity and efficacy of this conjugate to serve as a drug-delivery platform was further demonstrated *in vitro* and *in vivo*. The modified

aptamer retains its specificity and can load much more Dox than the unmodified aptamer. The specificity of this system was further demonstrated by treatment of human normal liver cells, which lack the aptamer binding target. The aptamer-Dox conjugate prevents the nonspecific uptake of Dox, decreasing cellular toxicity to non-target cells, and potentially reducing side-effects increasing the therapeutic index for the drug. Furthermore, the *in vivo* experiment showed better tumor inhibition by the TLS11a-GC-Dox group compared to all other control groups, indicating the successful delivery of Dox by the modified aptamer. This targeting specificity assured a higher local Dox concentration in the tumor. In addition, aptamer-Dox conjugates are smaller than antibody-based drug delivery systems, allowing faster penetration and fewer immunoreactions. We anticipate that the design of aptamer modification and aptamer-Dox conjugation platform technology based on the intercalation of anthracyclines may be utilized in distinct ways to develop novel targeted therapeutic modalities for more effective cancer chemotherapy.

In Chapter 4, the functional role of a biomarker, PTK7, was investigated by siRNA silencing. Suppression of PTK7 significantly increases apoptosis and inhibits cell proliferation in HCT 116 cells, indicating that PTK7 may play an important role in maintaining cancer cell viability. Apoptosis induced by knock down of PTK7 was caspase-10-dependent, and caspase-10 activation was downstream of mitochondrial damage. Therefore, the use of PTK7 siRNA, or other methods that counteracts PTK7 function, may be valuable in the development of cancer therapeutic agents.

Future Work

Biomarker Discovery

Cell membrane proteins are of considerable interest for diseases diagnosis and therapeutic applications, so it is important to identify these proteins of interest. A lot of approaches have been investigated to achieve this, such as antibodies. However most of these antibody targets are also expressed on normal cells, which limit their relevance in diagnostic and therapeutic applications. Therefore, it is important to identify unknown biomarkers with differential expression on cancer cells as opposed to healthy ones. One of the advantages of cell-SELEX is its ability to develop molecular probes for upregulated or unique targets without prior knowledge of the identity of those targets. The target of an aptamer can be identified through affinity precipitation and subsequent polyacrylamide gel electrophoresis (PAGE) and mass spectrometry.[76,77] Once the targets of these aptamers are identified, they will provide an opportunity to expand the aptamer‘s application.

So far, a lot of effort has been made to identify the target protein of aptamer TLS11a, but we have not yet been successful. In the future, we will try cross-linking to increase the interaction between the aptamer and target protein. This method was used to find the target to TD05, IgM in Ramos cells, and the scheme for that method is shown in Figure 5-1. Briefly, aptamer TLS11a will be modified with biotin and photoactive 5-dUI, which will facilitate the cross-linking between TLS11a and the target protein and help to maintain the aptamer-protein complex through the cell membrane protein isolation and solubilization. Then the aptamer-protein complex will be extracted by streptavidin conjugated magnetic beads. The enriched proteins will then be separated by PAGE and identified by mass spectrometry.[77]

Clinical Application

There is always a concern whether cell culture data can be translated to real clinical samples. Though cultured cells can grow unchecked and proliferate rapidly, providing readily assessable tumor specimen in cancer research, established cell lines often change in morphology and protein expression from their parental tumor as a result of their isolation and maintenance outside the body. Furthermore, creating a useful test to define a cancer type usually requires multiple cancer-specific molecular probes. In view of this, to really assess the real-world applicability of our selected liver cancer, theyneed to be tested on real clinical samples.

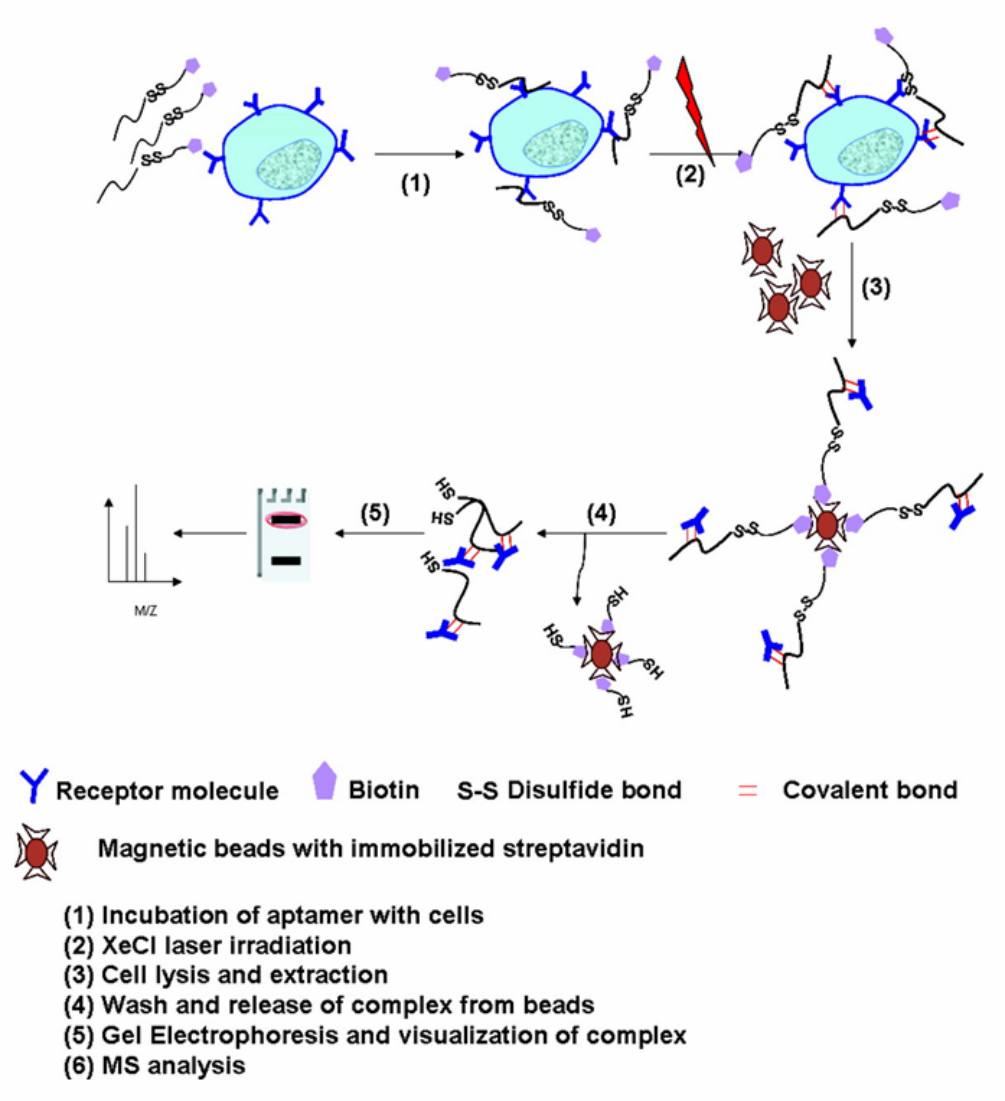

Figure 5-1. Outline of the protocol for the identification of IGHM on Ramos cells using selected aptamers targeting whole cells.[77]

LIST OF REFERENCES

(1) Anand, P.; Kunnumakkara, A. B.; Sundaram, C.; Harikumar, K. B.; Tharakan, S. T.; Lai, O. S.; Sung, B.; Aggarwal, B. B. *Pharm Res* **2008**, *25*, 2097-116.

(2) Society, A. C. *Cancer Facts & Figures* **2010**.

(3) Weber, B. L. *Cancer Cell* **2002**, *1*, 37-47.

(4) Ferrando, A. A.; Neuberg, D. S.; Staunton, J.; Loh, M. L.; Huard, C.; Raimondi, S. C.; Behm, F. G.; Pui, C. H.; Downing, J. R.; Gilliland, D. G.; Lander, E. S.; Golub, T. R.; Look, A. T. *Cancer Cell* **2002**, *1*, 75-87.

(5) Golub, T. R.; Slonim, D. K.; Tamayo, P.; Huard, C.; Gaasenbeek, M.; Mesirov, J. P.; Coller, H.; Loh, M. L.; Downing, J. R.; Caligiuri, M. A.; Bloomfield, C. D.; Lander, E. S. *Science* **1999**, *286*, 531-7.

(6) Alizadeh, A. A.; Eisen, M. B.; Davis, R. E.; Ma, C.; Lossos, I. S.; Rosenwald, A.; Boldrick, J. C.; Sabet, H.; Tran, T.; Yu, X.; Powell, J. I.; Yang, L.; Marti, G. E.; Moore, T.; Hudson, J., Jr.; Lu, L.; Lewis, D. B.; Tibshirani, R.; Sherlock, G.; Chan, W. C.; Greiner, T. C.; Weisenburger, D. D.; Armitage, J. O.; Warnke, R.; Levy, R.; Wilson, W.; Grever, M. R.; Byrd, J. C.; Botstein, D.; Brown, P. O.; Staudt, L. M. *Nature* **2000**, *403*, 503-11.

(7) Basso, K.; Liso, A.; Tiacci, E.; Benedetti, R.; Pulsoni, A.; Foa, R.; Di Raimondo, F.; Ambrosetti, A.; Califano, A.; Klein, U.; Dalla Favera, R.; Falini, B. *J Exp Med* **2004**, *199*, 59-68.

(8) Osborne, C. K.; Hamilton, B.; Titus, G.; Livingston, R. B. *Cancer Res* **1980**, *40*, 2361-6.

(9) Olsson, A. K.; Dimberg, A.; Kreuger, J.; Claesson-Welsh, L. *Nat Rev Mol Cell Biol* **2006**, *7*, 359-71.

(10) Ariad, S.; Seymour, L.; Bezwoda, W. R. *Breast Cancer Res Treat* **1991**, *20*, 11-7.

(11) Chan, J. M.; Stampfer, M. J.; Giovannucci, E.; Gann, P. H.; Ma, J.; Wilkinson, P.; Hennekens, C. H.; Pollak, M. *Science* **1998**, *279*, 563-6.

(12) Hosen, N.; Park, C. Y.; Tatsumi, N.; Oji, Y.; Sugiyama, H.; Gramatzki, M.; Krensky, A. M.; Weissman, I. L. *Proc Natl Acad Sci U S A* **2007**, *104*, 11008-13.

(13) Hopkins, A. L.; Groom, C. R. *Nat Rev Drug Discov* **2002**, *1*, 727-30.

(14) Zola, H. *Mol Med* **2006**, *12*, 312-6.

(15) Osborne, S. E.; Ellington, A. D. *Chem Rev* **1997**, *97*, 349-370.

(16) Ciesiolka, J.; Yarus, M. *RNA* **1996**, *2*, 785-93.

(17) Hofmann, H. P.; Limmer, S.; Hornung, V.; Sprinzl, M. *RNA* **1997**, *3*, 1289-300.

(18) Rajendran, M.; Ellington, A. D. *Anal Bioanal Chem* **2008**, *390*, 1067-75.

(19) Geiger, A.; Burgstaller, P.; von der Eltz, H.; Roeder, A.; Famulok, M. *Nucleic Acids Res* **1996**, *24*, 1029-36.

(20) Connell, G. J.; Illangesekare, M.; Yarus, M. *Biochemistry* **1993**, *32*, 5497-502.

(21) Harada, K.; Frankel, A. D. *EMBO J* **1995**, *14*, 5798-811.

(22) Wallis, M. G.; Streicher, B.; Wank, H.; von Ahsen, U.; Clodi, E.; Wallace, S. T.; Famulok, M.; Schroeder, R. *Chem Biol* **1997**, *4*, 357-66.

(23) Wallace, S. T.; Schroeder, R. *RNA* **1998**, *4*, 112-23.

(24) Nieuwlandt, D.; Wecker, M.; Gold, L. *Biochemistry* **1995**, *34*, 5651-9.

(25) Williams, K. P.; Liu, X. H.; Schumacher, T. N.; Lin, H. Y.; Ausiello, D. A.; Kim, P. S.; Bartel, D. P. *Proc Natl Acad Sci U S A* **1997**, *94*, 11285-90.

(26) Tuerk, C.; MacDougal, S.; Gold, L. *Proc Natl Acad Sci U S A* **1992**, *89*, 6988-92.

(27) Chen, H.; McBroom, D. G.; Zhu, Y. Q.; Gold, L.; North, T. W. *Biochemistry* **1996**, *35*, 6923-30.

(28) Dang, C.; Jayasena, S. D. *J Mol Biol* **1996**, *264*, 268-78.

(29) Kubik, M. F.; Stephens, A. W.; Schneider, D.; Marlar, R. A.; Tasset, D. *Nucleic Acids Res* **1994**, *22*, 2619-26.

(30) Green, L. S.; Jellinek, D.; Jenison, R.; Ostman, A.; Heldin, C. H.; Janjic, N. *Biochemistry* **1996**, *35*, 14413-24.

(31) Wiegand, T. W.; Williams, P. B.; Dreskin, S. C.; Jouvin, M. H.; Kinet, J. P.; Tasset, D. *J Immunol* **1996**, *157*, 221-30.

(32) Davis, K. A.; Lin, Y.; Abrams, B.; Jayasena, S. D. *Nucleic Acids Res* **1998**, *26*, 3915-24.

(33) Smith, D.; Kirschenheuter, G. P.; Charlton, J.; Guidot, D. M.; Repine, J. E. *Chem Biol* **1995**, *2*, 741-50.

(34) Mallikaratchy, P.; Stahelin, R. V.; Cao, Z.; Cho, W.; Tan, W. *Chem Commun (Camb)* **2006**, 3229-31.

(35) Mendonsa, S. D.; Bowser, M. T. *Anal Chem* **2004**, *76*, 5387-92.

(36) Morris, K. N.; Jensen, K. B.; Julin, C. M.; Weil, M.; Gold, L. *Proc Natl Acad Sci U S A* **1998**, *95*, 2902-7.

(37) Hicke, B. J.; Marion, C.; Chang, Y. F.; Gould, T.; Lynott, C. K.; Parma, D.; Schmidt, P. G.; Warren, S. *J Biol Chem* **2001**, *276*, 48644-54.

(38) Wang, C.; Zhang, M.; Yang, G.; Zhang, D.; Ding, H.; Wang, H.; Fan, M.; Shen, B.; Shao, N. *J Biotechnol* **2003**, *102*, 15-22.

(39) Cerchia, L.; Duconge, F.; Pestourie, C.; Boulay, J.; Aissouni, Y.; Gombert, K.; Tavitian, B.; de Franciscis, V.; Libri, D. *PLoS Biol* **2005**, *3*, e123.

(40) Shangguan, D.; Cao, Z. C.; Li, Y.; Tan, W. *Clin Chem* **2007**, *53*, 1153-5.

(41) Shangguan, D.; Meng, L.; Cao, Z. C.; Xiao, Z.; Fang, X.; Li, Y.; Cardona, D.; Witek, R. P.; Liu, C.; Tan, W. *Anal Chem* **2008**, *80*, 721-8.

(42) Tang, Z.; Shangguan, D.; Wang, K.; Shi, H.; Sefah, K.; Mallikratchy, P.; Chen, H. W.; Li, Y.; Tan, W. *Anal Chem* **2007**, *79*, 4900-7.

(43) Chen, H. W.; Medley, C. D.; Sefah, K.; Shangguan, D.; Tang, Z.; Meng, L.; Smith, J. E.; Tan, W. *ChemMedChem* **2008**, *3*, 991-1001.

(44) Sefah, K.; Tang, Z. W.; Shangguan, D. H.; Chen, H.; Lopez-Colon, D.; Li, Y.; Parekh, P.; Martin, J.; Meng, L.; Phillips, J. A.; Kim, Y. M.; Tan, W. H. *Leukemia* **2009**, *23*, 235-44.

(45) Pan, W.; Craven, R. C.; Qiu, Q.; Wilson, C. B.; Wills, J. W.; Golovine, S.; Wang, J. F. *Proc Natl Acad Sci U S A* **1995**, *92*, 11509-13.

(46) Kumar, P. K.; Machida, K.; Urvil, P. T.; Kakiuchi, N.; Vishnuvardhan, D.; Shimotohno, K.; Taira, K.; Nishikawa, S. *Virology* **1997**, *237*, 270-82.

(47) Misono, T. S.; Kumar, P. K. *Anal Biochem* **2005**, *342*, 312-7.

(48) Gopinath, S. C.; Misono, T. S.; Kawasaki, K.; Mizuno, T.; Imai, M.; Odagiri, T.; Kumar, P. K. *J Gen Virol* **2006**, *87*, 479-87.

(49) Tang, Z.; Parekh, P.; Turner, P.; Moyer, R. W.; Tan, W. *Clin Chem* **2009**, *55*, 813-22.

(50) Bruno, J. G.; Kiel, J. L. *Biosens Bioelectron* **1999**, *14*, 457-64.

(51) Hamula, C. L.; Zhang, H.; Guan, L. L.; Li, X. F.; Le, X. C. *Anal Chem* **2008**, *80*, 7812-9.

(52) Ellington, A. D.; Szostak, J. W. *Nature* **1990**, *346*, 818-22.

(53) Gopinath, S. C. *Anal Bioanal Chem* **2007**, *387*, 171-82.

(54) Chou, S. H.; Chin, K. H.; Wang, A. H. *Nucleic Acids Res* **2003**, *31*, 2461-74.

(55) Fang, X.; Sen, A.; Vicens, M.; Tan, W. *Chembiochem* **2003**, *4*, 829-34.

(56) Guo, K.; Wendel, H. P.; Scheideler, L.; Ziemer, G.; Scheule, A. M. *J Cell Mol Med* **2005**, *9*, 731-6.

(57) Daniels, D. A.; Chen, H.; Hicke, B. J.; Swiderek, K. M.; Gold, L. *Proc Natl Acad Sci U S A* **2003**, *100*, 15416-21.

(58) Blank, M.; Weinschenk, T.; Priemer, M.; Schluesener, H. *J Biol Chem* **2001**, *276*, 16464-8.

(59) Schmidt, K. S.; Borkowski, S.; Kurreck, J.; Stephens, A. W.; Bald, R.; Hecht, M.; Friebe, M.; Dinkelborg, L.; Erdmann, V. A. *Nucleic Acids Res* **2004**, *32*, 5757-65.

(60) Di Giusto, D. A.; Wlassoff, W. A.; Gooding, J. J.; Messerle, B. A.; King, G. C. *Nucleic Acids Res* **2005**, *33*, e64.

(61) Shangguan, D.; Tang, Z.; Mallikaratchy, P.; Xiao, Z.; Tan, W. *Chembiochem* **2007**, *8*, 603-6.

(62) Sefah, K.; Phillips, J. A.; Xiong, X.; Meng, L.; Van Simaeys, D.; Chen, H.; Martin, J.; Tan, W. *Analyst* **2009**, *134*, 1765-75.

(63) Mairal, T.; Ozalp, V. C.; Lozano Sanchez, P.; Mir, M.; Katakis, I.; O'Sullivan, C. K. *Anal Bioanal Chem* **2008**, *390*, 989-1007.

(64) Navani, N. K.; Li, Y. *Curr Opin Chem Biol* **2006**, *10*, 272-81.

(65) Lee, J. O.; So, H. M.; Jeon, E. K.; Chang, H.; Won, K.; Kim, Y. H. *Anal Bioanal Chem* **2008**, *390*, 1023-32.

(66) Willner, I.; Zayats, M. *Angew Chem Int Ed Engl* **2007**, *46*, 6408-18.

(67) Lai, R. Y.; Plaxco, K. W.; Heeger, A. J. *Anal Chem* **2007**, *79*, 229-33.

(68) Wu, Z. S.; Guo, M. M.; Zhang, S. B.; Chen, C. R.; Jiang, J. H.; Shen, G. L.; Yu, R. Q. *Anal Chem* **2007**, *79*, 2933-9.

(69) Su, S.; Nutiu, R.; Filipe, C. D.; Li, Y.; Pelton, R. *Langmuir* **2007**, *23*, 1300-2.

(70) Xiao, Y.; Piorek, B. D.; Plaxco, K. W.; Heeger, A. J. *J Am Chem Soc* **2005**, *127*, 17990-1.

(71) Rupcich, N.; Nutiu, R.; Li, Y.; Brennan, J. D. *Anal Chem* **2005**, *77*, 4300-7.

(72) Huang, Y. C.; Ge, B.; Sen, D.; Yu, H. Z. *J Am Chem Soc* **2008**, *130*, 8023-9.

(73) Fischer, N. O.; Tarasow, T. M.; Tok, J. B. *Anal Biochem* **2008**, *373*, 121-8.

(74) Zhou, L.; Ou, L. J.; Chu, X.; Shen, G. L.; Yu, R. Q. *Anal Chem* **2007**, *79*, 7492-500.

(75) Yang, L.; Fung, C. W.; Cho, E. J.; Ellington, A. D. *Anal Chem* **2007**, *79*, 3320-9.

(76) Shangguan, D.; Cao, Z.; Meng, L.; Mallikaratchy, P.; Sefah, K.; Wang, H.; Li, Y.; Tan, W. *J Proteome Res.* **2008**, *7*, 2133-2139.

(77) Mallikaratchy, P.; Tang, Z.; Kwame, S.; Meng, L.; Shangguan, D.; Tan, W. *Mol Cell Proteomics* **2007**, *6*, 2230-8.

(78) Shangguan, D.; Li, Y.; Tang, Z.; Cao, Z. C.; Chen, H. W.; Mallikaratchy, P.; Sefah, K.; Yang, C. J.; Tan, W. *Proc Natl Acad Sci U S A* **2006**, *103*, 11838-43.

(79) White, R. R.; Shan, S.; Rusconi, C. P.; Shetty, G.; Dewhirst, M. W.; Kontos, C. D.; Sullenger, B. A. *Proc Natl Acad Sci U S A* **2003**, *100*, 5028-33.

(80) Sullenger, B. A.; Gilboa, E. *Nature* **2002**, *418*, 252-8.

(81) Nimjee, S. M.; Rusconi, C. P.; Harrington, R. A.; Sullenger, B. A. *Trends Cardiovasc Med* **2005**, *15*, 41-5.

(82) Famulok, M.; Hartig, J. S.; Mayer, G. *Chem Rev* **2007**, *107*, 3715-43.

(83) Osborne, S. E.; Matsumura, I.; Ellington, A. D. *Curr Opin Chem Biol* **1997**, *1*, 5-9.

(84) Hicke, B. J.; Stephens, A. W. *J Clin Invest* **2000**, *106*, 923-8.

(85) Healy, J. M.; Lewis, S. D.; Kurz, M.; Boomer, R. M.; Thompson, K. M.; Wilson, C.; McCauley, T. G. *Pharm Res* **2004**, *21*, 2234-46.

(86) Willis, M.; Forssen, E. *Adv Drug Deliv Rev* **1998**, *29*, 249-271.

(87) Hicke, B. J.; Stephens, A. W.; Gould, T.; Chang, Y. F.; Lynott, C. K.; Heil, J.; Borkowski, S.; Hilger, C. S.; Cook, G.; Warren, S.; Schmidt, P. G. *J Nucl Med* **2006**, *47*, 668-78.

(88) Shi, H.; Tang, Z.; Kim, Y.; Nie, H.; Huang, Y. F.; He, X.; Deng, K.; Wang, K.; Tan, W. *Chem Asian J*, *5*, 2209-13.

(89) Farokhzad, O. C.; Jon, S.; Khademhosseini, A.; Tran, T. N.; Lavan, D. A.; Langer, R. *Cancer Res* **2004**, *64*, 7668-72.

(90) Dellaire, G.; Nisman, R.; Eskiw, C. H.; Bazett-Jones, D. P. *Nucleic Acids Res* **2004**, *32*, e165.

(91) Borbas, K. E.; Ferreira, C. S.; Perkins, A.; Bruce, J. I.; Missailidis, S. *Bioconjug Chem* **2007**, *18*, 1205-12.

(92) Bagalkot, V.; Zhang, L.; Levy-Nissenbaum, E.; Jon, S.; Kantoff, P. W.; Langer, R.; Farokhzad, O. C. *Nano Lett* **2007**, *7*, 3065-70.

(93) Bagalkot, V.; Farokhzad, O. C.; Langer, R.; Jon, S. *Angew Chem Int Ed Engl* **2006**, *45*, 8149-52.

(94) Dhar, S.; Gu, F. X.; Langer, R.; Farokhzad, O. C.; Lippard, S. J. *Proc Natl Acad Sci U S A* **2008**, *105*, 17356-61.

(95) Farokhzad, O. C.; Cheng, J.; Teply, B. A.; Sherifi, I.; Jon, S.; Kantoff, P. W.; Richie, J. P.; Langer, R. *Proc Natl Acad Sci U S A* **2006**, *103*, 6315-20.

(96) Wang, A. Z.; Bagalkot, V.; Vasilliou, C. C.; Gu, F.; Alexis, F.; Zhang, L.; Shaikh, M.; Yuet, K.; Cima, M. J.; Langer, R.; Kantoff, P. W.; Bander, N. H.; Jon, S.; Farokhzad, O. C. *ChemMedChem* **2008**, *3*, 1311-5.

(97) Zhang, L.; Radovic-Moreno, A. F.; Alexis, F.; Gu, F. X.; Basto, P. A.; Bagalkot, V.; Jon, S.; Langer, R. S.; Farokhzad, O. C. *ChemMedChem* **2007**, *2*, 1268-71.

(98) Chu, T. C.; Marks, J. W., 3rd; Lavery, L. A.; Faulkner, S.; Rosenblum, M. G.; Ellington, A. D.; Levy, M. *Cancer Res* **2006**, *66*, 5989-92.

(99) Tong, G. J.; Hsiao, S. C.; Carrico, Z. M.; Francis, M. B. *J Am Chem Soc* **2009**, *131*, 11174-8.

(100) McNamara, J. O., 2nd; Andrechek, E. R.; Wang, Y.; Viles, K. D.; Rempel, R. E.; Gilboa, E.; Sullenger, B. A.; Giangrande, P. H. *Nat Biotechnol* **2006**, *24*, 1005-15.

(101) Dassie, J. P.; Liu, X. Y.; Thomas, G. S.; Whitaker, R. M.; Thiel, K. W.; Stockdale, K. R.; Meyerholz, D. K.; McCaffrey, A. P.; McNamara, J. O., 2nd; Giangrande, P. H. *Nat Biotechnol* **2009**, *27*, 839-49.

(102) Zhou, J.; Li, H.; Li, S.; Zaia, J.; Rossi, J. J. *Mol Ther* **2008**, *16*, 1481-9.

(103) Zhou, J.; Swiderski, P.; Li, H.; Zhang, J.; Neff, C. P.; Akkina, R.; Rossi, J. J. *Nucleic Acids Res* **2009**, *37*, 3094-109.

(104) Wullner, U.; Neef, I.; Eller, A.; Kleines, M.; Tur, M. K.; Barth, S. *Curr Cancer Drug Targets* **2008**, *8*, 554-65.

(105) Chu, T. C.; Twu, K. Y.; Ellington, A. D.; Levy, M. *Nucleic Acids Res* **2006**, *34*, e73.

(106) Tasch, J.; Gong, M.; Sadelain, M.; Heston, W. D. *Crit Rev Immunol* **2001**, *21*, 249-61.

(107) Zhou, J.; Rossi, J. J. *Silence* **2010**, *1*, 4.

(108) Ng, E. W.; Shima, D. T.; Calias, P.; Cunningham, E. T., Jr.; Guyer, D. R.; Adamis, A. P. *Nat Rev Drug Discov* **2006**, *5*, 123-32.

(109) Griffin, L. C.; Toole, J. J.; Leung, L. L. *Gene* **1993**, *137*, 25-31.

(110) Li, W. X.; Kaplan, A. V.; Grant, G. W.; Toole, J. J.; Leung, L. L. *Blood* **1994**, *83*, 677-82.

(111) Bates, P. J.; Laber, D. A.; Miller, D. M.; Thomas, S. D.; Trent, J. O. *Exp Mol Pathol* **2009**, *86*, 151-64.

(112) Teng, Y.; Girvan, A. C.; Casson, L. K.; Pierce, W. M., Jr.; Qian, M.; Thomas, S. D.; Bates, P. J. *Cancer Res* **2007**, *67*, 10491-500.

(113) Farazi, P. A.; DePinho, R. A. *Nat Rev Cancer* **2006**, *6*, 674-87.

(114) El-Aneed, A.; Banoub, J. *Anticancer Res* **2006**, *26*, 3293-300.

(115) Jayasena, S. D. *Clin Chem* **1999**, *45*, 1628-50.

(116) Breaker, R. R. *Nature* **2004**, *432*, 838-45.

(117) Yang, C. J.; Jockusch, S.; Vicens, M.; Turro, N. J.; Tan, W. *Proc Natl Acad Sci U S A* **2005**, *102*, 17278-83.

(118) Nutiu, R.; Li, Y. *Angew Chem Int Ed Engl* **2005**, *44*, 5464-7.

(119) Liu, J.; Lu, Y. *Angew Chem Int Ed Engl* **2005**, *45*, 90-4.

(120) Cerchia, L.; Hamm, J.; Libri, D.; Tavitian, B.; de Franciscis, V. *FEBS Lett* **2002**, *528*, 12-6.

(121) Brown, M.; Wittwer, C. *Clin Chem* **2000**, *46*, 1221-9.

(122) ATCC *http://www.atcc.org/common/catalog/numSearch/numResults.cfm?atccNum)TIB-75*

(123) Tatsumi, T.; Takehara, T.; Kanto, T.; Miyagi, T.; Kuzushita, N.; Sugimoto, Y.; Jinushi, M.; Kasahara, A.; Sasaki, Y.; Hori, M.; Hayashi, N. *Cancer Res* **2001**, *61*, 7563-7.

(124) Rougier, P.; Mitry, E.; Barbare, J. C.; Taieb, J. *Semin Oncol* **2007**, *34*, S12-20.

(125) Wang, X. W.; Hussain, S. P.; Huo, T. I.; Wu, C. G.; Forgues, M.; Hofseth, L. J.; Brechot, C.; Harris, C. C. *Toxicology* **2002**, *181-182*, 43-7.

(126) Lee, H. C.; Kim, M.; Wands, J. R. *Front Biosci* **2006**, *11*, 1901-15.

(127) Thorgeirsson, S. S.; Lee, J. S.; Grisham, J. W. *Hepatology* **2006**, *43*, S145-50.

(128) Paradis, V.; Bedossa, P. *J Hepatol* **2007**, *46*, 9-11.

(129) Seow, T. K.; Liang, R. C.; Leow, C. K.; Chung, M. C. *Proteomics* **2001**, *1*, 1249-63.

(130) Carter, P. J.; Senter, P. D. *Cancer J* **2008**, *14*, 154-69.

(131) Chari, R. V. *Acc Chem Res* **2008**, *41*, 98-107.

(132) Huang, Y. F.; Shangguan, D.; Liu, H.; Phillips, J. A.; Zhang, X.; Chen, Y.; Tan, W. *Chembiochem* **2009**, *10*, 862-8.

(133) Mallikaratchy, P.; Tang, Z.; Tan, W. *ChemMedChem* **2008**, *3*, 425-8.

(134) Flinders, J.; DeFina, S. C.; Brackett, D. M.; Baugh, C.; Wilson, C.; Dieckmann, T. *Chembiochem* **2004**, *5*, 62-72.

(135) Patel, D. J.; Suri, A. K.; Jiang, F.; Jiang, L.; Fan, P.; Kumar, R. A.; Nonin, S. *J Mol Biol* **1997**, *272*, 645-64.

(136) Zhu, H.; Dong, H.; Eksioglu, E.; Hemming, A.; Cao, M.; Crawford, J. M.; Nelson, D. R.; Liu, C. *Gastroenterology* **2007**, *133*, 1649-59.

(137) Chaires, J. B.; Herrera, J. E.; Waring, M. J. *Biochemistry* **1990**, *29*, 6145-53.

(138) Lipscomb, L. A.; Peek, M. E.; Zhou, F. X.; Bertrand, J. A.; VanDerveer, D.; Williams, L. D. *Biochemistry* **1994**, *33*, 3649-59.

(139) N. Husain; R. A. Agbaria; Warner, I. M. *J. Phys. Chem.* **1993**, *97*, 10857-10861.

(140) Yan, Q.; Priebe, W.; Chaires, J. B.; Czernuszewicz, R. S. *Biospectroscopy* **1997**, *3*, 307-316.

(141) Haj, H. T.; Salerno, M.; Priebe, W.; Kozlowski, H.; Garnier-Suillerot, A. *Chem Biol Interact* **2003**, *145*, 349-58.

(142) Cory, A. H.; Owen, T. C.; Barltrop, J. A.; Cory, J. G. *Cancer Commun* **1991**, *3*, 207-12.

(143) Salvesen, G. S. *Cell Death Differ* **2002**, *9*, 3-5.

(144) Ghavami, S.; Hashemi, M.; Ande, S. R.; Yeganeh, B.; Xiao, W.; Eshraghi, M.; Bus, C. J.; Kadkhoda, K.; Wiechec, E.; Halayko, A. J.; Los, M. *J Med Genet* **2009**, *46*, 497-510.

(145) Lee, Y.; Park, S. Y.; Mok, H.; Park, T. G. *Bioconjug Chem* **2008**, *19*, 525-31.

(146) Boudeau, J.; Miranda-Saavedra, D.; Barton, G.; Alessi, D. *Trends Cell Biol.* **2006**, *16*, 443-452.

(147) Mossie, K.; Jallal, B.; Alves, F.; Sures, I.; Plowman, G.; Ullrich, A. *Oncogene* **1995**, *11*, 2179-2184.

(148) Park, S.-K.; Lee, H.-S.; Lee, S.-T. *J. Biochem* **1996**, *119*, 235-239.

(149) Kroiher, M.; Miller, M.; Steele, R. *Bioessays.* **2001**, *23*, 69-76.

(150) Saha, S.; Bardelli, A.; Buckhaults, P.; Velculescu, V. E.; Rago, C.; Croix, B. S.; Romans, K. E.; Choti, M. A.; Lengauer, C.; Kinzler, K. W.; Vogelstein, B. *Science* **2001**, *294*, 1343-1346.

(151) Gorringe, K. L.; Boussioutas, A.; Bowtell, D. D. *Genes Chromosomes Cancer* **2005**, *42*, 247-259.

(152) Endoh, H.; Tomida, S.; Yatabe, Y.; Konishi, H.; Osada, H.; Tajima, K.; Kuwano, H.; Takahashi, T.; Mitsudomi, T. *J Clin Oncol.* **2004**, *22*, 811-819.

(153) Müller-Tidow, C.; Schwäble, J.; Steffen, B.; Tidow, N.; Brandt, B.; Becker, K.; Schulze-Bahr, E.; Halfter, H.; Vogt, U.; Metzger, R.; Schneider, P.; Büchner, T.; Brandts, C.; Berdel, W.; Serve, H. *Clin Cancer Res.* **2004**, *10*, 1241-1249.

(154) Katoh, M.; Katoh, M. *Int J Mol Med.* **2007**, *20*, 405-409.

(155) Lu, X.; Borchers, A.; Jolicoeur, C.; Rayburn, H.; Baker, J.; Tessier-Lavigne, M. *Nature* **2004**, *430*, 93-98.

(156) Shin, W.; Maeng, Y.; Jung, J.; Min, J.; Kwon, Y.; Lee, S. *Biochem Biophys Res Commun.* **2008**, *371*, 793-798.

(157) Alnemri, E.; Livingston, D.; Nicholson, D.; Salvesen, G.; Thornberry, N.; Wong, W.; Yuan, J. *Cell* **1996**, *18*, 171.

(158) Thornberry, N.; Lazebnik, Y. *Science* **1998**, *281*, 1312-1316.

(159) Earnshaw, W.; Martins, L.; Kaufmann, S. *Annu Rev Biochem.* **1999**, *68*, 383-424.

(160) Boatright, K.; Salvesen, G. *Curr Opin Cell Biol.* **2003**, *15*, 725-731.

(161) Carlo-Stella, C.; Lavazza, C.; Locatelli, A.; Vigano, L.; Gianni, A. M.; Gianni, L. *Clin Cancer Res* **2007**, *13*, 2313-7.

(162) Green, D.; Kroemer, G. *Science* **2004**, *305*, 626-629.

(163) Scaffidi, C.; Fulda, S.; Srinivasan, A.; Friesen, C.; Li, F.; Tomaselli, K.; Debatin, K.; Krammer, P.; Peter, M. *EMBO J.* **1998**, *17*, 1675-1687.

(164) Fernandes-Alnemri, T.; Armstrong, R.; Krebs, J.; Srinivasula, S.; Wang, L.; Bullrich, F.; Fritz, L.; Trapani, J.; Tomaselli, K.; Litwack, G.; Alnemri, E. *Proc Natl Acad Sci U S A.* **1996**, *93*, 7464-7469.

(165) Filomenko, R.; Prévotat, L.; Rébé, C.; Cortier, M.; Jeannin, J.; Solary, E.; Bettaieb, A. *Oncogene* **2006**, *7*, 7635-7645.

(166) Harada, K.; Toyooka, S.; Shivapurkar, N.; Maitra, A.; Reddy, J.; Matta, H.; Miyajima, K.; Timmons, C.; Tomlinson, G.; Mastrangelo, D.; Hay, R.; Chaudhary, P.; Gazdar, A. *cancer Res.* **2002**, *62*, 5897-5901.

(167) MS, S.; HS, K.; CS, K.; WS, P.; SY, K.; SN, L.; JH, L.; JY, P.; JJ, J.; CW, K.; SH, K.; JY, L.; NJ, Y.; SH, L. *Blood* **2002**, *99*, 409404099.

(168) Shin, M.; Kim, H.; Lee, S.; Lee, J.; Song, Y.; Kim, Y.; Park, W.; Kim, S.; Lee, S.; Park, J.; Lee, J.; Xiao, W.; Jo, K.; Wang, Y.; Lee, K.; Park, Y.; Kim, S.; Lee, J.; Yoo, N. *Oncogene* **2002**, *21*, 4129-4136.

(169) Park, S.; Wu, C.; Gordon, J.; Zhong, X.; Emami, A.; Safa, A. *J Biol Chem.* **2004**, *278*, 51057-51067.

(170) Fire, A.; Xu, S.; Montgomery, M.; Kostas, S.; Driver, S.; Mello, C. *Nature* **1998**, *391*, 806-811.

(171) Zhao, Y.; Srivastava, D. *Trends Biochem Sci* **2007**, *32*, 189-97.

(172) Pillai, R. S.; Bhattacharyya, S. N.; Filipowicz, W. *Trends Cell Biol* **2007**, *17*, 118-26.

(173) Zamore, P.; Tuschl, T.; Sharp, P.; Bartel, D. *Cell* **2000**, *101*, 25-33.

(174) Siomi, H.; Siomi, M. C. *Nature* **2009**, *457*, 396-404.

(175) Vermeulen, A.; Behlen, L.; Reynolds, A.; Wolfson, A.; Marshall, W. S.; Karpilow, J.; Khvorova, A. *RNA* **2005**, *11*, 674-82.

(176) Castanotto, D.; Rossi, J. J. *Nature* **2009**, *457*, 426-33.

(177) Qiu, S.; Adema, C. M.; Lane, T. *Nucleic Acids Res* **2005**, *33*, 1834-47.

(178) Ahlquist, P. *Science* **2002**, *296*, 1270-3.

(179) Elbashir, S.; Harborth, J.; Lendeckel, W.; Yalcin, A.; Weber, K.; Tuschl, T. *Nature* **2001**, *411*, 494-498.

(180) McNamara, J. n.; Andrechek, E.; Wang, Y.; Viles, K.; Rempel, R.; Gilboa, E.; Sullenger, B.; Giangrande, P. *Nat Biotechnol.* **2006**, *24*, 1005-1015.

(181) Devi, G. *Cancer Gene Ther.* **2006**, *13*, 819-829.

(182) Karagiannis, T.; El-Osta, A. *Cancer Gene Ther.* **2005**, *12*, 787-795.

(183) Towbin, H.; Staehelin, T.; Gordon, J. *Proc Natl Acad Sci U S A* **1979**, *76*, 4350-4.

(184) Renart, J.; Reiser, J.; Stark, G. R. *Proc Natl Acad Sci U S A* **1979**, *76*, 3116-20.

(185) Zipper, H.; Brunner, H.; Bernhagen, J.; Vitzthum, F. *Nucleic Acids Res* **2004**, *32*, e103.

(186) Mackay, I. M.; Arden, K. E.; Nitsche, A. *Nucleic Acids Res* **2002**, *30*, 1292-305.

(187) Matlashewski, G.; Lamb, P.; Pim, D.; Peacock, J.; Crawford, L.; Benchimol, S. *EMBO J* **1984**, *3*, 3257-62.

(188) Bunz, F.; Dutriaux, A.; Lengauer, C.; Waldman, T.; Zhou, S.; Brown, J. P.; Sedivy, J. M.; Kinzler, K. W.; Vogelstein, B. *Science* **1998**, *282*, 1497-501.

(189) Kaeser, M. D.; Pebernard, S.; Iggo, R. D. *J Biol Chem* **2004**, *279*, 7598-605.

(190) Dornburg, R.; Pomerantz, R. J. *Adv Pharmacol* **2000**, *49*, 229-61.

(191) Dykxhoorn, D. M.; Novina, C. D.; Sharp, P. A. *Nat Rev Mol Cell Biol* **2003**, *4*, 457-67.

BIOGRAPHICAL SKETCH

Ling Meng was born in Urumchi, China in 1980. She spent her childhood mainly in Binzhou, Shandong. After completing the basic and senior high school, she attended the Shandong University and obtained her bachelor's degree in Microbiology in 2003. Inspired by the environment of the school, her family and friends, she decided to go abroad to continue her research career. She joined the University of Florida in 2005 and received her PhD degree in Chemistry in December 2010 under the tutorage of Dr Weihong Tan.